Theoretical Studies on Reactions of Transition-Metal Complexes

Shuqiang Niu[†] and Michael B. Hall*

Department of Chemistry, Texas A&M University, College Station, Texas 77843

Received September 21, 1999

Contents

I. Introduction

Stoichiometric and catalytic transition-metal reactions have attracted great interest for their many applications in industrial and synthetic processes. Transition-metal reactions are critical in many thermodynamically feasible processes because they accelerate the reaction by opening a lower activation-energy pathway, often one that was symmetry forbidden. These metal-centered reactions consist of one or more elementary reactions such as substitution, oxidative addition, reductive elimination, migratory insertion, hydrogen exchange, β-hydrogen transfer, σ-bond metathesis, and nucleophilic addition. Numerous experimental and theoretical studies have been undertaken in order to understand these fundamental transformations.[1] Recent progress in computational chemistry has shown that many important chemical and physical properties of the species involved in these reactions can be predicted from first principles by various computational techniques.[2] This ability is especially important in those cases where experimental results are difficult to obtain.

In the past 8 years, several excellent reviews have appeared that describe the application of ab initio molecular orbital (MO) and density functional theory (DFT) methods to reactions containing transition metals.[3] The reviews by Koga and Morokuma,[3a] Musaev and Morokuma,[3b] and Siegbahn and Blomberg[3c] give an overview of theoretical studies of transition-metal-catalyzed chemical reactions. Those by Ziegler[3d] and Salahub et al.[3e] review DFT methods and their applications to transition-metal reactions. Siegbahn[3f] has recently reviewed applications of both conventional ab initio quantum methods and DFT methods to transition-metal systems. Recent books on applications of ab initio MO theory include those edited by Dedieu[3g] and van Leeuwen et al.[3h] on theoretical aspects of transition-metal hydrides and homogeneous catalysis, respectively.

Here, we focus on reactions of transition-metal complexes and review recent studies which use the latest computational techniques. First, we briefly review recent developments in the computational methodologies that are used in studies on transition-metal reactions. Then, we review applications to various classes of elementary reactions such as substitution, migratory insertion, hydrogen transfer, oxidative addition/reductive elimination, metathesis, and nucleophilic addition. Finally, some recently studied catalytic processes are discussed.

II. General Methods

In the last several years, the enormous progress in computational techniques is reflected in higher level applications of ab initio Hartree−Fock (HF), post-HF, and density functional theory (DFT) to real reaction systems containing transition metals.[2−4] Treatment of the reactions with quantum chemical methods involves calculations of geometries and energetics of reactants, intermediates, transition states, and products. The accuracy of the calculations, which affects the thermodynamic and kinetic data as well as details of the reaction mechanism, depends on a combination of the theoretical method and basis set.[4]

Figure 1 illustrates the strategic use of a sequence of model chemistries definable via the computational method and basis set in studies of transition-metal

[†] Presently at Pacific Northwest National Laboratory, Richland, WA 99352.

10.1021/cr980404y CCC: $35.00
Published on Web 01/26/2000

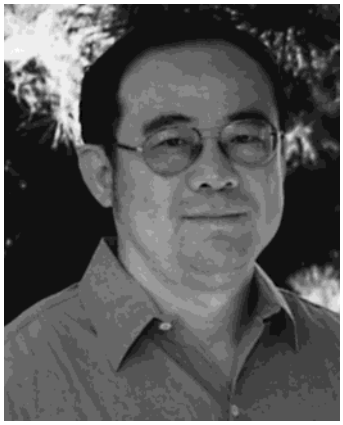

Shuqiang Niu was born in Beijing, China, and received his B.S. and M.S. degrees (with Professor Chengming Lai) in Physical Chemistry from Nankai University. After a two-year teaching career at Nankai University, he joined Professor R. Gleiter's group at University Heidelberg, Germany, in 1989 and completed his Ph.D. degree there in 1994, where he studied Ziegler–Natta catalytic systems. From 1994 to 1999, he did research with Professor Michael B. Hall at Texas A&M University as a Welch Foundation Postdoctoral Fellow and then as an Assistant Research Scientist, investigating reaction processes of organometallic and bioinorganic systems. He currently works at the Pacific Northwest National Laboratory as an Associated Western Universities research staff member. His research interests include the structure, reaction mechanism, and reactivity of organic, organometallic, and bioinorganic systems.

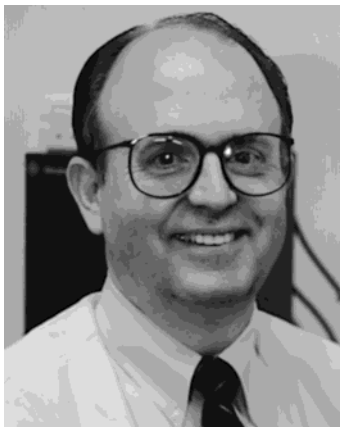

Professor Hall was born in Pennsylvania and graduated from Juniata College with a B.S. degree in Chemistry in 1966. After completing his Ph.D. degree with Richard Fenske at the University of Wisconsin in 1971, he accepted an AEI fellowship to study ab initio quantum chemistry with Ian Hillier at the University of Manchester, England. He accepted an appointment as Assistant Professor of Chemistry at Texas A&M University in 1975, rose through the ranks, and served as Head of the Department from 1986 to 1994. He currently directs the Laboratory for Molecular Simulation and serves as Associate Dean for Research and Information Technology in the College of Science. His research interests are primarily directed toward understanding chemical structures and reactions through the application of state-of-the-art quantum calculations. He serves on the Editorial Advisory Board of *Theoretical Chemistry Accounts*.

reactions.[2−5] The theoretical level increases from HF through DFT,[3d,6] Møller−Plesset (MP) perturbation series (MP2, MP3, and MP4),[7] multiconfigurational self-consistent field (MCSCF),[8] modified coupled pair functional (MCPF),[9] quadratic configuration interaction with singles and doubles (QCISD),[10] and coupled cluster with singles and doubles (CCSD)[11] to QCISD and CCSD with perturbative corrections for triples (QCISD(T) and CCSD(T)).[10,12] On the other coordinate, atomic basis sets from minimal basis sets on the left through the double- and triple-ζ basis sets

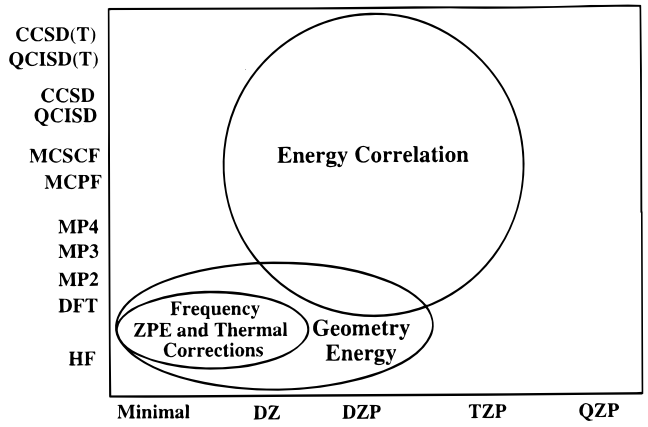

Figure 1. Illustration for the strategic use of a sequence of model chemistries definable via the computational method and basis set in studies of transition-metal reactions.

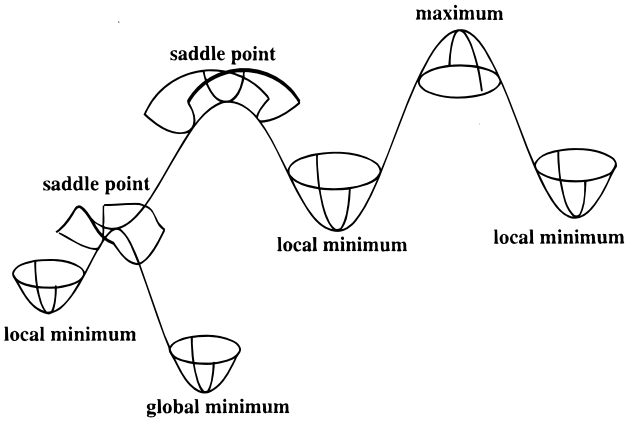

Figure 2. Illustration of the types of stationary points on a potential energy surface.

(DZ and TZ) with additional polarization functions (DZP and TZP) to the quadruple-ζ basis sets with polarization functions (QZP) on the right lead to an increase in the relative accuracy of various model calculations.[4,5] Highly accurate methods and large basis sets lead to higher computational cost, especially for experimentally accurate reaction models. Thus, the strategic use of computational chemistry in transition-metal reactions ultimately depends not only on established levels of performance, but also on practical considerations such as cost.

A. Geometry

Geometry optimization is one of the most important steps in the theoretical treatment of transition-metal reactions. Accurate application of molecular orbital theory and reliable determination of the reaction and activation energies require reasonable molecular geometries of reactants, transition states, intermediates, and products. The geometry optimization of reactants, intermediates, and products of transition-metal reactions involves minimization of the energy with respect to each independent geometrical parameter, while a corresponding treatment of a transition state (TS) seeks a saddle point on the potential surface as shown in Figure 2.[2,13] With the development of efficient analytical energy gradient and

second-derivative (Hessian matrix) methods, complete optimization of geometric parameters for minima and saddle points has become more common. A minimum with all positive eigenvalues in Hessian matrix corresponds to an equilibrium structure, while a saddle point with one negative eigenvalue in a Hessian matrix corresponds to a transition-state structure usually connecting two stationary structures. The nature of stationary points on the potential energy surface can be characterized by the number of imaginary frequencies: zero for a minima, one for a TS (first-order saddle point), and two or more (x) for a "maximum" (x-order saddle point).[4,5] It is important to note that the normal mode corresponding to the imaginary frequency of a saddle point must be determined so that the nature of the transition-state structure can be analyzed. The eigenvectors of the imaginary frequency of the transition-state structure show which geometrical parameters are involved in the reaction coordinate (RC). Animating the vibrations with a chemical visualization package (for example, Cerius[2] from MSI and ECCE from PNNL) is often sufficient for this analysis. Sometimes it is necessary to perform an intrinsic reaction coordinate (IRC)[14] calculation to follow the RC both in the forward and reverse directions to be assured that the TS connects the anticipated minima. Since searching for a desired transition-state structure is much more difficult than searching for a local minimum, a good initial structure is especially important in the TS optimization. The linear synchronous transit (LST)[15] and the synchronous transit-guided quasi-Newton (STQN)[16] methods are useful for locating transition-state structures. In some reaction systems, important insight can be gained by scanning the potential energy surface along one or two RCs.

Currently, the most common geometry optimizations for studies of reactions containing transition metals are performed at the HF, MP2, and DFT levels of theory. In the last several years, the HF and MP2 methods have been employed successfully to obtain molecular structures, electronic structures, and thermodynamic and kinetic data for second- and third-row transition-metal systems.[2−5] Relativistic effective core potentials (RECPs)[17] generated from the relativistic HF atomic core are especially valuable for heavy transition-metal system such as second- and third-row transition-metal complexes because the most important relativistic effects are incorporated into the ECP.[18] Generally, first-row transition-metal complexes are significantly more difficult to treat with the HF and MP2 methods than complexes of the second- and third-row transition metals. The major reason for this is that the 3d orbitals are much more compact than the 4s orbitals.[3f] The compactness of the 3d orbital leads to the presence of strong near-degeneracy effects because of weak overlap between the 3d orbitals and the ligand orbitals.[3f] Because the 4d and 5d orbitals are larger relative to the atom's size, the influence of near-degeneracy effects on complexes of the second- and third-row transition metals is smaller. Near-degeneracy problems often lead to multireference character in the state of interest, and in principle, these states cannot be described correctly by single-reference methods such as HF or MP2. A poor description of the electronic state by HF or MP2 may lead to incorrect results for the geometry optimization. Recent progress in DFT has shown clearly that the new generation of gradient-corrected DFT methods such as Becke's three-parameter hybrid exchange potential (B3)[19] with the Lee−Yang−Parr (LYP),[20] Perdue (P86),[21] or Perdue−Wang (PW91)[22] correlation functional are efficient and accurate computational methods in studies of transition-metal reactions, especially for treating much larger systems and complexes containing first-row transition metals.

Table 1. RHF, B3LYP, MP2, and CISD Fully Optimized Geometries and Experimental Values of the Product $CpCo(N(O)CH_3)PH_3$ (4b)

	RHF/DZ	DFT/DZ	MP2/DZ	CISD/DZ	exp
Co−Cp	2.076	1.849	1.731	1.888	1.718
Co−P	2.511	2.287	2.164	2.360	2.174
Co−N	1.991	1.772	1.711	1.787	1.780
N−O	1.226	1.324	1.378	1.295	1.282
N−C	1.487	1.514	1.527	1.504	1.484
P−Co−N	96.8	95.8	94.4	96.0	92.4
Co−N−O	124.2	126.4	128.3	125.4	125.6
Co−N−C	121.2	123.5	124.5	123.5	124.4
av % dev	7.65	2.95	2.48	3.25	

To examine the quality of the geometric optimization for transition-metal reactions at different levels of theory, we have selected the insertion of NO into a $Co-CH_3$ σ bond followed by PH_3 addition to generate the nitroso complex, $CpCo(PH_3)(N(O)CH_3)$ (**4**; reaction 1).[23,24]

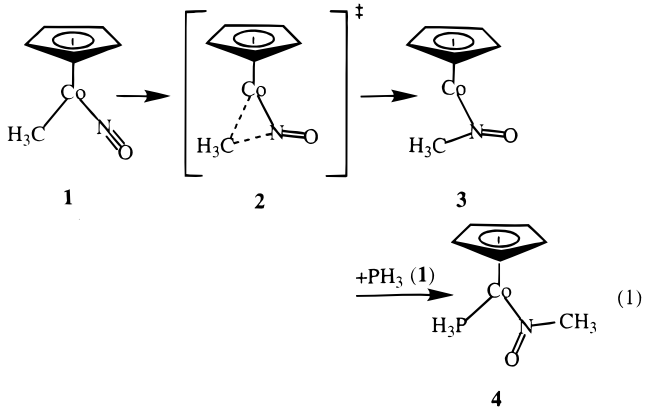

1 **2** **3** **4** (1)

The HF/DZ, DFT-B3LYP/DZ, MP2/DZ, and CISD/DZ fully optimized geometries of the product $CpCo(PH_3)(N(O)CH_3)$ (**4**) are given in Table 1.[25] Compared to the experimental values of Weiner and Bergman,[23] the overall average percent deviation is 7.65% at the HF level, where the metal−ligand bond lengths are generally too long in this basis set. The B3LYP, MP2, and CISD geometries of **4** are in much better agreement with the X-ray structure with average percent deviations of 2.95%, 2.48%, and 3.25%, respectively. The optimized geometry at the B3LYP level is very similar to the one at the CISD level. The largest differences between B3LYP, CISD and MP2 values are for the Co−Cp, Co−P, and Co−N metal−ligand distances, which are all shorter at the MP2 level.

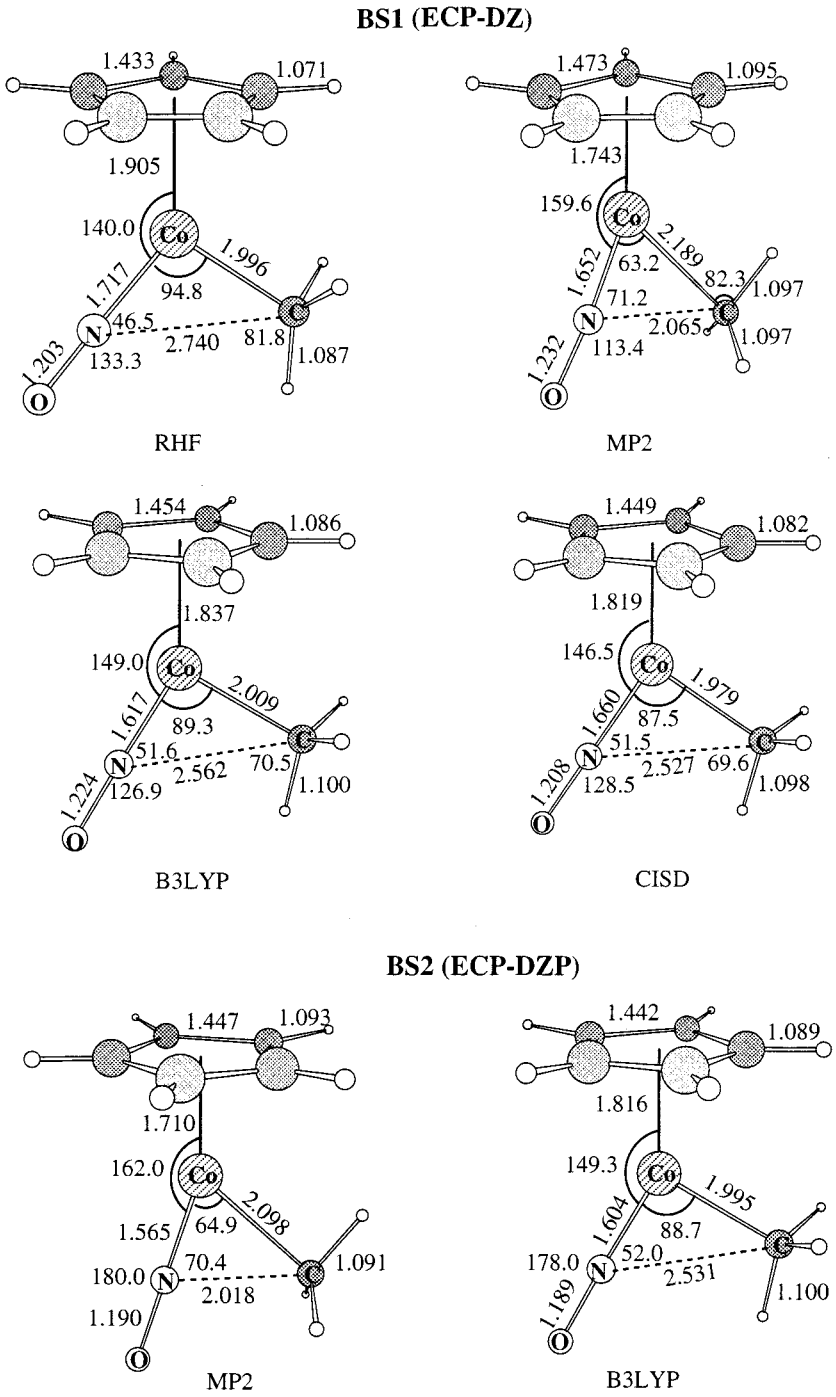

Figure 3. HF/DZ, B3LYP/DZ, MP2/DZ, CISD/DZ, MP2/DZP, and B3LYP/DZP fully optimized geometries of the reactant $CpCo(CH_3)(NO)$ (**1**).

Compared with the experimental values, the MP2 bond lengths for Co−Cp and Co−P are better than those of B3LYP and CISD but the MP2 value for the Co−N is worse. The short MP2 Co−N bond length and the long MP2 N−O bond length indicate that the strength of the "backdonation" is exaggerated by the MP2 method.

As an additional example, the HF/DZ, B3LYP/DZ, MP2/DZ, CISD/DZ, MP2/DZP, and B3LYP/DZP fully optimized geometries of the reactant $CpCo(CH_3)(NO)$ (**1**) are shown in Figure 3. Compared with the CISD/DZ-optimized geometry, the HF/DZ-optimized Cp−Co, Co−NO, and N−CH_3 distances are all longer while the Co−CH_3 distance is close to CISD result. The B3LYP geometry is in very good agreement with that at the CISD level; the average percent deviation is less than 2.6%. However, the MP2/DZ- and MP2/DZP-optimized structures of **1** are both quantitatively and qualitatively different from the B3LYP/DZ- or B3LYP/DZP- and CISD/DZ-optimized ones in having a much shorter N−CH_3 distance and a rotated and distorted methyl group. Note that the addition of polarization functions does not significantly improve the MP2 results. Calculations with higher level correlation methods, QCISD and CCSD, indicate that the B3LYP/DZ and CISD/DZ geometries of **1** are 15−23 kcal/mol lower in energy than the MP2/DZ geometry. Complete active-space multiconfiguration SCF

Table 2. Optimized Geometries for the Singlet Ni(H)(OH) Insertion Product and Transition State

method	Ni−H	Ni−O	H−Ni−OH	Ni−O−H
		Product		
HF	1.60	1.74	131.4	151.5
MP2	1.39	1.71	89.6	122.2
CASSCF	1.51	1.75	109.2	136.7
MCPF	1.40	1.71	103.8	116.1
DFT-LSD	1.42	1.68	98.6	110.6
		Transition State		
HF	1.65	1.78	48.7	131.8
MP2	1.26	1.74	66.4	110.2
CASSCF	1.69	1.89	48.5	128.2
QCISD	1.57	1.85	49.6	112.8
MCPF	1.57	1.82	46.2	113.1

(CASSCF)[26] calculations and CCSD T_1 diagnostic analysis[27] at the B3LYP geometry of the reactant (**1**) show that it has a significantly larger multireference character than the insertion TS (**2**) or intermediate (**3**). Thus, the reactant (**1**) has strong near-degeneracy effects from the interaction between the low-lying unoccupied π^* orbitals of the NO group and high-lying occupied Co orbitals.[24] The consequence of these near-degeneracy effects is that the MP2 geometry of **1** migrates toward the TS (**2**) for this insertion reaction. Thus, near-degeneracy problems can affect the accuracy of both HF and MP2 geometry optimization.

Similar results have been observed in the OH insertion into the Ni−H bond to generate Ni(OH_2) (reaction 2).[28]

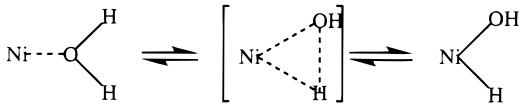

(2)

The optimized geometric parameters and relative energies of the OH insertion into the Ni−H bond at the difference levels of theory are given in Table 2.[28] Here, one again encounters problems for the geometry optimization. Since near-degeneracy effects are quite severe for this system, with a larger CI coefficient of 0.30 appearing in the wave function, the geometry optimizations of Ni(H)(OH) at the HF and MP2 levels give very different H−Ni−CH_3 angles (too large at the HF level and too small at the MP2 level) with respect to those at the DFT, CASSCF, and MCPF levels. In contrast, the MP2-optimized H−Ni−OH angle of the transition state is larger by about 20° than that at the higher levels of theory.[28a] Clearly, at the MP2 level these near-degeneracy effects exaggerate the geometric difference.

B. Energy

Calculations of the energy at the optimized geometry are an equally important step in theoretical studies of transition-metal reactions. Many predicted chemical properties are directly related to the energy.[2−5] Generally, accurate relative energies such as reaction energies and activation energies in transition-metal reactions can obtained by a series of energy corrections, which include electron correlation

Table 3. Calculated and Experimentally Observed First Bond Dissociation Energies (FBDE) (kcal/mol)

	$Cr(CO)_6$	$Mo(CO)_6$	$W(CO)_6$	ref
HF/DZ	21.0	26.3	34.8	31a
HF/DZ	20.3	28.4	37.7	33a
MP2/DZP	58.0	46.1	54.9	31a
CCSD(T)//MP2/DZP	45.8 (32.5)	40.4	48.0	31a
LDA	62.1	52.7	48.4	33b
LDA/NL	35.1	28.4	33.9	33c
LDA/NL	44.6	37.4	33.5	33b
LDA/NL+FO	45.1	39.8	41.8	33b
NL-SCF	45.9	38.2	38.8	33b
NL-SCF/FO	46.8	40.6	47.2	33b
NL-SCF-QR	46.2	39.7	43.7	33b
NL-SCF+QR	43.1	39.9	46.0	33d
exp	38.7	30.1	39.7	34
exp	37 ± 5	34 ± 5	38 ± 5	35
exp	36.8 ± 2	40.5 ± 2	46.0 ± 2	36

corrections from higher levels of theory with larger basis sets, basis-set superposition error (BSSE) corrections,[29a,b] zero-point energy (ZPE), and thermal, solvation, and relativistic (spin−orbit, etc.) corrections. In most studies of transition-metal reactions, factors that are related to a counterion or a solvent are either neglected or just qualitatively discussed. Currently, the higher level methods for electron correlation in transition-metal reactions are MCSCF, MCPF, QCISD, CCSD, QCISD(T), and CCSD(T). Applications of one or more of these methods may be essential not only for accurate energy calculations but also for examining the outcome of geometry optimization at various levels of theory. Since spin-unrestricted wave functions are not eigenfunctions of the S^2 operator, the potential energy surfaces obtained for open-shell reaction systems by spin-unrestricted methods can be significantly distorted by contamination from higher spin states. The spin-projected UMPn (PUMPn) and higher level methods based on UHF such as UCCSD can overcome some of these spin contamination problems.[29c,d]

The problems encountered in geometry optimizations affect energy calculations in similar ways. It is well-known that Møller−Plesset (MP) perturbation methods have given reliable results for systems involving second- and third-row transition metals.[3,30] Frenking and co-workers[31] have studied a series of transition-metal carbonyl complexes, $M(CO)_6$ (M = Cr, Mo, Hf^{2-}, Ta^-, W, Re^+, Os^{2+}, Ir^{3+}), $M(CO)_5$ (M = Fe, Ru, Os), and $M(CO)_4$ (M = Ni, Pd, Pt), where the MP2/DZP-optimized geometries, CO stretching frequencies, and CCSD(T)/DZP//MP2/DZP first bond dissociation energies (FBDE) of the second- and third-row carbonyl complexes are in excellent agreement with experimental values. However, large oscillations in the total energy differences were found in the application of perturbation theory to some reactions involving first-row transition metals.[31a,32]

Table 3 compares the calculated[31,33] and experimental[34,35] first bond dissociation energies (FBDE) of $M(CO)_6$ (M = Cr, Mo, and W). One can find that (i) the HF FBED values are too low by 12−15 kcal/mol, a result which is also reflected in the long M−CO bonds calculated at the HF level, (ii) the

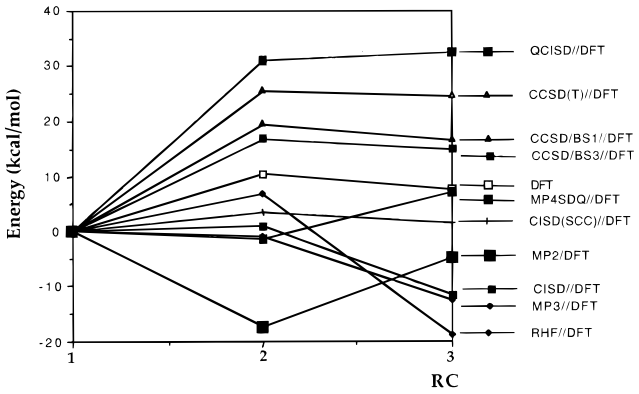

Figure 4. Energy profiles for the migratory insertion step (reaction 1) based on the calculations of the HF/DZ, B3LYP/DZ, MP2/DZ, MP3/DZ, MP4/DZ, CISD/DZ, CISD(SCC)/DZ, QCISD/DZ, CCSD/DZ, CCSD(T)/DZ, and CCSD/DZP, at the B3LYP/DZ geometries.

FBDE values are too high at MP2/DZP and LDA, particularly for $Cr(CO)_6$, for which shorter M−CO bond lengths are calculated by MP2 and LDA, and (iii) the DFT/NL and CCSD(T) FBDE values are lower than those at MP2 and LDA but higher than those at HF. It noteworthy that the "best" theoretical values for $Cr(CO)_6$, 43.1 (NL-SCF+QR) and 45.8 kcal/mol (CCSD(T)/DZP//MP2/DZP), are larger than the best experimental estimate of 38.8 kcal/mol.[31,33,36] Ehlers and Frenking attributed the deviation with experiment to deficiencies in the optimized geometries,[31a] a near-degeneracy problem. Ziegler et al. argue that the DFT discrepancy with experimental values for chromium is due to a problem in the analysis of the experiment.[33b] Nevertheless, the values at CCSD(T) and DFT/NL compare well with the available experimental estimates for $Mo(CO)_6$ and $W(CO)_6$.

The perturbation series (MP2, MP3, MP4) for the migratory insertion step (reaction 1) also fails to converge during the energy calculations.[24] Since it was already mentioned above that the DFT-B3LYP geometries are somewhat more accurate than the HF and MP2 geometries, the energetics by the higher order methods (CISD/DZ, CISD(SCC)/DZ, QCISD/DZ, CCSD/DZ, CCSD(T)/DZ, and CCSD/DZP) at the B3LYP/DZ geometries were investigated. These results, Figure 4, clearly show that the Møller−Plesset perturbation series for the electron correlation of this insertion reaction fails to converge, where substantial oscillations appear in the energetic order of the reactant (**1**), the transition state (**2**), and the η^1-intermediate (**3**). These severe oscillations again suggest a serious near-degeneracy problem in this system. The consequences of this problem are that both MP2 and MP4 overestimate the stability of the B3LYP transition state (**2**) with respect to **1** and **3**. However, the B3LYP energetic order from **1** through **2** to **3** is in very good agreement with the higher order electron correlation methods (CISD/DZ, CISD(SCC)/DZ, QCISD/DZ, CCSD/DZ, CCSD(T)/DZ, and CCSD/DZP) at the B3LYP/DZ geometries. The calculated activation barriers of the migratory insertion step **1** → **3** at the B3LYP, CCSD/DZ//B3LYP, and CCSD/DZP//B3LYP levels are 10.4, 19.5, and 16.9 kcal/mol, respectively. When compared to the estimated experimental activation enthalpy of 14.5 kcal/mol,[37] the calculated barrier heights are quite reasonable, especially the CCSD value in the DZP basis set. Thus, DFT-B3LYP gives a much better and more reliable description of the geometries and relative energies in this first-row transition-metal system than either the HF or the MP2 approach.

In the another example of a first-row transition-metal reaction system (reaction 3),[38] the calculations for this intramolecular C−H bond activation process at the MP2, DFT-B3P86, QCISD, and QCISD(T) levels show that (i) geometries obtained at the B3P86 level compared favorably with an available experimental structure,[39] (ii) the DFT-B3P86 geometries of **5** and **7** are better than the MP2 geometries, the QCISD energies are 18−25 kcal/mol lower in energy for the B3D86 geometries, and (iii) the activation free energy from **5** to **7** obtained at the QCISD//B3P86/DZP level are in excellent agreement with the experimental value (within 1 kcal/mol).

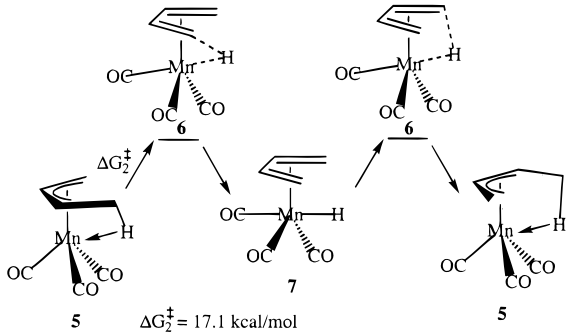

(3)

Thus, one must again conclude that (i) the Møller−Plesset perturbation series is not sufficiently convergent for the final energy determinations in first-row transition-metal reaction systems and (ii) the DFT methods generally give a much better and more reliable description of the geometries and relative energies in these first-row transition-metal reaction systems.

The final example, a counter example, will be taken from recent applications to agostic M···H−C bonding such as that found in the precursor complex for the methane C−H bond activation by transition-metal complexes (reaction 4).

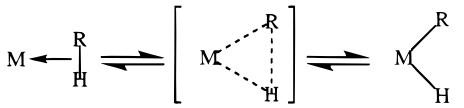

(4)

Bergman et al.[40] directly measured the rates of reactions between the 16-electron complex, Cp*Rh(CO), and alkanes in the gas phase. They estimated the bonding energy from Cp*Rh(CO) and alkane to the σ complex, Cp*Rh(CO)(η^2-alkane), to be about 10 kcal/mol. The quantitative variations in the bonding energy from the different calculations in Table 4 arise from differences in theoretical methods.[41] These calculations gave values from −7.7 to −14.8 for the conventionally correlated ab initio methods and from

Table 4. Calculated Bonding Energy (kcal/mol) between CpRh(CO) and Methane at the Difference Levels of Theory

method	ΔE	ref
MP2//HF	−14.8	41b
MP2//MP2	−12.3	41d
	−7.7	41c
	−13.6	41e
MCPF//MP2	−10.1	41d
PCI-80//MP2	−12.5	41d
CASPT2//MP2	−11.7	41d
B3LYP//MP2	−5.6	41d
B3P86//MP2	−8.0	41d
DFT-LDA	−6.9	41a
B3LYP//B3LYP	−6.4	41e
exp	−10	40a

−5.6 to −8.0 for the DFT methods. The conventional ab initio methods overestimate this binding because of the lack of BSSE correction, while the DFT calculations underestimate this α-agostic interaction between CpRh(CO) and CH_4. Other work on the binding of alkanes to tungsten pentacarbonyl, alkane−$W(CO)_5$, also shows that the conventional ab initio methods give an excellent description of these weak bonding energies, especially in the larger basis sets.[42] The problem here, of course, is that current functionals do not correctly describe the dispersion energy, which is well described by MP2 calculations.

In summary, DFT methods generally give a much better and more reliable description of the geometries and relative energies than HF or MP2 methods except for some weak bonding interactions.[43] During the past 4 years, the DFT methods such as B3LYP and B3P86 became the dominant computational tool for treating the transition-metal reaction systems. The DFT methods appear less basis-set sensitive, more efficient, and more accurate. Only CC methods, which are very costly, would appear to equal or exceed the accuracy of the best DFT methods.

III. Substitution Reactions

Ligand substitution at a transition-metal center is one of the most basic reactions and a crucial step in homogeneous catalytic reactions.[1] Substitution reactions are usually classified into four types of mechanisms: D (dissociative), I_d (dissociative interchange), I_a (associative interchange), and A (associative).[44] These mechanisms are distinguished on the basis of thermodynamic activation parameters such as $\Delta H^{\ddagger}$, $\Delta S^{\ddagger}$, $\Delta G^{\ddagger}$, or $\Delta V^{\ddagger}$. Recent kinetic studies have shown that the substitutional ability and mechanism of transition-metal complexes can be explained qualitatively in terms of the stability of the transition state or intermediate involved.[45] For example, it has been shown that the first CO substitution by a phosphine ligand is about 10^{10}-fold faster for the 17-e$^-$ vanadium hexacarbonyl, $V(CO)_6$, than it is for the analogous 18-e$^-$ chromium complex, $Cr(CO)_6$.[46] The kinetic evidence indicates that substitution reactions of 17-e$^-$ metal carbonyl complexes proceed via a low-energy associative mechanism (A) while those of 18-e$^-$ complexes proceed via a higher energy dissociative (D) or dissociative interchange (I_d) one (reaction 5).[45]

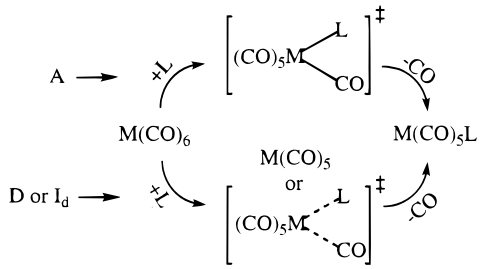

(5)

Using ab initio MO methods, Lin and Hall studied the substitution mechanisms of the 17-e$^-$ metal hexacarbonyls, $M(CO)_6$ (M = V, Nb, and Ta), and the analogous 18-e$^-$ complexes, $M(CO)_6$ (M = Cr, Mo, and W), by the CO and PH_3 ligands.[33a] They determined geometries for the transition states and investigated the effect of electron correlation on these systems. The energetics of carbonyl exchange reactions of hexacarbonyl complexes is summarized in Table 5. Since the calculated activation energies from the associative reaction mechanism and the calculated first CO dissociation energies (FBDE) (ΔE_d) are similar for the 18-e$^-$ complexes and both the entering and leaving ligands are far from the metal in the calculated transition state for the associative reaction, this reaction resembles an I_d mechanism.[33a,b] Although the HF calculations underestimate the difference in the activation energies (ΔE_a) between the 17-e$^-$ complex and the 18-e$^-$ complex compared to the DFT and CI calculations, even for third-row transition-metal complexes, the trend at the HF level shows that substitution reactions of the 17-e$^-$ transition-metal hexacarbonyl complexes proceed via an associative mechanism. The calculations on carbonyl substitution by phosphine in $M(CO)_6$ also show a significant difference in activation energies (ca. 11 kcal/mol) between the two (18-e$^-$ and 17-e$^-$) substitution reactions. The valence-electron Laplacian ($-\nabla^2\rho$)[47] plots of the transition states (Figure 5) show that (i) in the substitution reaction of the 18-e$^-$ metal carbonyl complexes, the "associative" transition state corresponds to a 20-e$^-$ system and the valence-electron charge concentrations are located in the direction of metal−entering/leaving ligand bonds and (ii) for the 19-e$^-$ transition state, the two maxima in the charge concentration are not directed toward the entering/leaving ligands and both entering and leaving ligands are linked to the metal by dative bonds. Thus, the relatively more stable transition state observed for the substitution reactions of 17-e$^-$ transition-metal complexes is reflected in significant differences in the valence-electron distributions of their associative transition states.

In substitution reactions of transition-metal complexes, the reaction mechanism not only depends on the valence-electron distributions of the metal−entering/leaving ligand bonds in their transition state, but also on the spectator ligands. For example, although four-coordinate $Ni(CO)_4$ slowly undergoes substitution through a dissociative mechanism,[48a,b] its isoelectronic analogues $Co(CO)_3(NO)$,[48c] $Fe(CO)_2(NO)_2$,[48d] and $Mn(CO)(NO)_3$[48e] readily react through

Table 5. Activation Energies (ΔE_a), First CO Dissociation Energies (FBDE) (ΔE_d), and Selected Structural Parameters of Hartree−Fock Transition States for $M(CO)_6 + CO$

	ΔE_a (kcal/mol)	structural parameters		$\Delta\Delta E_a$ (kcal/mol)	ΔE_d (kcal/mol)
		α (deg)	M···CO (Å)		
$Cr(CO)_6 + CO$	19.1[a] (47.0)[b]	62.5	4.23	2.7	20.3 (46.2)
$V(CO)_6 + CO$	16.9	61.4	4.22		
$Mo(CO)_6 + CO$	27.3 (40.4)	60.0	4.23	6.5	28.4 (39.7)
$Nb(CO)_6 + CO$	20.8	59.5	3.38		
$W(CO)_6 + CO$	35.8 (35.8)	57.4	3.91	15.0	37.7 (43.7)
$Ta(CO)_6 + CO$	20.8	70.0	2.29		

[a] CISD//HF/DZ, ref 33a. [b] LDA/DZ, ref 33b.

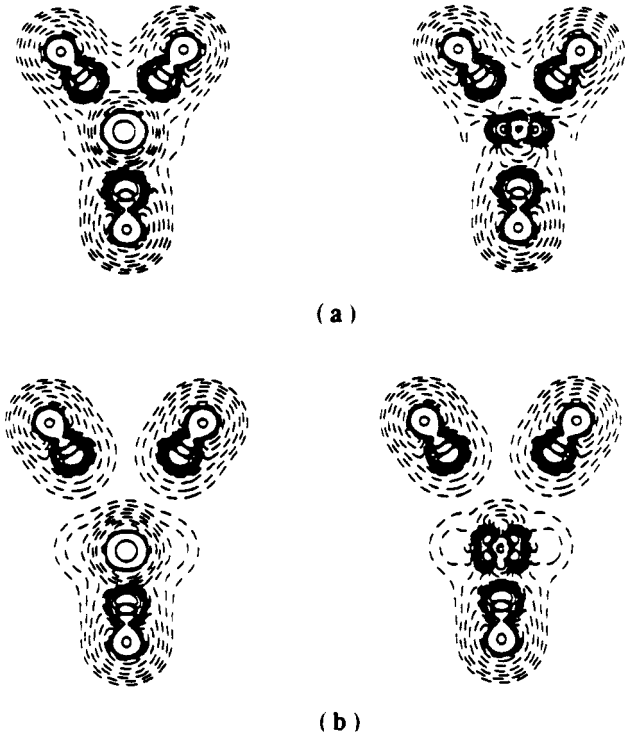

Figure 5. Valence-electron Laplacian ($-\nabla^2\rho$) plots of the transition states in the $Ta(CO)_6 + CO$ (a) and $W(CO)_6 + CO$ (b) carbonyl exchange reactions. (Reprinted with permission from ref 33a. Copyright 1992 American Chemical Society.)

an associative process. Carbonyl substitution in five-coordinate $Fe(CO)_5$[49a] and six-coordinate $Cr(CO)_6$[49b] occurs by a dissociative mechanism, while their isoelectronic counterparts $Mn(CO)_4(NO)$[49a] and $V(CO)_5(NO)$[46] react by an associative pathway. Recent experimental studies on $W(CO)_4(NO)X$ (X = Cl, Br, or I) show that CO substitution proceeds through an associative route with strong nucleophiles such as P(*n*-Bu)$_3$ but through a dissociative or dissociative interchange mechanism (I_d) for weaker nucleophiles such as PPh_3.[50a] However, this associative pathway apparently is not accessible to the isoelectronic metal carbonyl $Re(CO)_5X$.[50b] The explanation for a low-energy associative mechanism is not obvious at first as the 20-e$^-$ transition state should have a very high energy. However, as distinct from CO, NO is more versatile; it can function as either a 3-e$^-$ ligand or an 1-e$^-$ ligand (reaction 6). Thus, as a spectator ligand, the nitrosyl can change the transition-metal electron count through bending.

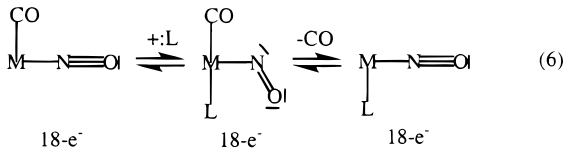

(6)

Constructing the potential energy surfaces from ab initio calculations, Song and Hall investigated CO substitution in these isoelectronic metal carbonyl complexes.[52] The calculations for the attack by PMe_3 on $W(CO)_4(NO)Cl$ predict an associative mechanism with a seven-coordinate intermediate, in which the W−N−O angle is bent to 135.7° (Figure 6). The Laplacian of the total charge density displays a process in which electrons shift from the metal to the nitrogen, create an additional N lone pair, and vacate a coordinate site for the entering ligand (Figure 6). In contrast, substitution by PR_3 (R = H, Me) in $Re(CO)_5Cl$ proceeds by a dissociative or I_d mechanism since the CO ligand cannot accommodate an additional electron pair and resists bending to maintain a strong Re−CO bond. Although the nitrosyl bends strongly for PMe_3, it is unable to provide a low-energy associative path for the substitution by the PH_3 ligand. The PH_3 ligand, as a poor donor, cannot stabilize an associative intermediate with a bent W−N−O bond. On the basis of experimental[53] and theoretical results,[52] Song and Hall have offered the following four nucleophiles in the descending order of strength P(*n*-Bu)$_3$ ≈ P(Me)$_3$ > PPh_3 > PH_3.

A bent Co−nitrosyl complex has been experimentally observed through replacing PPh_3 with PEt_3 by Weiner and Bergman (reaction 1).[23] The DFT and CCSD calculations by Niu and Hall show that the bent nitrosyl intermediate, $CpCo(PH_3)(CH_3)(NO)$, is less stable by 16 and 18 kcal/mol than the reactants, $CpCo(CH_3)(NO)$ and PH_3, since PH_3 is a poorer nucleophile than either PPh_3 or PEt_3.[24] Thus, the substitution reaction mechanism is directly related to the stabilizing interactions between the metal and the entering ligands and between the metal and the spectator ligands in the transition state or intermediate.

Copolymerization of an olefin with carbon monoxide has attracted much attention from an industrial viewpoint due to the useful chemical and physical properties introduced into the polymer chain by the presence of ketone groups.[54−56] Although the experimental and theoretical work of Brookhart,[56] Ziegler,[57] Morokuma,[58] Siegbahn,[58] Hall,[59] and co-workers show that the Pd(II)-assisted alternating copolymerization

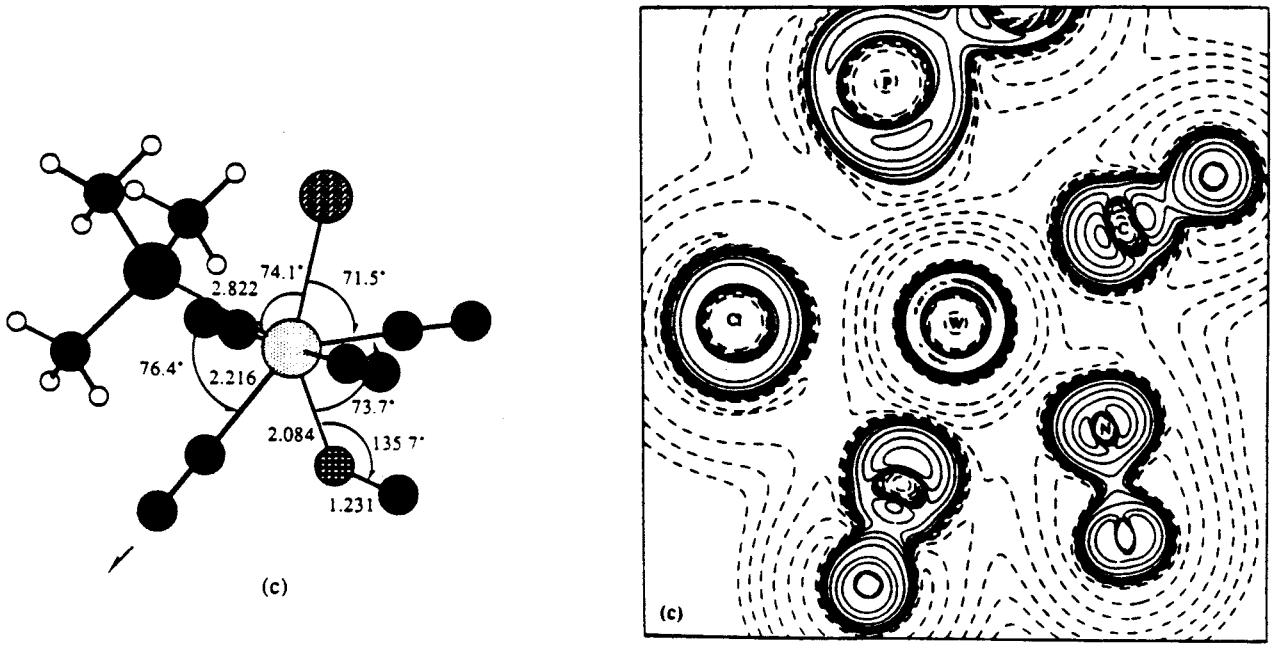

Figure 6. Optimized geometry and the Laplacian ($-\nabla^2\rho$) contour plot of the seven-coordinate intermediate along the associative path for the CO substitution by PMe_3 in $W(CO)_4(NO)Cl$. The absolute value of the smallest contour is 0.01465 e/a_0. (Reprinted with permission from ref 52. Copyright 1993 American Chemical Society.)

of olefin and CO (reaction 7) is kinetically favored over homopolymerization of olefin or CO, the competition of CO/olefin substitution with CO/olefin insertion thermodynamically as well as kinetically dominates reaction routes (see next section).

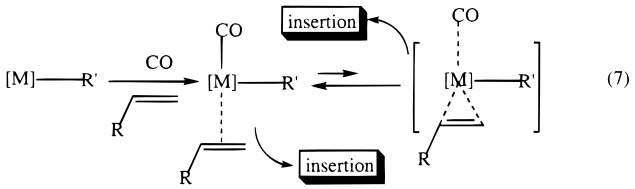

(7)

Since the Pd(II) complex will form a stronger bond to the CO in the Dewar−Chatt−Duncanson model, CO association is favorable (−10 kcal/mol) over olefin association. The olefin complex converts to the CO complex through an associative mechanism. As a consequence of this equilibrium, the rate of olefin insertion into the M−R bond will decrease.[59]

Generally, one can rationalize the *trans*-effect order in substitution reactions of square-planar complexes by a combination of σ-donating and π-accepting abilities of the ligands:[1e,60] C_2H_4, CO, CN^- > PR_3, H^- > CH_3^- > $C_6H_5^-$, NO_2^-, SCN^-, I^- > Br^-, Cl^- > Py, NH_3, OH^-, H_2O.

In an early ab initio MO study, the substitution reactions of square-planar transition-metal complexes were investigated by Lin and Hall.[61a] The calculations show a pseudo-trigonal-bipyramidal transition state with a very small leaving-ligand to metal to entering-ligand (L−M−E) angle in this system. The *trans*-effect order (CO > H^- > CH_3^- > Cl^- > NH_3) predicted by the calculations agrees with the experimental order. In addition, the ligand dissociation process was determined for the following reactions by Lin and Hall (reaction 8). As expected, the dissociation energies are much higher than the activation energies of the associative mechanism. Therefore, it is unlikely that a dissociative reaction mechanism can contribute much to the substitution rates of these square-planar complexes.

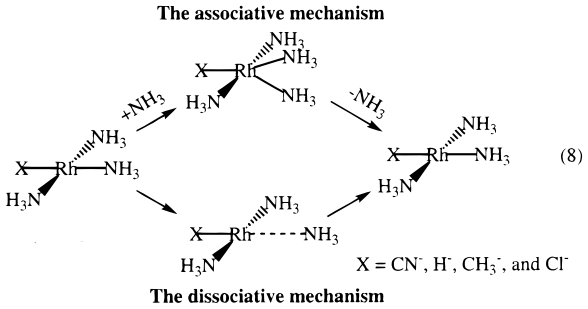

(8)

Recently, Yates and co-workers investigated the model ligand substitution reaction $Pd(N-O)(CH_3)(PH_3) + CO \rightarrow Pd(N-O)(CH_3)(CO) + PH_3$ (N−O = $NHCHCOO^-$) with density functional and conventional ab initio MO methods.[61b−d] The calculations show that the exchange of CO for PH_3 is an endothermic process that should proceed with only a small activation energy of 3.7 kcal/mol. The stabilization of the five-coordinate intermediate with respect to the four-coordinate species generally precludes the formation of three-coordinate species, where higher barriers of 29−57 kcal/mol are calculated. Thus, an associative mechanism is favored over a dissociative one in this model system.

IV. Migratory Insertion Reactions

A. Olefin Insertions

Olefin insertion reactions (reaction 9) are fundamental elementary steps in a variety of C−C bond-forming reactions such as polymerization, copolym-

Scheme 1

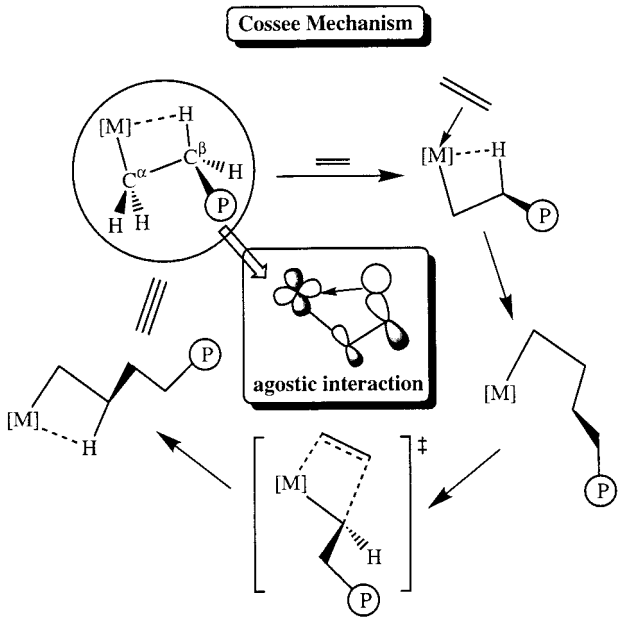

erization, hydroformylation, hydrogenation, and isomerization.[1] Numerous experimental and theoreti-

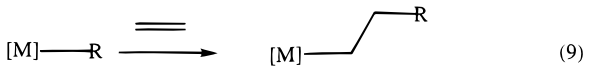

(9)

R = alkyl, acyl, and H

cal studies have been concerned with the kinetic and thermodynamic behavior of these transformations in order to discover the basic principles and to search for more selective or more efficient catalysts.

Recent experimental studies show that in addition to metallocenes and geometry-constrained catalysts of the early transition metals (d^0 and d^0f^n; Ziegler−Natta catalysts being the archetype), various Fe(II), Co(III), Ni(II), Pd(II), and Ru(II) complexes also catalyze olefin polymerization or oligomerization reactions. Numerous real and model insertion reactions have been investigated with density functional theory (DFT) and ab initio molecular orbital theory, and this work has been reviewed by Koga and Morokuma,[3a] Musaev and Morokuma,[3b] Siegbahn and Blomberg,[3c] and Yoshida et al.[3i]

For **early transition metals**, recent experimental work provides compelling support for the identification of the d^0 and d^0f^n metallocenes species as active catalysts[1,62,63] as well as for the widely accepted Cossee mechanism.[64] Nearly all of the theoretical work also supports the general aspects of this mechanism.[65−80] According to the Cossee mechanism, the propagation step in the polymerization of olefins occurs via a prior π-coordination to a vacant coordination site on the active catalyst, followed by olefin insertion through a four-center transition state in a $2\pi + 2\sigma$ reaction involving the C−C π bond and metal−alkyl σ bond as shown in Scheme 1.[64] In the four-center transition state, the occupied σ_{M-R} and π_{Olefin} orbitals interact with the vacant π^*_{Olefin} and σ^*_{M-R} orbitals as illustrated in Figure 7.[65,70b] The $\pi-\pi^*$ mixing involved in these interactions shifts

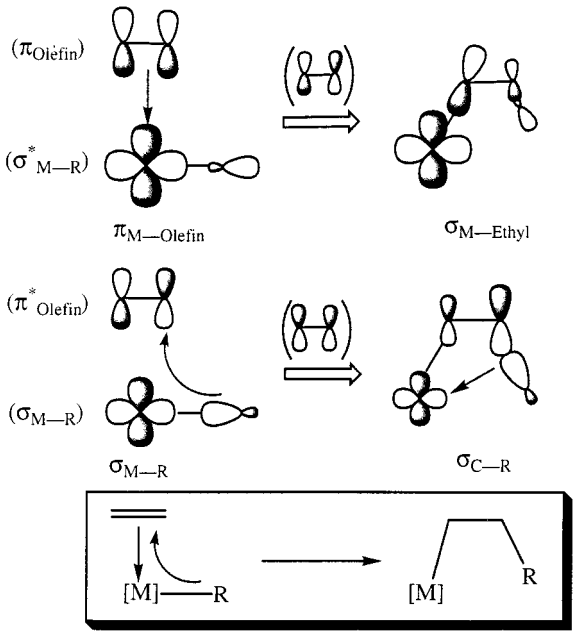

Figure 7. Schematic bonding interactions between d^0 metal−alkyl and olefin.

electron densities to the C^α which is forming the new σ_{M-R} bond and away from the C^β which is forming the new σ_{C-R} bond. In other words, the $\pi-\pi^*$ mixing helps to break the π bond and in olefin insertions it polarizes the olefin, $^-CH_2-CH_2^+$, so that the cationic center is available to form the C−R bond while the anionic center is available to form the new M−C bond. Thus, a combination of electron transfer from the π_{Olefin} orbital to the σ^*_{M-R} orbital and the $\pi-\pi^*$ mixing leads to a new $\sigma_{M-Alkyl}$, while the combination of electron transfer from the σ_{M-R} bond to the π^*_{C-C} orbital of the olefin and the $\pi-\pi^*$ mixing leads to a new σ_{C-R} bond. The d^0/d^0f^n metal center plays a dual role as an electron acceptor and electron donor during the electron-transfer process.[70b] Agostic interactions[81] between a low-lying unoccupied d orbital and an inside occupied C−H or C−C orbital (see Scheme 1) have been shown by numerous theoretical investigations to be vital throughout the insertion process since they provide extra stabilization for the carbon network and lower the insertion barrier during the bond rearrangement process.[65−80]

Recently, Ziegler and co-workers investigated the ethylene insertion reaction with $Cp_2MCH_3^+$ and $HN(SiH_2)CpMCH_3^+$ (M = Ti, Zr, and Hf) by DFT methods,[75a−c] and Yoshida, Koga, and Morokuma studied the mechanism of ethylene polymerization with silyene-bridged metallocenes, $H_2SiCp_2MCH_3^+$ (M = Ti, Zr, and Hf), at the HF (for geometry optimization), MP2, MP3, MP4, and QCISD levels of theory.[66g] The important calculated energetic parameters involved in insertion process are summarized in Table 6. In general, these newer computational results at higher levels of theory support the earlier studies, which found that ethylene association is exothermic and ethylene insertion from the π complex through the insertion TS to the agostic complex is exothermic with a low barrier as shown in Scheme 2. Although there are some differences in the opti-

Table 6. Relative Energies (kcal/mol) of Olefin Insertion into the M−R Bond of (L)M−R$^+$ + C_2H_4 to (L)MC_2H_4R$^+$ for Early Transition Metals

M	L[a]	R	method	reactant	π-complex	TS	product	ref
Ti(IV)	[1]	CH_3	BP86	0.0	−20.8	−17.8	−33.6	75a−c
	[3]	CH_3	QCISD	0.0	−21.9	−14.8	−29.3	66g
	[1]	C_2H_5	BP86	0.0	−1.9	1.7		75a−c
	[2]	C_2H_5	BP86	0.0	−17.2	−15.3	−28.2	75a−c
Zr(IV)	[1]	CH_3	BP86	0.0	−22.9	−22.2	−31.0	75a−c
	[2]	CH_3	BP86	0.0	−24.2	−19.1	−32.4	75a−c
	[3]	CH_3	BP86	0.0	−26.3	−25.3	−34.0	75a−c
	[3]	CH_3	QCISD	0.0	−29.1	−19.7	−33.4	66g
	[1]	C_2H_5	BP86	0.0	−10.5	−5.5		75a−c
Hf(IV)	[2]	CH_3	BP86	0.0	−25.7	−10.0	−33.6	75a−c
	[3]	CH_3	QCISD	0.0	−27.6	−17.5	−32.1	66g
	[1]	C_2H_5	BP86	0.0	−15.1	−10.8		75a−c

[a] [1] = Cp_2^{2-}; [2] = NH−Si(H)$_2$−$C_5H_4^{2-}$; [3] = $H_2SiCp_2^{2-}$.

Scheme 2

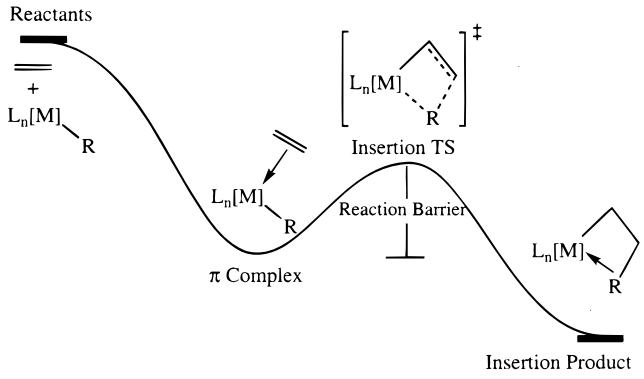

mized geometries, both DFT and QCISD methods give quite similar relative energies for ethylene insertion into the M−CH_3 and M−C_2H_5 σ bonds, where the ethylene binding energies of the corresponding π complexes and the insertion barriers increase slightly in the order Ti < Zr < Hf. By comparing the calculated results for unbridged and bridged systems, Ziegler and co-workers have found their steric differences cause only small differences in the energetics of ethylene insertion into the M−CH_3 σ bond, although they have different sized coordination sites and different electron deficiency on the metal center. However, as the polymer chain propagates, there is a destabilization of the potential energy surface from the π complex through the insertion TS to the product. Now the steric effect of the spectator ligands significantly affects the polymerization rate and selectivity (see Table 6).

Morokuma and co-workers investigated a new class of olefin polymerization catalysts, zirconium- and titanium-chelated alkoxide complexes, [X(C_6H_4O)$_2$-MCH_3]$^+$ (M = Ti, Zr; X = S (S-bridged), CH_2 (CH_2-bridged), nothing (directly bridged)).[66h] In comparison to metallocene complexes, the bridged chelating ligands in these catalysts are more flexible. In the case of the S-bridged species, there is a definite interaction between the metal center and the S atom. This interaction stabilizes the reactant as the complexes prefer to be four-coordinate. Because the incoming olefin competes with the S donation, this system has a destabilized precursor, π complex. Since Ti complexes generally have weaker metal−olefin bonds and lower insertion barriers, the S-bridged titanium catalyst has the lowest predicted barrier, a result that agrees with its experimentally high activity. The CH_2− and directly bridged species cannot have such a direct interaction with the metal, and thus their insertion barriers are much larger. Overall, the titanium S-bridged system has an activity comparable to the very active metallocene systems.

Table 7. Agostic Stabilizing Energies and Relative Energies (kcal/mol) of Olefin Insertion into the M−R Bond of [L]M−R^n + C_2H_4 to (L)MC_2H_4R^n (n = 0 and +1) for Early Transition Metals[75g,h]

M	[L][a]	R	method	agostic	π-complex	barrier
Sc(III)	[4]	C_2H_5	BP86	1.8	−11.0	4.1
	[5]	C_2H_5	BP86	1.8	−11.0	2.6
	[6]	C_2H_5	BP86	1.4	−9.1	2.6
Y(III)	[4]	C_2H_5	BP86	2.4	−12.7	6.2
	[5]	C_2H_5	BP86	1.9	−13.1	6.2
	[6]	C_2H_5	BP86	1.4	−12.0	5.5
La(III)	[4]	C_2H_5	BP86	1.9	−9.1	6.7
	[5]	C_2H_5	BP86	1.9	−9.6	9.1
	[6]	C_2H_5	BP86	1.2	−8.6	6.9
Ti(IV)	[4]	C_2H_5	BP86	2.6	−26.1	8.1
	[5]	C_2H_5	BP86	3.1	−24.4	5.5
	[6]	C_2H_5	BP86	4.5	−22.9	4.3
Zr(IV)	[4]	C_2H_5	BP86	3.1	−26.1	8.6
	[5]	C_2H_5	BP86	2.9	−26.8	8.1
	[6]	C_2H_5	BP86	5.0	−24.9	7.6
Hf(IV)	[4]	C_2H_5	BP86	0.5	−24.1	17.0
	[5]	C_2H_5	BP86	0.5	−20.6	15.3
	[6]	C_2H_5	BP86	0.7	−20.8	12.9

[a] [4] = $(OH)_2^{2-}$; [5] = $(CH_3)_2^{2-}$; [6] = $(NH_2)_2^{2-}$.

More recently, Margl, Deng, and Ziegler systematically investigated olefin insertion into the M−R bond for a number of d^0 [L]M−R^n fragments (M = Sc(III), Y(III), La(III), Ti(IV), Zr(IV), Hf(IV), Ce(IV), Th(IV), and V(V); L = NH−$(CH)_2$−NH^{2-}, N(BH_2)−$(CH)_2$−$(BH_2)N^{2-}$, O−$(CH)_3$−O^-, Cp_2^{2-}, NH−Si(H)$_2$−$C_5H_4^{2-}$, [(oxo)(O−$(CH)_3$−O)]$^{3-}$, $(NH_2)_2^{2-}$, $(OH)_2^{2-}$, $(CH3)_2^{2-}$, NH−$(CH_2)_3$−NH^{2-}, and O−$(CH_2)_3$−O^{2-}; R = H, CH_3, and C_2H_5; n = 0, +1, and +2).[75g,h] In Table 7, where the calculated energetic parameters of the insertion reaction of sterically unencumbered systems are summarized, one finds that (i) the β-agostic bond strength in the [L]M$C_2H_5^n$ (n = 0 and +1) precursor follows the order Ti ≈ Zr > Hf and Sc ≈ Y ≥ La with agostic interactions for uncharged precursor complexes (with a higher lying d orbital) generally being weaker than for cationic ones (with a lower lying d orbital), (ii) the ethylene association energy to the [L]-M$C_2H_5^n$ (n = 0 and +1) precursor can be predicted to within ±4.8 kcal/mol by a simple empirical rule,

Scheme 3

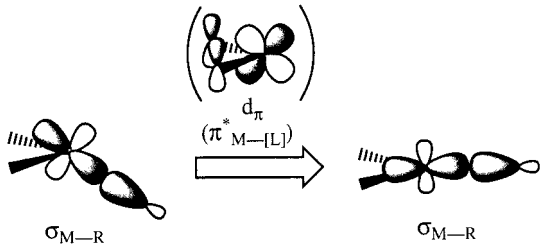

Scheme 4

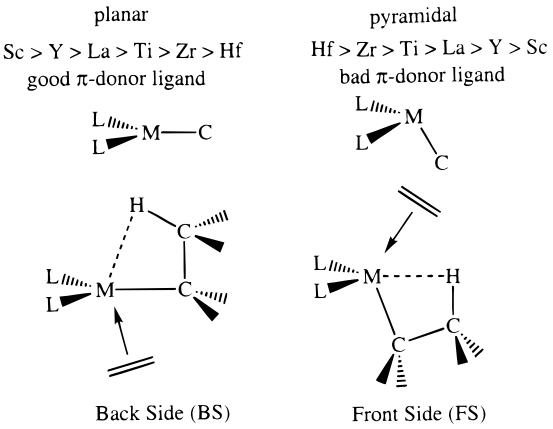

based on the accessible metal surface of the [L]-$MC_2H_5^n$ fragment and its gross charge, (iii) ethylene insertion barriers follow the order Sc < Y < La and Ti < Zr < Hf and are generally lower for group 3 than for group 4 because the aptitude of the $[L]MC_2H_5^n$ fragment to occupy the trigonal-planar arrangement, a structure close to the TS, tends to be Sc > Y > La > Ti > Zr > Hf, and (iv) good π-donor spectator ligands have an increased tendency to form trigonal arrangements because the π-donor interaction between the spectator ligands and the d_π orbital leads to a decrease of the d_π character in the σ_{M-R} orbital, as shown in Scheme 3.

Extensive studies of the reactivity of unbridged metallocenes, $Cp_2MR^{0/+1}$, bridged metallocenes, $HN(SiH_2)CpMR^+$, and constrained geometry complexes, $H_2SiCp_2MR^+$, by Morokuma,[66] Ziegler,[75a−f] and coworkers show that the olefin π-association energy is subtly influenced by the steric characteristics of the spectator ligands and that it is hard to predict beyond an accuracy of ±4.8 kcal/mol without detailed first-principles calculations. Thus, steric crowding by spectator ligands generally lowers the insertion barrier, since compression of the active site favors the transition-state geometry over the π-complex geometry.

For the chain propagation step, Ziegler and coworkers have studied an alternative ethylene insertion pathway, the so-called backside insertion (BS) as shown in Scheme 4.[75d−h] The conformation of the π complex (backside (BS) vs front side (FS)) is influenced by the nature of the metal and the spectator ligand. The propensity to form a FS complex increases from 3d to 5d metals and from group 3 to group 4 metals. Spectator ligands that are good donors or sterically bulky tend to enhance BS complexation. BS insertion barriers depend only weakly on the identity of the metal center as BS insertion requires little deformation of the metal−ligand framework.

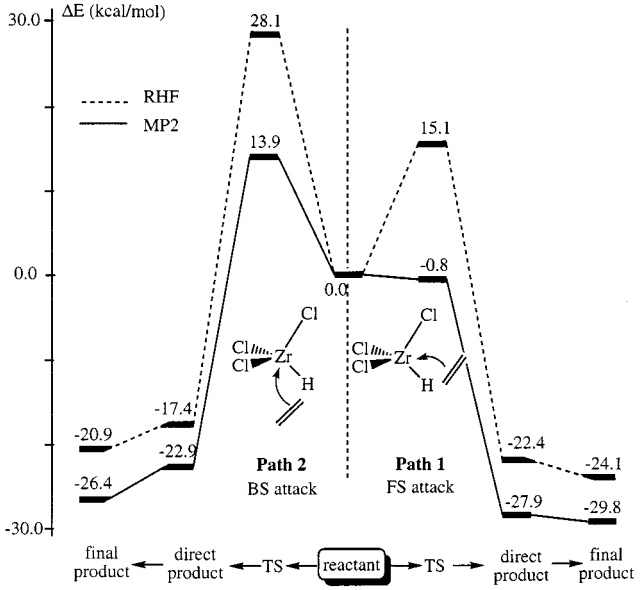

Figure 8. Relative potential energy profiles from reactants to products for hydrozirconation of ethylene.

In previous work, Endo, Koga, and Morokuma[66f] reported similar pathways for insertion of ethylene into the Zr−R bond of the $Cp_2Zr(R)Cl$ complex (R = H and CH_3), the so-called hydrozirconation reaction, as shown in Figure 8. In this system, ethylene can attack between the hydride and the chloride ligands, a front-side (FS) insertion pathway (pathway 1), or it can attack from the opposite side of the chloride, a backside (BS) insertion pathway (pathway 2). The FS insertion is found to be more favorable than the BS insertion because of a smaller repulsion between the hydride and the chloride ligand. The calculated activation barrier for the FS pathway of hydrozirconation of ethylene at the RHF and MP2 levels of theory is very small, consistent with the experimental result that the reaction is fast.

More recently, Petitjean et al. have revisited the FS, BS, and stepwise backside (SBS) mechanisms of ethylene polymerization by metallocene catalysts with DFT calculations.[72] Only FS and SBS mechanisms appear to be competitive, and energy barriers in both FS and SBS mechanisms are on the order of 3 kcal/mol, a value which is compatible with the experimental and other theoretical values for similar processes.

Among the early-transition-metal systems, the d^1 and d^2 complexes are quite different from the d^0 ones because the one filled or partly filled d_π orbital can stabilize metal−ligand interactions and facilitate electron transfer during the insertion process.[65,70b] In particular, this orbital can stabilize the metal−olefin bond by back-donation to the π^*_{olefin} orbital as illustrated in Figure 9. Generally, this interaction leads to a much larger olefin association energy than that for d^0 complexes.[75g] The formation of this stronger π complex destabilizes the π^*_{olefin} orbital, which strongly affects the $\pi-\pi^*$ mixing during the new σ_{M-C}

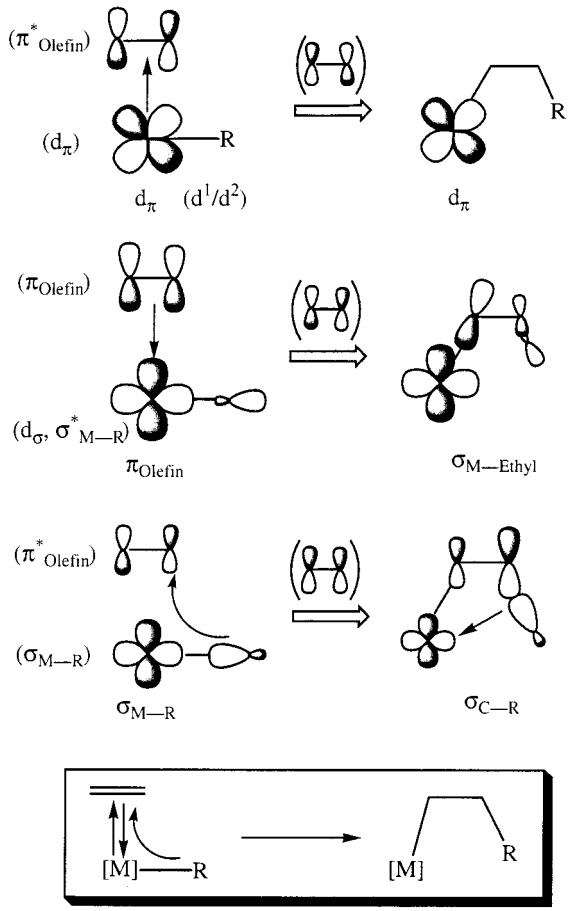

Figure 9. Schematic bonding interactions between d^1 or d^2 metal−alkyl and olefin.

and σ_{C-R} bond formation in the olefin insertion process and usually results in a higher olefin insertion barrier than that for d^0 complexes.[75h]

To compare the reactivity of the d^1/d^2 complexes with the d^0 complexes, Ziegler and co-workers investigated the insertion process of $[L]NbC_2H_5^n + C_2H_4 \rightarrow [L]Nb(butyl)^n$ ($n = 0$ and $+2$; L = NH−$(CH)_2$−NH^{2-}).[75g,h] The olefin association energy for this d^2 system (−49.5 kcal/mol) is much larger than that for d^0 metals due to the donation of high-lying metal d_π electrons into the lower lying olefin π^* orbital. Also, the insertion barrier for the d^2 complex is 46.8 kcal/mol, a value which is nearly 10 times larger than that for the analogous Sc(III) d^0 complex. Similarly, adding an extra electron to $[L]TiC_2H_5(C_2H_4)^+$ (giving $[L]TiC_2H_5(C_2H_4)$; L = $(NH_2)_2^{2-}$) results in an olefin insertion barrier of 22.0 kcal/mol, a value that is 4.8 kcal/mol larger than that for the d^0 parent complex. From these results, Margl, Deng, and Ziegler conclude that d^1 or d^2 complexes will generally not be good olefin insertion catalysts, unless the interfering d electrons can either be stabilized by a ligand orbital so that they are not available to the olefin π^* orbital or be forced to occupy a metal orbital that is orthogonal the olefin π^* orbital. An example of this has been given experimentally by Nakamura et al.,[82] who reported living olefin polymerization with complexes of the type $M(\eta^5\text{-}C_5Me_5)(\eta^5\text{-diene})X_2$ (M = Nb(III) and Ta(III)). In this case, the d electron pair can donate into the empty diene π^* orbital instead of the olefin−polymer π^* orbital.

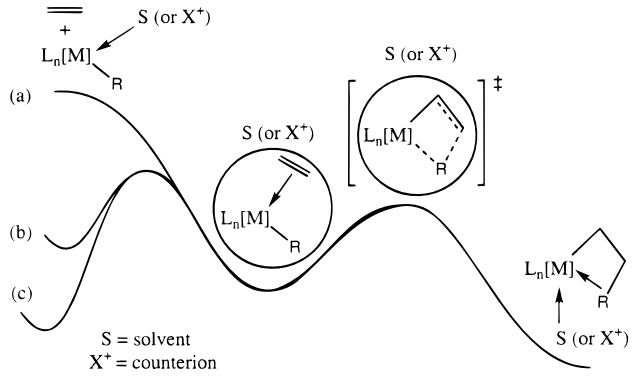

Figure 10. Three possible solution-phase energy profiles for olefin insertion reactions.

Table 8. Energetics, Enthalpy, and Free Energy Changes (kcal/mol) in the Gas Phase[a] and Free Energy Changes in Toluene[b] for Reaction Steps Involving Insertion Reactions (eqs 10, 11, 12, and 13) for the Cp_2ZrR^+ and $(CpCH_2Cp)ZrR^+$ Cataylsts

	Cp_2ZrR^+				$(CpCH_2Cp)ZrR^+$			
	eq 10	eq 11	eq 12	eq 13	eq 10	eq 11	eq 12	eq 13
ΔE^c	−19.8	−9.5	−10.8	−13.8	−21.6	−14.7	−14.7	−16.9
ΔH^c_{298}	−18.1	−7.1	−8.5	−11.3	−20.2	−12.6	−12.8	−15.0
ΔG^c_{298}	−6.7	4.4	5.8	0.8	−9.9	−1.2	−1.0	−3.3
ΔG^c_s	−0.6	5.8	6.9	2.5	0.0	2.3	1.0	2.0
ΔE^r	−8.1	−9.9	−10.0	−4.0	−7.7	−9.7	−8.8	−2.5
ΔH^r_{298}	−6.2	−9.0	−8.9	−3.1	−5.8	−7.1	−7.5	−1.3
ΔG^r_{298}	−3.4	−7.9	−9.0	−2.4	−3.1	−5.3	−6.8	0.5
ΔG^r_s	−3.5	−8.5	−9.4	−1.9	−3.4	−5.8	−6.6	−0.1
$\Delta E^‡$	6.5	3.5	7.2	7.2	7.1	6.0	6.4	9.6
$\Delta H^‡_{298}$	6.6	2.9	7.7	6.9	7.1	5.3	6.7	9.2
$\Delta G^‡_{298}$	7.9	4.5	9.6	9.4	10.1	6.9	9.2	11.7
$\Delta G^‡_s$	7.8	3.2	9.7	10.3	10.2	5.7	9.3	11.2

[a] Using B3LYP hybrid DFT. [b] Calculated by ZSM1.

Recently, Cavallo et al. presented a theoretical study of olefin polymerization with a model for the heterogeneous Ziegler−Natta catalyst, Mg_2Cl_6Ti-(III)−R.[80a] The calculated results show that (i) the olefin association in $eq_{||}$ orientation is exothermic by −7.3 kcal/mol without an energy barrier, (ii) the insertion reaction's overall activation barrier of 6.6−8.6 kcal/mol is facilitated by a weak α-agostic interaction, and (iii) the insertion reaction is exothermic by 25.2−27.6 kcal/mol. In this case, the steric interaction between catalyst and olefin may affect the d electron donation into the olefin π^* orbital.

So far, most discussions on olefin insertion are based on results calculated in the gas phase. In the solution phase, energy profiles obtained in the gas phase should change due to placement of weakly coordinated solvent molecules or counterions. In a previous study,[74] Bierwagen et al. suggested that there should be a barrier for the olefin association step in solution, although calculations of the solvent effects were not performed in this work. The consequences of such a barrier result in three possible solution-phase energy profiles as shown in Figure 10. For scandium, the insertion step is expected to be rate determining since the olefin association step would be endothermic (due to the large reorganization energy, small intrinsic binding energy, and

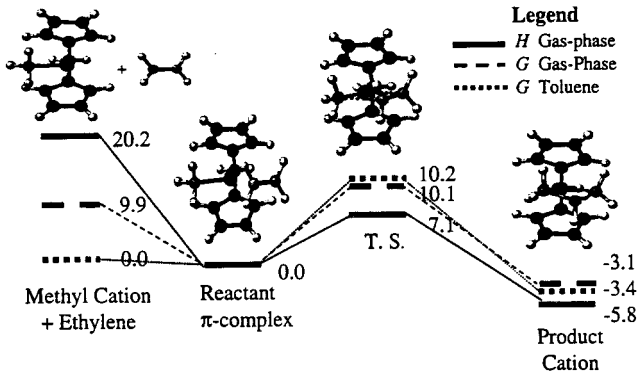

Figure 11. Relative enthalpies (ΔH, kcal/mol) and free energies (ΔG, kcal/mol) in the gas phase (H and G Gas-Phase) and toluene (G Toluene) for the insertion reaction from the reactants to insertion product for $[CpCH_2Cp]ZrCH_3^+ + C_2H_4$. (Reprinted with permission from ref 66i. Copyright 1999 Oxford University Press.)

energy required for solvent displacement) (Figure 10a). For Ti(IV), the association step should be exothermic as illustrated in Figure 10b. In the third situation, the association step with a barrier due to solvent or counterion displacement may be rate determining if the insertion barrier is small enough (Figure 10c).

More recently, Das et al. investigated two structurally distinct zirconocene catalyst systems, Cp_2ZrR^+ and $(CpCH_2Cp)ZrR^+$, in the gas phase using DFT and integrated methods.[66i] The effects of solvation upon the energetics of the various insertion steps were examined by employing continuum and explicit representations of the solvent (toluene). Energy, enthalpy, and free energy changes in the gas phase and in toluene for reaction steps involving insertion reactions, eqs 10, 11, 12, and 13, are summarized in Table 8.

$$L_nZrCH_3^+ + CH_2{=}CH_2 \rightarrow L_nZr\ CH_2CH_2CH_3^+ \quad (10)$$

$$L_nZr\ CH_2CH_2CH_3^+ + CH_2{=}CH_2\ (FS) \rightarrow L_nZr\ CH_2CH_2CH_2CH_2CH_3^+ \quad (11)$$

$$L_nZr\ CH_2CH_2CH_3^+ + CH_2{=}CH_2\ (BS) \rightarrow L_nZr\ CH_2CH_2CH_2CH_2CH_3^+ \quad (12)$$

$$L_nZr\ CH_2CH_2CH_3^+ + CH_2{=}CHCH_3 \rightarrow L_nZr\ CH_2CH(CH_3)CH_2CH_2CH_3^+ \quad (13)$$

Relative enthalpies and free energies for the insertion reaction from the reactants to insertion products are shown in Figure 11. One can see that both entropy and the solvation play a significant role in the initial step of insertion reactions. As expected, a large negative entropy, ΔS, occurs in the olefin association to a metal center. Consideration of the solvation effect of toluene, which effects the energy in the same direction, finally makes the olefin association step endothermic rather than exothermic.

In earlier work,[73] Siegbahn studied the olefin insertion into transition-metal−hydrogen and metal−methyl bonds for the entire sequence of second-row transition-metal atoms at the HF and MCPF levels. The relative energies of the reactants, the olefin π complexes, the transition states, and the insertion products of the insertion reactions A−C, $(H)_nM{-}H + C_2H_4 \rightarrow (H)_nMC_2H_5$ (M = Y, Zr, Nb, Mo, Tc, Ru, Rh, Pd; $n = 0, 1, 2$), are shown in Table 9. Although the results show no relationship between the barrier heights for insertion and the bond strengths of the initial metal hydride or the strength of the π-bonded complexes, repulsion between nonbonding metal electrons and the electrons on the olefin was shown to play a dominant role in the size of the insertion barrier.[73a] In short, the main effect of adding hydride ligands is a general reduction in the size of the insertion barriers because the spectator hydride ligands help to remove the repulsive nonbonding electrons from metal. This result reflects, in part, the hydride ligand's affect on the donation of high-lying metal d_π electrons into the lower-lying olefin π^* orbital. It seems that this effect is especially important for early transition metals, which are electropositive (good donors). Another mechanism to remove the repulsive nonbonding electrons from the metal is sd hybridization. The consequences of metal−ligand repulsion can be seen clearly in Table 9, where a comparison for reaction A between Rh on one hand and Ru and Pd on the other is particularly revealing. Rhodium has a dramatically lower barrier since for rhodium the s^0 state is low lying and the covalent d bond that is required at the transition state can be easily formed. For ruthenium, a substantial promotion energy is required to reach the s^0 state, and for palladium, the s^0 state has a closed d shell that

Table 9. Relative Energies[a] (kcal/mol) of the Reactants, Olefin π Complexes, Transition States, and Insertion Products of Insertion Reactions A−C, $(H)_nM{-}H + C_2H_4 \rightarrow (H)_nMC_2H_5$

metal (M)	π complex	TS (barrier)	product
	$M{-}H + C_2H_4 \rightarrow MC_2H_5$ (Reaction A)		
Y	−15.1	−5.2 (9.9)	−32.2
Zr	−43.3	−11.7 (31.6)	−36.4
Nb	−30.9	−11.7 (19.2)	−29.4
Mo	−10.6	16.1 (26.7)	−29.1
Tc	−33.1	19.5 (52.6)	−30.9
Ru	−21.4	6.7 (28.1)	−26.1
Rh	−27.5	−12.8 (14.7)	−24.9
Pd	−17.8	6.9 (24.7)	−27.0
	$(H)M{-}H + C_2H_4 \rightarrow (H)MC_2H_5$ (Reaction B)		
Y	−25.1	−6.9 (18.2)	−30.5
Zr	−53.3	−3.1 (50.2)	−32.4
Nb	−43.3	−10.7 (32.6)	−33.3
Mo	−18.3	4.3 (22.6)	−31.1
Tc	−13.4	2.4 (15.8)	−28.3
Ru	−18.4	−2.4 (16.0)	−26.4
Rh	−18.0	−0.9 (17.1)	−24.8
Pd	−36.8	−1.4 (35.4)	−25.7
	$(H)_2M{-}H + C_2H_4 \rightarrow (H)_2MC_2H_5$ (Reaction C)		
Y		−7.9	−29.4
Zr	−18.6	−15.9 (2.7)	−33.9
Nb	−40.3	−17.7 (22.6)	−32.2
Mo	−15.6	−6.0 (9.6)	−30.1
Tc	−10.1	−10.1 (0.0)	−27.0
Ru	−5.6	−12.3 (-6.7)	−27.0
Rh		−3.6	−25.7
Pd			

[a] Calculated by MCPF//HF/DZPD.

cannot form any d bonds unless it is promoted to the d^9s state.

Among **late transition metals** there have been observations that some of the d^6 or d^8 metal complexes are active as olefin polymerization catalysts.[83] For example, Bookhart and co-workers have recently developed diimine Ni- and Pd-based d^8 catalyst systems, which give branched polymers with highly desirable strength and processing properties.[84] Generally, the olefin insertion into M−R bonds seems to be kinetically more favorable for the d^0 and d^0f^n early transition metals than for late to middle transition metals.[1−3] The different behaviors observed for the late-transition-metal complexes are attributable to electronic structure differences, some of which have been mentioned above.

For d^0 systems, as shown in Figure 7, the stabilization of the reactant π-olefin complex by metal d_π to olefin π^* back-donation is lacking since the metal d_π orbital is unoccupied.[65,70b] Thus, the electron transfer from the π_{olefin} orbital to the σ^*_{M-R} orbital by olefin $\pi-\pi^*$ mixing, which leads to a new $\sigma_{M-Alkyl}$ bond during the insertion process, is facile. Meanwhile, the low-lying olefin π^* orbital can easily accept the electron pair of the σ_{M-R} bond, which leads to a new σ_{C-R} bond. The better $\pi-\pi^*$ mixing in d^0 systems lowers the energy barrier of the insertion reaction. In the late transition systems, the metal's d_π orbital is occupied so that the π complex, $[M](C_2H_4)R$, is stabilized by metal d_π to olefin π^* back-donation.[65,66b,85] As in the case of d^1 and d^2 systems, the filled d_π orbital is stabilized by the π^*_{olefin} orbital of the olefin as illustrated in Figure 9.[59] In turn, the π^*_{olefin} orbital is destabilized so that it cannot easily serve in the $\pi-\pi^*$ mixing. Generally, the insertion reaction is thermodynamically less favorable for late-transition-metal systems.

In early work,[66b,86] Morokuma and co-workers investigated a series of olefin insertions into the d^6 and d^8 metal−hydride bonds (M = Rh, Ni, Pd, Pt) using the HF method. These studies have been reviewed by Koga and Morokuma.[3a] Recently, Sakaki et al. reported a theoretical study with the MP4SDQ method of olefin insertion into Pt−H and Pt−SiH_3 bonds of the complex $PtH(SiH_3)(PH_3)$.[87a,b] As shown in Scheme 5, the three isomers of $Pt(H)(PH_3)(SiH_3)$, **8**−**10**, coordinate with olefin to form the three π complexes, **11**−**13**, where the olefin is trans to the spectator ligands, hydride (**11**), SiH_3 (**12**), and PH_3 (**13**), respectively. Then, the reactions proceed through the transition states, **14**, **16**, **18**, and **20**, of the insertion process to generate insertion products, **15**, **17**, **19**, and **21**, respectively. The relative energies of intermediates and transition states, **11**−**21**, of olefin insertion into Pt−SiH_3 and Pt−H bonds are shown in Table 10.[87a] In the T-shaped ML_3 fragment, the trans spectator ligand (trans to the vacant position that will be occupied by ethylene) has substantial influence on the metal d_σ orbital (LUMO, which has some s and p) as illustrated in Scheme 6.[85c] The calculations show that with respect to the olefin the *trans*-influence of the ligand becomes stronger in the order $PH_3 \ll H < SiH_3$. The situation for **10** is the worst because the H and SiH_3 ligands, both having strong *trans*-influence, weaken each other's metal−ligand bond. Thus, **10** is less stable than either **8** or **9**. The *trans*-influence of the H, SiH_3, and PH_3 ligands also exerts significant effects on the C_2H_4 insertion into the Pt−H and Pt−SiH_3 bonds. When the H ligand lies at the trans position to olefin, olefin insertion into the Pt−SiH_3 bond is endothermic by 31 kcal/mol with a high activation barrier of 54 kcal/mol. When the SiH_3 ligand lies at the trans position to olefin, olefin insertion into the Pt−H bond is endothermic by 21 kcal/mol with a lower barrier of 21 kcal/mol. When the PH_3 ligand is at the trans

Scheme 5

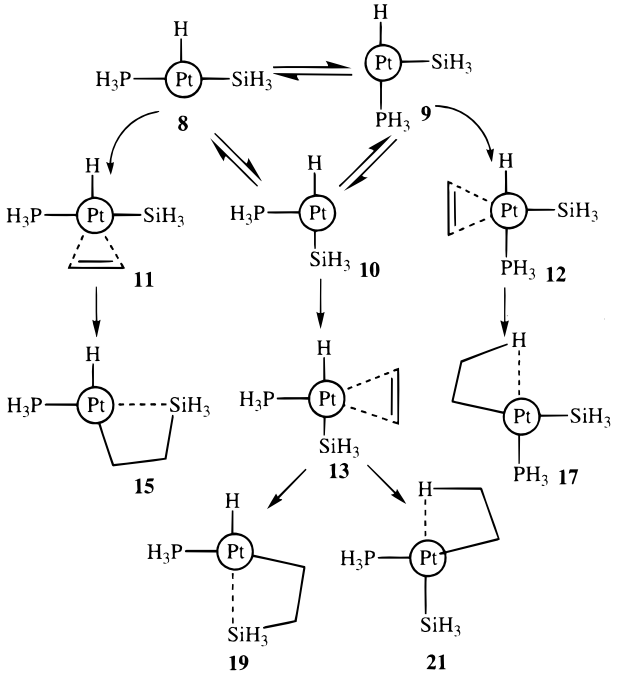

Table 10. Relative Energies (kcal/mol) of Olefin Insertion into Pt−SiH_3 and Pt−H Bonds

complex	HF	MP2	MP3	MP4DQ	MP4SDQ
Olefin Insertion into Pt−H of **11**					
11	0.0	0.0	0.0	0.0	0.0
14	20.1	19.7	18.6	20.3	20.6
15	20.1	20.0	19.7	20.5	20.8
Olefin Insertion into Pt−SiH_3 of **12**					
12	0.0	0.0	0.0	0.0	0.0
16	45.9	54.9	50.2	53.4	53.9
17	21.7	31.3	27.0	29.8	30.5
Olefin Insertion into Pt−SiH_3 of **13**					
13	0.0	0.0	0.0	0.0	0.0
18	17.8	16.2	15.0	16.2	16.3
19	−6.3	2.4	−2.0	−0.2	0.6
Olefin Insertion into Pt−H of **13**					
13	0.0	0.0	0.0	0.0	0.0
20	5.1	4.0	4.6	4.6	4.4
21	−21.6	−19.7	−19.4	−18.6	−18.4

Scheme 6

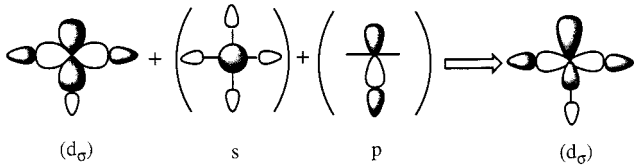

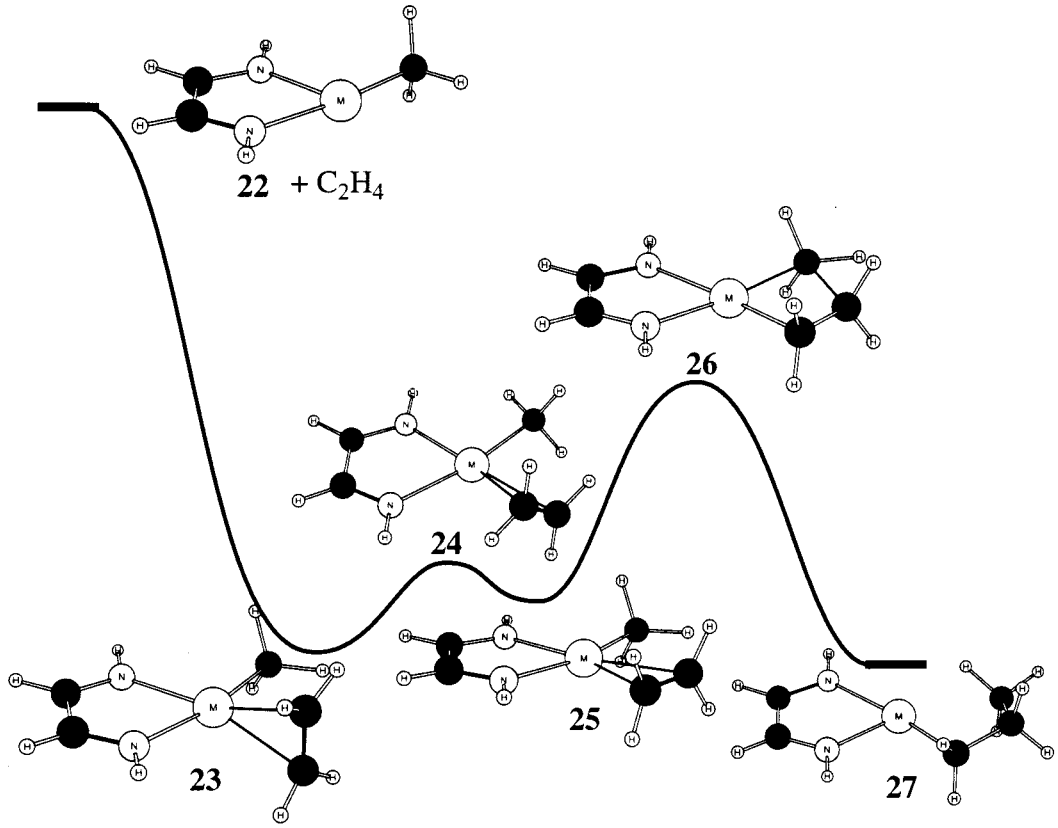

Figure 12. Relative potential energy profiles from reactants (**22**) to products (**27**) for ethylene insertion into the M−CH_3 bond of to the diimine complex.

position to olefin, olefin insertion has much lower barriers, 16 kcal/mol for the Pt−SiH_3 bond and only 4.4 kcal/mol for the Pt−H bond. Thus, olefin insertion into the Pt−H bond is favored over insertion into the Pt−SiH_3 bond and the *trans*-influence of the spectator ligands is an important factor in the insertion barrier.

In a more recent study, Coussens and co-workers investigated the insertion of propene into the Pt−H bond of the cationic $Pt(PR_3)_2(H)^+$ complexes (R = H, F, CH_3) with both B3PW91 and traditional ab initio (HF, MP2, QCISD) methods.[88] In general, insertion and β-hydrogen-transfer barriers tend to be small. In comparison to the B3PW91 calculations, the HF method overestimates all barriers while the MP2 method is generally in better agreement. Which method, MP2 or B3PW91, should be considered to be the most reliable is difficult to assess. For relative stabilities, higher level calculations at the QCISD level of theory as well as available experimental data strongly suggest that the B3PW91 method is more reliable than the MP2 method. Insertion barriers are found to be 2.4−3.6 kcal/mol for R = H, 0.7−2.2 kcal/mol for R = CH_3, and 0.5−1.0 kcal/mol for R = F. Thus, even though the differences are small, the clear trend of decreasing insertion barriers is in the order PH_3 > PMe_3 > PF_3.

More recently, focusing on catalytic properties of the late-transition-metal complexes, Morokuma, Ziegler, Siegbahn, Hall, Rösch, and co-workers studied d^8 metal-catalyzed olefin polymerization.[59,89−92] As shown in Figure 12, the olefin insertion proceeds from reactants (the metal−methyl complex, **22**, and ethylene) through the π complexes (**23** and **25**), olefin rotation transition state (**24**), and insertion transition state (**26**) to generate the γ-agostic palladium−propyl complexes (**27**). The calculated relative energetic parameters at different levels of theory are summarized in Table 11. As seen from Figure 12 and Table 11, the rate-determining step of these reactions is the migratory insertion of the olefin into a metal−alkyl bond, as it was for the early-metal complexes. Generally, upon going from Ni to Pd to Pt, the olefin coordination energy to $[L_2M(CH_3)]^+$ increases while the stability of transition state **26** relative to the reactants does not change much. As a result, the insertion barrier from π complex **23** to **27** increases in the order Ni < Pd < Pt. This order is consistent with the well-known increase in the M−L binding energy, Ni < Pd < Pt, which has been explained in terms of electronic and size effects.[93,94] Thus, one may conclude that the catalytic activity of the d^8 M(II) complexes will decrease as Ni > Pd > Pt, in agreement with experiment.[84a] On the other hand, compared to the diimine complex,[91a] the potential energy surface of the diamine complex rises slightly because of the diimine's greater trans influence.[59] This trans influence is especially important in the π complex and insertion transition state.

Very recently, Hall and co-workers investigated the olefin and acetylene insertion reactions of the higher oxidation state Ir(III) system, $CpIr(PH_3)(CH_3)^+$.[95] Because of strong back-donation, the optimized geometry of the π complex shows strong covalent bond character between the olefin and the metal. Thus, the reaction has a large olefin association energy of

Table 11. Calculated Relative Energetic Parameters (kcal/mol) of Olefin Insertion into the Metal−Methyl Bond

metal	L_2	23	24	25	26	27	ref
			Olefin Insertion into M−CH_3				
Ni	NH=CHCH=NH	−27.9		−21.6	−18.0	−33.3	89a,d
Ni	NH=CHCH=NH	−35.3	−29.3	−30.6	−24.2	−38.4	90a
Ni	NAr=CMeCMe=NAr	−20.4			−16.6	−30.4	89e
Ni	NH=CHCH=NH	−27.0			−16.8	−38.5	91b
Pd	NH=CHCH=NH	−31.7		−26.1	−15.5	−31.8	89a,c
Pd	NAr=CMeCMe=NAr	−29.8			−15.7	−33.6	89e
Pd	NH=CHCH=NH	−31.7	−26.6	−26.8	−15.5	−31.8	89c,d
Pd	NH=CHCH=NH	−33.9	−28.9	−29.3	−17.6	−33.9	89c
Pd	NH=CHCH=NH	−29.8			−13.4	−36.8	91b
Pd		−43.9			−25.6	−40.8	91a
Pd	$(NH_3)_2$	−27.3			−9.3	−34.8	91a
Pd	NH=CHCH=NH	−29.8			−13.4	−36.8	91a
Pd	NH=CHCH=NH	−31.8	−26.6	−27.1	−15.5	−31.6	59
Pt	NH=CHCH=NH	−43.6			−18.3		89d
Pt	NH=CHCH=NH	−41.5			−16.0	−38.9	91b
			Olefin Insertion into M−Aryl				
Pd	$(NCH_2)_2$	−5.3		−4.8	+6.2	−15.1	92
Pd	$(NCH_2)_2^+$	−19.5		−19.4	−11.2	−34.8	92

32 kcal/mol, which leads to a high activation barrier of about 33 kcal/mol for the insertion of the olefin. In similar work, Han, Deng, and Ziegler reported studies of the insertion of olefin into the M−H and M−CH_3 bonds in $CpM(PH_3)(CH_2CH_2)R^+$ (R = H, CH_3; M = Co, Rh, Ir).[96] Relative to the π complex, the olefin insertion into the M−H bond is slightly exothermic for Co (ΔH_e = −3.4 kcal/mol) and Rh (ΔH_e = −1.0 kcal/mol) but endothermic for Ir (ΔH_e = 3.7 kcal/mol). The corresponding reaction barriers for this insertion are 0.3 (Co), 2.7 (Rh), and 6.1 kcal/mol (Ir). Furthermore, the olefin insertion into the M−CH_3 bond is exothermic for Co (ΔH_e = −12.7 kcal/mol), Rh (ΔH_e = −8.5 kcal/mol), and Ir (ΔH_e = −5.3 kcal/mol) in comparison to the π complex. The corresponding reaction barriers for this insertion are 15.2 (Co), 19.8 (Rh), and 23.2 kcal/mol (Ir). Thus, the insertion reaction becomes kinetically and thermodynamically less favorable down the triad. On the other hand, hydride migration is kinetically more favorable as the spherically symmetric 1s orbital is better able to stabilize the transition state than the directional p orbital of the methyl group.

B. Acetylene Insertions

Acetylene insertion reactions and metathesis reactions have been reported. Even multiple-insertion products of relevance to alkyne oligomerization and polymerization are known.[97] For early transition metals, many 14-e$^-$ d^0 complexes have been found and characterized as the products of the insertion reactions of bulky alkyne with $Cp_2MCH_3^+$ (M = Ti, Zr).[98] For late transition metals, the alkyne insertion reaction has been postulated for the primary step in the metal-catalyzed dimerization of alkynes.[99] Because of the similarity in the electronic structure of olefins and alkynes, the alkyne insertion is also believed to proceed by the Cossee mechanism for the olefin polymerization.[64,65,70b] However, alkynes should have different reactivity because they have lower lying occupied π orbitals and higher lying unoccupied π^* orbitals than olefins. In Table 12, we have summarized the calculated energetic parameters involved in the acetylene insertion process from recent theoretical studies.

Table 12. Calculated Energetic Parameters (kcal/mol) Involved in the Acetylene Insertion Process[a]

complex	method	ΔE_1[b]	ΔE_2[c]	ΔE_3[b]	ref
Cl_2ScH	GVB-CI//RHF	−20.2	6.9	−45.2	100
Cl_2ZrH^+	RHF	−43.9	0.2	−79.3	70b
	MP2//RHF	−51.6	0.2	−86.9	70b
$Cl_2ZrCH_3^+$	RHF	−38.2	10.1	−55.3	70b
	MP2//RHF	−41.5	5.1	−53.3	70b
$CuCH_3$	RHF	−11.1	46.6	−34.4	101
	MP2//RHF	−17.1	45.4		101
$TpRu(PH_3)H$	B3LYP	0.0[c]	9.0[c]	−16.3[c]	102
$Tp'Ru(PH_3)H$	B3LYP	0.0[c]	9.6[c]	−11.0[c]	102
$Tp'Ru(PH_3)(CCH)$	B3LYP	0.0[c]	22.1[c]	−11.7[c]	102
	CCSD//B3LYP	0.0[c]	30.9[c]	−12.1[c]	102
$CpIr(PH_3)CH_3^+$	B3LYP	−28.0	24.8	−45.5	95
	CCSD//B3LYP	−32.6	30.6	−35.9	95
$Pd(Cl)(NH_3)CH_3$	SCF	0.0[c]	20.5[c]	−26.0[c]	103
	CAS-SCF	0.0[c]	22.6[c]	−19.3[c]	103
	CI	0.0[c]	17.1[c]	−22.4[c]	103
$PtH(PH_3)(SiH_3)$	MP2	0.0[c]	14.3[c]	−16.5	87c
	MP4SDQ	0.0[c]	12.8[c]	−21.4	87c
$PtSiH_3(PH_3)(H)$	MP2	0.0[c]	23.8[c]	−6.7	87c
	MP4SDQ	0.0[c]	20.9[c]	−11.7	87c

[a] ΔE_1, ΔE_2, and ΔE_3 are the acetylene association energy, activation barrier, and reaction energy, respectively. [b] Energy is given relative to the reactants. [c] Energy is given relative to the π complex.

Using all-electron HF and MP2 methods, Hyla-Kryspin, Niu, and Gleiter investigated acetylene insertion reactions with the model compounds Cl_2ZrH^+ and $Cl_2ZrCH_3^+$.[70b] Although the Zr−H bond is stronger than the Zr−CH_3 bond, insertion of acetylene into the Zr−H bond of Cl_2ZrH^+ occurs more easily than that into the Zr−CH_3 bond of $Cl_2ZrCH_3^+$. The insertion process is calculated to have a barrier from the π complex of 0.2 and 5.1 kcal/mol, respectively, and to be exothermic with respect to the reactants by 86.9 and 53.3 kcal/mol, respectively. A major reason for this difference is the sphericity of the hydride orbital compared to the directionality of the methyl orbital, but both steric effects and the overall exothermicity play roles. The large exothermicities suggest that the insertion reaction of acetylene into both Zr−H and Zr−CH_3 bonds of Cl_2ZrH^+

and $Cl_2ZrCH_3^+$ should be irreversible, a result which agrees with experimental observations.

In a comparison of the relative reactivity of acetylene vs olefin, Zakharov et al. calculated the intermediates, transition states, and products for the insertion reaction of acetylene and olefin with $H_2Ti(III)CH_3$ using the HF method.[104] They found that the reactivity decreases in the order $C_2H_2 > C_2H_4 > C_3H_6$. Because the d_π orbital of $H_2Ti(III)CH_3$ is occupied, the energy of the π and π^* orbital of monomers parallels their relative reactivity in the insertion reaction.

Endo, Koga, and Morokuma also investigated the insertion of acetylene into the Zr−R bond of the $Cp_2Zr(R)Cl$ complex (R = H and CH_3), a reaction known as hydrozirconation of acetylene.[66f] As in the hydrozirconation of olefins, acetylene could attack between the hydride and the chloride ligands, a frontside (FS) insertion pathway (pathway 1), or it could attack from the opposite side of the chloride, a backside (BS) insertion pathway (pathway 2). The FS insertion is found to be more favorable than the BS insertion because of a smaller repulsion between the hydride and the chloride ligand. The calculated activation barriers are low for the FS pathway of hydrozirconation of both ethylene and acetylene at the HF and MP2 levels of theory. In a comparison, hydrozirconation is thermodynamically more favorable and kinetically less favorable for acetylene. These results seem to disagree with the experimental ones, which show that hydrozirconation is much faster for alkynes than for alkenes. However, steric repulsion between the Cp ligands and the substituted alkene or alkyne used in the experiment could account for the differences since one would expect the activation energy for the reaction of substituted alkenes to be higher than that for substituted alkynes.

As in olefin insertion, acetylene insertion into the M−R bond of a late-transition-metal complex has a higher barrier than that for an early-transition-metal complex (Table 12). Recently, Hall and co-workers studied several insertion reactions of acetylene into the M−H, M−CH_3, and M−acetylide bonds using DFT and CCSD methods.[95,102] In comparison to the olefin insertion reaction, the insertion reactions of acetylene with $CpIr(PH_3)R^+$ are more exothermic with lower activation barriers because of the weaker back-donating interaction between acetylene and the metal center in the π complex and the stronger π-bonding interaction between the vinyl ligand and the metal center in the Ir vinyl complex.

More recently, Sakaki and co-workers investigated acetylene insertion into Pt(II)−H and Pt(II)−SiH_3 bonds of $PtH(SiH_3)(PH_3)$ using RHF, MP2, and MP4SDQ methods.[87c] They found that the insertion into Pt−H was predicted to proceed with a smaller activation energy (12.8 kcal/mol) than that into Pt−SiH_3 (20.9 kcal/mol). The reaction energy (ΔE) of the insertion into Pt−H is exothermic by 21.4 kcal/mol, 10 kcal/mol smaller than that for insertion into Pt−SiH_3, which reflects differences in bond energies between C−H and C−Si and between Pt−H and Pt−SiH_3. In their study, de Vaal and Dedieu[103] found that the C_2H_2 insertion reaction into the Pd−CH_3 bond is quite exothermic by about 22 kcal/mol with an energy barrier of 17 kcal/mol. Thus, as seen from Table 12, the insertion of C_2H_2 is a feasible process, quite exothermic and with a moderate energy barrier.[95,103]

C. Carbonyl Insertions

Carbonyl migratory insertion into a M−R bond is a critical step in many transition-metal-catalyzed carbon−carbon bond-forming processes, such as hydroformylation and olefin/CO copolymerization reactions.[83,84,105] There have been numerous experimental and theoretical studies of the classical reaction, eq 14.[106−113]

$$Mn(CO)_5CH_3 + CO \rightarrow Mn(CO)_5(C(O)CH_3) \quad (14)$$

The previous theoretical work, which varies from extended Hückel calculations[107,108] through other approximate calculations[109,110] to ab initio, configuration-interaction studies,[111−113] has been reviewed by Koga and Morokuma.[3a] The notable conclusions of these studies on the migratory-insertion reaction are that (i) for middle to late transition metals, the CH_3 ligand migrates to a bound CO followed by the added CO filling the vacant coordination site to generate an η^1-M−acyl complex and the reaction is endothermic with a moderate energy barrier; (ii) for early transition metals, the reaction is exothermic because the bonding interaction between the lone pair of formyl oxygen and empty d orbital stabilizes the η^2-coordination; (iii) for the M−H bond, the insertion is more difficult than for a M−CH_3 bond because the M−H bond is stronger; and (iv) for third-row late transition metals, insertion is less favorable than for second-row late metals because the M−C bonds for third-row late transition metals are stronger.

The generally accepted mechanism for the migratory insertion of CO into an M−R bond involves a three-center transition state.[107−113] For late transition metals, as the methyl group migrates, the carbonyl group bends and the occupied σ_{M-R} orbital donates density to the vacant π^-_i(CO) orbital, which leads to a new σ_{M-acyl} bond as illustrated in Figure 13. Meanwhile, the occupied σ_{M-CO} orbital interacts with the vacant σ^*_{M-R} orbital to form a new σ_{C-C} bond and the in-plane π^+_i(CO) orbital becomes a lone pair at the oxygen atom.[59] Although there is mixing among all these orbitals, the three-center CO insertion is somewhat different than the four-center olefin insertion. Although the alkyl group attacks the CO as a nucleophile, the CO's carbon passes this density on to form the new σ_{M-acyl} bond not the new σ_{C-C}, which seems to arise mainly from the CO lone pair (σ_{M-CO}). Better $\sigma_{M-R}-\sigma^*_{M-R}$ mixing lowers the energy barrier of the insertion reaction. The electron transfer from the σ_{M-R} orbital to the high-lying π^-_i(CO) orbital costs some energy due to the loss of the strong back-donating interaction between the CO and the metal center.

For early transition metals, the CO insertion into an M−R bond is quite different since there is no back-donating interaction between the CO and the metal center. In the early stage of the CO insertion, the

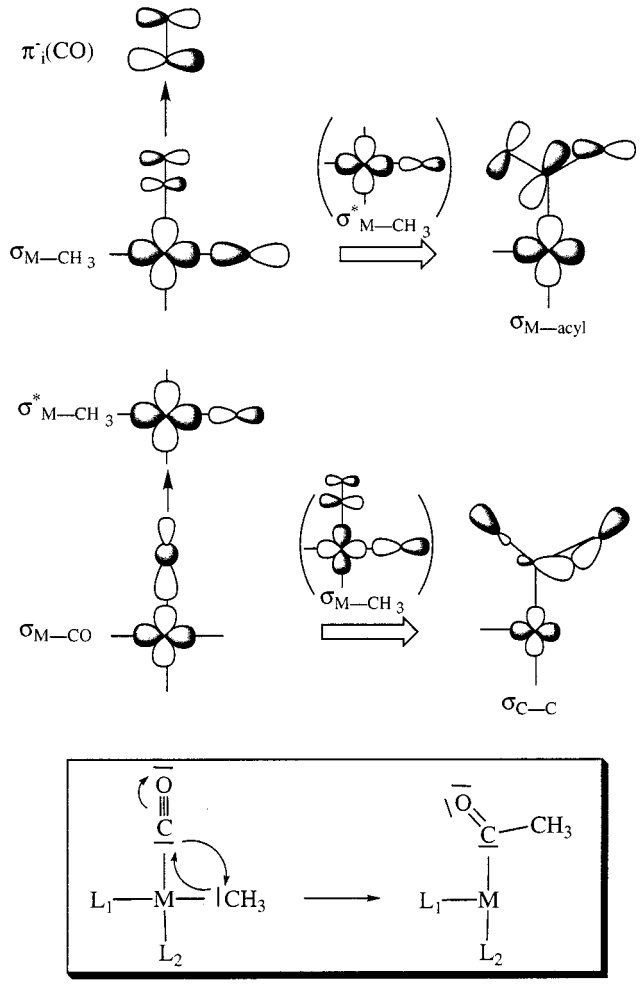

Figure 13. Schematic bonding interactions between metal–alkyl and CO.

electron-transfer process for the early transition metals is similar to that for the late transition metals but then becomes more like the olefin insertion later in the reaction. The occupied σ_{M-R} orbital interacts with the vacant π^{-}_{i}(CO) orbital, but this interaction now forms the new σ_{C-C} bond. Then the occupied CO lone pair (at the carbon atom) interacts with the vacant σ^{*}_{M-R} orbital to form a new σ_{M-acyl} bond and the in-plane π^{+}_{i}(CO) orbital becomes a lone pair at the oxygen atom.[113] As the carbonyl group inserts and bends, a stable η^2-acyl complex is ultimately formed as shown in Figure 14. Although the electronic rearrangement is quite analogous to that seen previously for the olefin insertion into an early-transition-metal M–R bond, there is no extra stabilizing interaction like the β-agostic interaction to lower the activation energy at the three-centered transition state. Generally, CO insertion into the M–R bond occurs with a higher barrier than that for the olefin insertion reaction.

In earlier work,[114] Siegbahn and co-workers studied CO insertion into transition-metal–hydrogen and metal–methyl bonds for the entire sequence of second-row transition-metal atoms, M–R + CO → MR(CO) → M–C(O)R (M = Y, Zr, Nb, Mo, Tc, Ru, Rh, Pd; R = H, CH_3), at the HF and MCPF levels. The energies of the MR(CO) complexes, the transition states, and the insertion products, relative to the

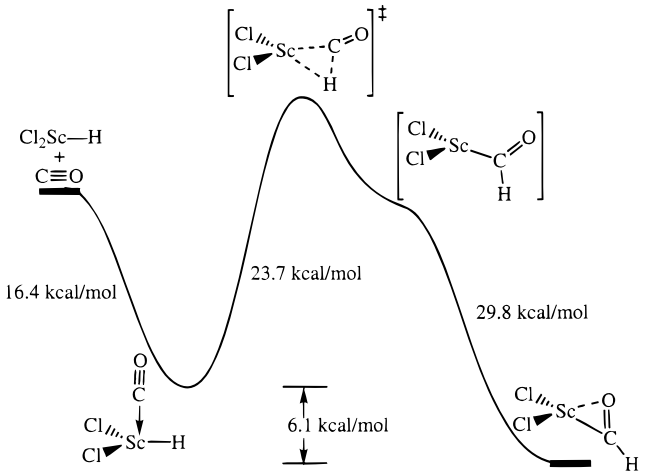

Figure 14. Reaction energy diagram for insertion of CO into the Sc–H σ bond of Cl_2ScH.

Table 13. Relative Energies (kcal/mol) of the Reactants, CO-Associated Complexes, Transition States, and Insertion Products of Insertion Reactions D–E, MR(CO) → M–C(O)R

metal (M)	associated complex	TS (barrier)	product
	M–H + CO → MC(O)H (Reaction D)		
Y	−3.4	−1.8 (1.6)	−16.4
Zr	−21.3	−13.6 (7.7)	−21.3
Nb	−25.0	−19.1 (5.9)	−14.6
Mo	−16.3	13.9 (30.2)	−0.2
Tc	−24.0	7.8 (31.8)	−2.4
Ru	−34.5	−3.0 (31.5)	0.6
Rh	−34.9	−19.7 (15.2)	−5.3
Pd	−17.9	7.7 (25.6)	−4.9
	M–CH_3 + CO → MC(CO)CH_3 (Reaction E)		
Y	−1.5	14.9 (16.4)	−15.4
Zr	−20.2	11.2 (31.4)	−14.8
Nb	−25.5	2.7 (28.2)	−16.8
Mo	−16.8	21.9 (38.7)	−3.0
Tc	−21.3	16.7 (38.0)	−2.5
Ru	−31.9	3.2 (35.1)	−5.6
Rh	−34.9	−12.0 (22.9)	−10.8
Pd	−19.7	13.5 (33.2)	−10.9

reactants, are given in Table 13. From experimental work, the gas-phase exothermicity of carbonyl insertion into the M–methyl bond is estimated to be about 10 kcal/mol. Compared to this expected value, one can see that the calculated exothermicities are (i) about 5 kcal/mol larger for the early transition metals due to η^2-complex formation, (ii) about 7–8 kcal/mol smaller for the middle transition metals due to a repulsive interaction between the oxygen lone pair and occupied 4d orbitals, and (iii) close to 10 kcal/mol for late transition metals due to formation of sd hybrids, which reduces the repulsion with the oxygen lone pair. The usual preference for CO insertion into the M–C bonds over M–H bonds is not apparent in the results of Siegbahn and co-workers.

Recently, Morokuma and co-workers reported a theoretical study on catalytic hydroformylation by $RhH(CO)(PH_3)_2$ at the MP2 level.[115a] The calculations show that in the reaction cycle the active intermediate, $RhH(CO)_2(PH_3)$, forms by CO–phosphine exchange, then the steps are olefin insertion, CO insertion, H_2 oxidative addition, and aldehyde reductive elimination. The CO insertion into the Rh–Et bond is the rate-determining step, which is endo-

Table 14. Calculated Relative Energetic Parameters[a] (kcal/mol) of CO Insertion into the M−Alkyl and M−Acyl Bonds

metal	L_2	**28**	**29**	**30**	ref
	CO Insertion into M−Alkyl				
Ni	NH=CHCH=NH	−39.6	−29.8 (9.8)[b]	−45.2	89a
Pd	NH=CHCH=NH	−41.1	−26.1 (15.0)	−32.7	89a
Pd	$PH_2CH=CHPH_2$	−60.9	−49.5 (11.4)	−56.4	90e
Pd	NH=CHCH=NH	−41.4	−26.3 (15.1)	−34.4	59
	CO Insertion into M−Acyl				
Ni	NH=CHCH=NH	−64.6	−39.7 (24.9)	−57.5	89a
Pd	NH=CHCH=NH	−67.4	−39.2 (28.2)	−51.9	89a
Pd	$PH_2CH=CHPH_2$	−82.5	−56.4 (26.1)	−63.3	90e
Pd	NH=CHCH=NH	−68.3	−39.3 (29.0)	−52.2	59

[a] Energy is given relative to the reactants, L_2MCH_3, 2CO, and C_2H_4. [b] Activation energy barrier relative to the CO-associated complex.

thermic by 14.2 kcal/mol with a moderate barrier of 26.1 kcal/mol. Overall, the reaction is exothermic.

In a combined experimental and theoretical study, Markies et al. investigated the CO insertion processes in the cationic model system $[Pd(CH_3)(NH_3)_3]^+ + CO$ and the neutral system $[Pd(CH_3)_2(NH_3)_2] + CO$ by ab initio calculations at the RHF, MP2//RHF, and CASSCF+CI//RHF levels.[115b] They found that the carbonylation reaction follows a hybrid pathway, i.e., a concerted replacement of NH_3 by CO followed by migratory insertion of CO into the Pd−H bond instead of a purely dissociative or associative mechanism. For both the neutral and the cationic systems, the rate-determining step is the migratory insertion, where the insertion barriers are 23.8 and 24.3 kcal/mol, respectively. The insertion process is enhanced by coordination of the dissociated amine and is slightly more favorable in neutral systems. Together with the low-energy replacement of NH_3 by CO, these results suggest that in both systems the rate of carbonyl insertion should be independent of the applied CO pressure.

More recently, Morokuma, Ziegler, Hall, and co-workers investigated the late-transition-metal-catalyzed olefin/CO copolymerization reaction.[59,89,90] In Table 14, we have summarized the calculated energetic parameters involved in the CO insertion process from these theoretical studies. The calculations show that relative to the CO-associated complex, the CO insertion into the M−alkyl bond from the associated complex **28** through the insertion TS **29** to the metal−acyl complex **30** is exothermic for Ni (ΔH_e = −5.6 kcal/mol) but endothermic for Pd (ΔH_e = 4.5−8.4 kcal/mol). The corresponding barrier for insertion (from **28** to **29**) is about 9.8−15.1 kcal/mol. However, the CO insertion into the M−acyl bond is endothermic for both Ni and Pd with higher barriers. The unfavorability of CO insertion into an M−acyl bonds arises from the lack of a stabilizing interaction like the β-agostic interaction to lower the activation energy at the three-centered transition state.

Employing nonlocal DFT and MP2 methods, a similar carbonylation system, $Pd(PH_3)(CH_3)(N-O) + CO \rightarrow Pd(PH_3)(COCH_3)(N-O)$ (N−O = $NHCHCOO^-$), has been studied by Yates and co-workers.[61b−d] After the exchange of CO for PH_3, four possible mechanisms were investigated. Of these four mechanisms,

Scheme 7

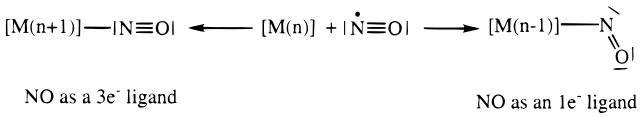

the rate-determining methyl migration step was found to be lowest in energy when proceeding from a novel five-coordinate intermediate in which the palladium−nitrogen bond is weakened.

In a combined experimental and theoretical study on CO/olefin insertions into Pd−C bonds of complexes containing flexible and rigid terdentate nitrogen ligands,[115c] Vrieze and co-workers found that the overall reaction is exothermic by 37.8 kcal/mol with two low-energy insertion barriers of 11.5 and 7.4 kcal/mol for the CO and olefin insertion steps, respectively, at the MP2 level. The calculations, which indicate that even rigid terdentate nitrogen ligands may coordinate in a bidentate fashion, are fully supported by the experimentally observed bidentate nitrogen coordination of both flexible and rigid terdentate nitrogen ligands in alkylpalladium complexes obtained after norbornadiene insertion and by the kinetic study of this insertion reaction.

A recently submitted paper by Cao, Niu, and Hall reports results on the oxidative acceleration of CO insertion into the $Fe-CH_3$ of $CpFe(CO)_2CH_3$ (reaction 15).[116] The calculated activation energies are 17.8 and

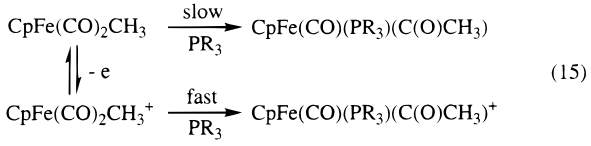

(15)

7.5 kcal/mol for the neutral and the cation reactions, respectively. In the neutral reaction, the methyl groups migrated as an anion, but in the cation reaction, the methyl group has considerable radical character induced by the Fe radical.

D. Nitric Oxide Insertions

Nitric oxide migratory insertion is an important reaction in metal nitrosyl complexes and biochemical reactions.[117−119] In contrast to the migratory-insertion reaction of CO into the metal−carbon bond, experimental and theoretical investigations on the migratory-insertion reaction of NO into the metal−carbon bond are more limited.

As distinct from CO, nitric oxide is a more versatile ligand; it can function as either a 3-e$^-$ or 1-e$^-$ ligand. Thus, it can accommodate a variation in the electronic structure of the coordinated metal center as shown in Scheme 7, and this variation can directly change the reactivity of the complex. As discussed earlier, it is well-known that bent NO plays an important role in providing a low-energy path in substitution reactions.[52,120] Although several experimental groups have suggested an intermolecular insertion process for the nitrosyl insertion,[121,122] Weiner and Bergman[123] show that an intramolecular

Scheme 8

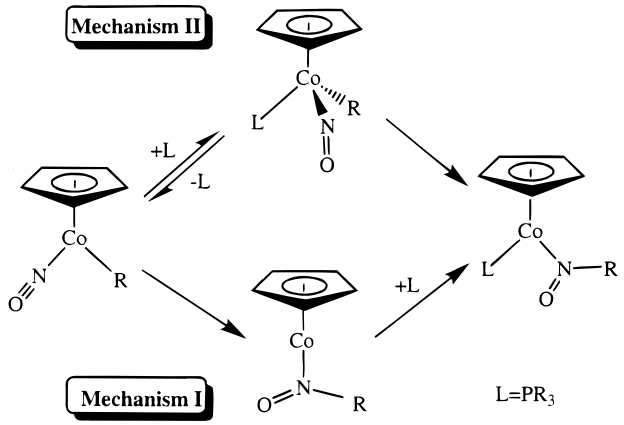

insertion process is operative in the insertion reaction of NO into the Co−CH_3 bond of reaction 16.

$$CpCo(NO)(CH_3) + PPh_3 \rightarrow CpCo(PPh_3)(N(O)CH_3) \quad (16)$$

Their labeling experiments and kinetic measurements suggest that this system proceeds through methyl migration followed by phosphine addition as illustrated in the bottom of Scheme 8.

Recently, Niu and Hall investigated this migratory-insertion reaction with and without phosphine association (Scheme 8) using the DFT (geometry) and CCSD (energy) methods.[24] As shown in Figure 15, the insertion without PH_3 (mechanism I) occurs with an activation energy of 10−20 kcal/mol and the intermediate, $CpCoN(O)CH_3$ (**3**), forms with an endothermicity of 8−17 kcal/mol at the B3LYP and CCSD levels of theory. The overall reaction to the product, $CpCoN(O)CH_3(PH_3)$ (**4b**), was exothermic by 10 to 16 kcal/mol depending on the level of theory. However, as illustrated in Figure 16, an alternative mechanism (mechanism II) begins with PH_3 association and NO bending, which is endothermic by 16−18 kcal/mol, and is immediately followed by a NO insertion barrier of 19−34 kcal/mol. Therefore, mechanism I is the favored pathway. These results are in very good agreement with the kinetic experiments of Weiner and Bergman. The difference between mechanism I and mechanism II can be explained in terms of the electronic structures of the reactant, transition state, and insertion product. Although the Co center plays a dual, electron acceptor and donor, role in the migratory insertion for both mechanisms I and II as shown in Figures 17 and 18, the actual electron-transfer process is different. Along mechanism I (Figure 17), it is very easy to transfer electron density from the original σ_{Co-C} orbital to the NO antibonding orbital (π^-_i(NO)) to form the new σ_{Co-N} bond due to the metal center remaining d^8. The better acceptor and donor character of the metal center results in lower activation energy. Obviously, this mechanism is similar to that of the CO insertion process. In contrast, for mechanism II (Figure 18), the original σ_{Co-C} orbital must rise higher in energy before it can transfer electron density to the NO antibonding orbital (π^-_o(NO)) to form the d_σ orbital of the product as it cycles from a d^8 ($18e^-$) complex at **1** to a d^6 ($18e^-$) intermediate (**34**) and back to a d^8 ($18e^-$) complex at **4b**, a cycle which requires a greater activation energy. In addition, a stable η^2-intermediate, **33**, where the O of NO coordinates to Co rather than an agostic C−H as found in **3**, could be involved in mechanism I. Although **33** is more stable by 7 kcal/mol than **3**, the insertion followed by PH_3 addition to form **4a** is favorable over the nitrosol group movement to **33** because of a higher barrier.

V. Hydrogen Transfer

Hydrogen-transfer reactions by transition-metal complexes are now well-recognized fundamental steps

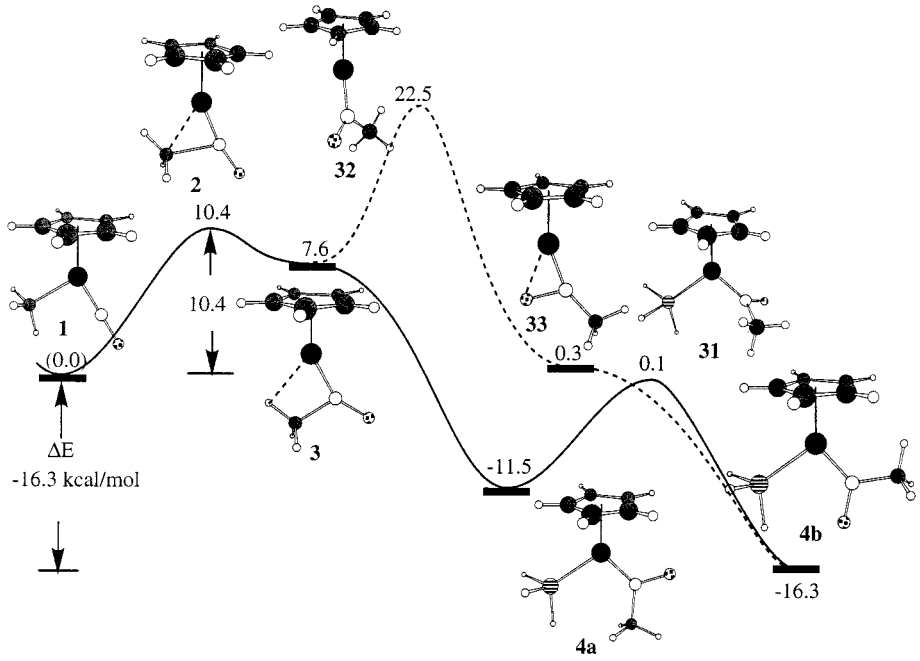

Figure 15. Profiles of the B3LYP potential energy surfaces for the NO insertion into Co−CH_3 along mechanism I.

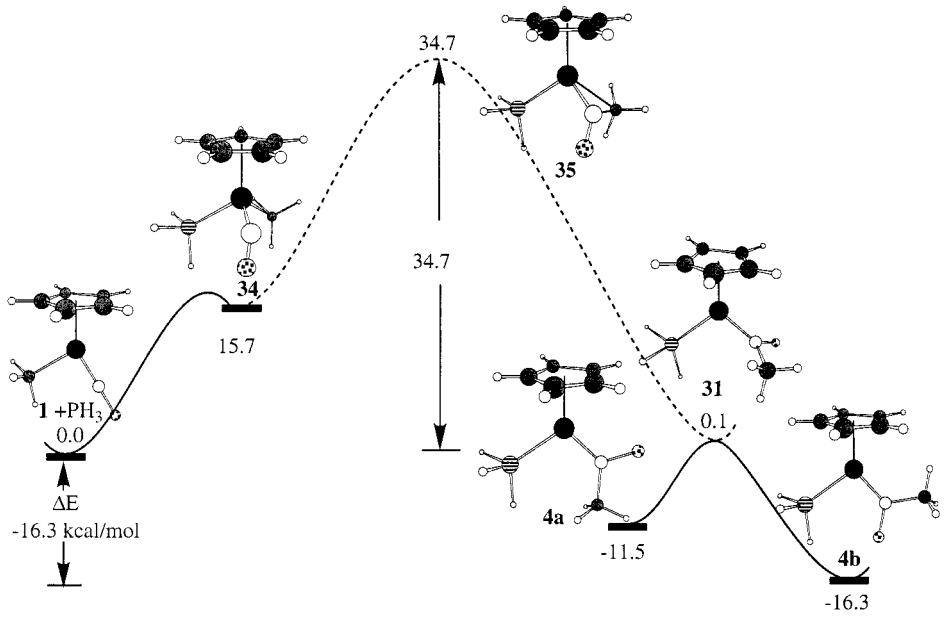

Figure 16. Profiles of the B3LYP potential energy surfaces for the NO insertion into Co−CH_3 along mechanism II.

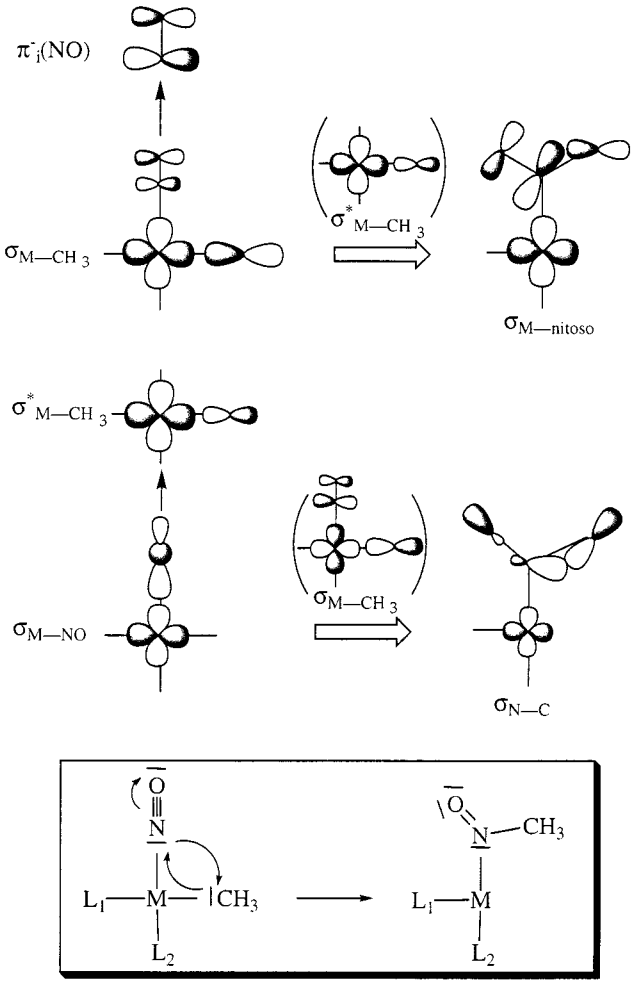

Figure 17. Schematic bonding interactions between Co−methyl and NO−CH_3 along mechanism I.

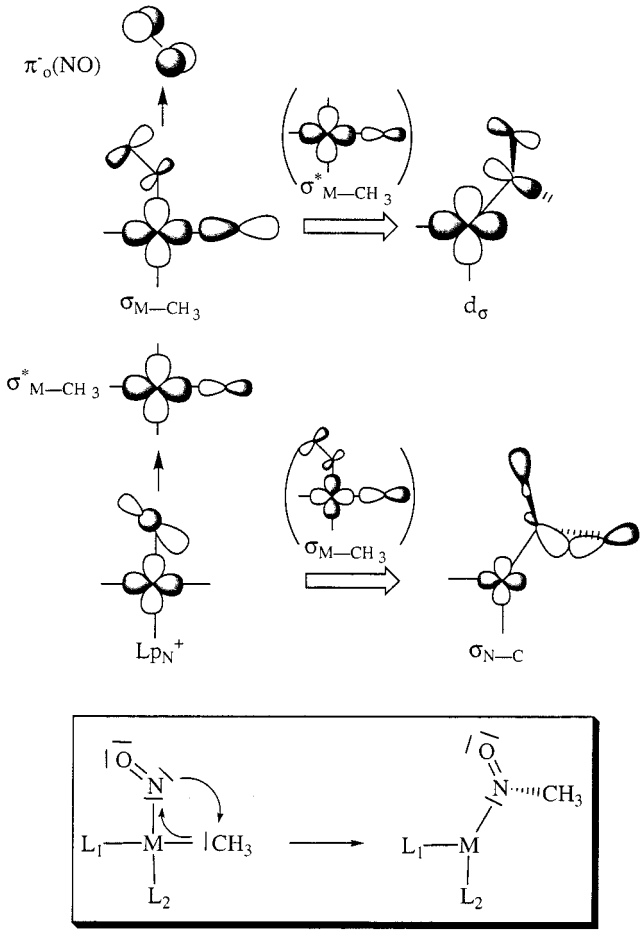

Figure 18. Schematic bonding interactions between Co−methyl and NO−CH_3 along mechanism II.

in several important catalytic cycles.[1] β-hydrogen-transfer, hydrogen-exchange, oxidative-addition, reductive-elimination, metathesis, and nucleophilic addition reactions can be regarded as several of the elementary reactions in hydrogen transfer. Recent experimental and theoretical studies show that the activation of X−H (X = H, CH_3, SiH_3, OH, etc.) bonds by homogeneous transition-metal complexes involve one of these processes.[1,3] Insight into the reactivity involved in metal-mediated hydrogen-transfer reactions will prove essential for the rational design of new catalysts for industrial production and practical hydrogen-storage systems.

A. β-Hydrogen Transfer

β-Hydrogen transfer is an important step in the chain termination of olefin polymerization and in the dehydrogenation of alkanes to alkenes.[1,63] In this reaction, which can be thought of as the reverse of insertion reactions, the metal−alkyl or −alkenyl complexes undergo β-H transfer to form a M−olefin or M−acetylene π complex. For early transition metals, this transformation is generally endothermic because the strong M−C and C−H bonds vanish while only a strong M−H bond and a weak π complexation form. For late-transition-metal alkyl complexes, the β-H transfer is generally much easier than that for early-transition-metal complexes due to the strong π complexation and the strong M−H bond formation. The agostic interaction can also lower the activation barrier of the β-H-transfer reaction for both early and late transition metals. However, weak metal−olefin and metal−hydride bonding interactions in the β-H-transfer transition state lead to higher barriers.

Paralleling their studies of chain propagation of olefin polymerization,[75g,h] Margl, Deng, and Ziegler presented a systematic investigation of chain termination processes for a number of d^0 [L]M−R^n fragments (M = Sc(III), Y(III), La(III), Ti(IV), Zr(IV), Hf(IV), Ce(IV), Th(IV), and V(V); L = $NH-(CH)_2-NH^{2-}$, $N(BH_2)-(CH)_2-(BH_2)N^{2-}$, $O-(CH)_3-O^-$, Cp_2^{2-}, $NH-Si(H)_2-C_5H_4^{2-}$, $[(oxo)(O-(CH)_3-O)]^{3-}$, $(NH_2)_2^{2-}$, $(OH)_2^{2-}$, $(CH3)_2^{2-}$, $NH-(CH_2)_3-NH^{2-}$, $O-(CH_2)_3-O^{2-}$, and DPZ; R = H, CH_3, and C_2H_5; $n = 0, +1$, and $+2$).[124] The calculations for group 3 and group 4 metals show that steric congestion around the metal center seems to influence strongly the β-H-transfer barrier. For large metal ions, the barrier can be lowered by increasing the steric bulk because the crowding destabilizes the metal alkyl complex relative to the metal hydrido olefin complex. For very small metal ions, adding steric bulk can increase the barrier since the π-complexation energy of the transition state vanishes for highly congested systems. They also found that the metal hydrido olefin complexes are usually 4.8−7.2 kcal/mol more stable than the β-H-transfer TS, except for Hf, which tends to have a very stable product (below the energy of the β-H-transfer TS by −12.0 kcal/mol). Overall, the barrier heights in [L]$MC_2H_5^n$ ($n = 0$ and $+1$) seem to follow the order of β-agostic bond strength: Ti ≈ Zr > Hf and Sc ≈ Y ≥ La.

In their studies of the mechanism of the ethylene polymerization reaction with homogeneous silyene-bridged metallocenes, $H_2SiCp_2MCH_3^+$ (M = Ti, Zr, and Hf),[66g] Yoshida, Koga, and Morokuma also investigated chain termination processes at the HF (for geometry optimization), MP2, MP3, MP4, and QCISD levels of theory. As shown in Table 15, the chain termination from **36** through the β-H transfer and olefin elimination to **39** is very endothermic: 52.8 (Ti), 45.6 (Zr), and 48.5 (Hf) kcal/mol, and hence, it is an unfavorable pathway. On the basis of the calculated results in the gas phase, Yoshida et al. suggested that the rapid olefin polymerization, where Hf is the best of these cationic catalysts, results in high-molecular-weight polymer.

Table 15. Calculated Relative Energetic Parameters (kcal/mol) of the β-H-Transfer Reactions of $H_2SiCp_2MCH_2CH_2CH_3^+$ (M = Ti, Zr, Hf) to $H_2SiCp_2MH^+$ and C_3H_7

method	β-agostic complex (**36**)	TS (**37**)	π complex (**38**)	[M]−H (**39**) + product
		$H_2SiCp_2TiCH_2CH_2CH_3^+$		
RHF	0.0	18.9	18.2	42.3
RMP2	0.0	18.6	20.9	61.6
RMP3	0.0	19.7	19.9	52.6
RMP4SDQ	0.0	18.0	18.8	57.7
QCISD	0.0	18.0	18.0	52.8
		$H_2SiCp_2ZrCH_2CH_2CH_3^+$		
RHF	0.0	16.3	10.5	36.0
RMP2	0.0	13.7	12.7	51.6
RMP3	0.0	14.8	12.0	47.4
RMP4SDQ	0.0	14.1	11.1	46.7
QCISD	0.0	13.9	10.9	45.6
		$H_2SiCp_2HfCH_2CH_2CH_3^+$		
RHF	0.0	17.0	10.9	36.8
RMP2	0.0	15.0	13.2	54.7
RMP3	0.0	15.7	12.3	50.0
RMP4SDQ	0.0	15.2	11.9	49.6
QCISD	0.0	15.0	11.6	48.5

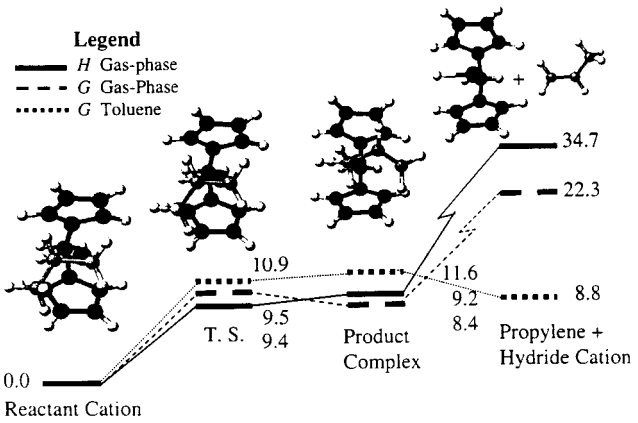

Figure 19. Relative enthalpies (Δ*H*, kcal/mol) and free energies (Δ*G*, kcal/mol) in the gas phase (*H* and *G* Gas-Phase) and toluene (*G* Toluene) for the β-H transfer from the β-agostic $(CpCH_2Cp)ZrCH_2CH_2CH_3^+$ reactant to the β-H-transfer products, $(CpCH_2Cp)ZrH^+$ and a free propene. (Reprinted with permission from ref 66i. Copyright 1999 Oxford University Press.)

However, this performance may change in the solution phase. Using DFT methods, Das et al. examined the effects of solvation upon the energetics of the chain termination processes employing continuum and explicit representations of the solvent (toluene).[66i] Relative enthalpies and free energies for the β-H transfer from the β-agostic $(CpCH_2Cp)ZrCH_2CH_2CH_3^+$ reactant to the β-H-transfer products, $(CpCH_2Cp)ZrH^+$ and a free propene, are shown in Figure 19. Although solvation effects on the transition-state free energy of the β-H-transfer step are nearly the same as they are on the reactant, solvation reduces the free energy change for the separation (dissociation) into products by approximately 16 kcal/mol. Thus, in the solution phase, chain termination through β-H transfer is a thermodynamically possible pathway in olefin polymerization and the rate-determining step could be the β-H transfer instead of olefin elimination. However, the barriers for olefin−solvent exchange have not been calculated.

Table 16. Calculated Relative Energetic Parameters (kcal/mol) of the β-H-Transfer Reactions of Late-Transition-Metal Complexes

metal	L_2	R	**36**	**37**	**38**	**39**	ref
Ni	NH=CHCH=NH	C_3H_7	0.0	*a*	13.6	52.2	89d
	NH=CHCH=NH	C_3H_7	0.0		11.0		91b
	NH=CHCH=NH	C_4H_9	0.0	*a*	8.9		91b
	NAr=CMeCMe=NAr[b]	C_3H_7	0.0		14.5	56.2	89e
	NAr=CMeCMe=NAr	C_3H_7	0.0		15.4	48.0	89e
Pd	$(NH_3)_2$	C_3H_7	0.0	5.4	3.7		91a
	$(NH_3)_2$	C_4H_9	0.0	7.7	4.0		91a
	NH=CHCH=NH	C_3H_7	0.0	5.0	4.8		91a
	NH=CHCH=NH	C_3H_7	0.0	5.9	5.4	47.3	89d
	NH=CHCH=NH	C_3H_7	0.0		4.8		91b
	NH=CHCH=NH	C_4H_9	0.0	5.0	3.6		91b
	NH=CHCH=NH[c]	C_4H_9	0.0	5.9	5.4	41.9	89c
	NH=CHCH=NH[d]	C_4H_9	0.0	5.2	5.0	43.9	89c
	NAr=CMeCMe=NAr[b]	C_3H_7	0.0		0.2	43.8	89e
	NAr=CMeCMe=NAr	C_3H_7	0.0		−1.2	35.1	89e
Pt	NH=CHCH=NH	C_3H_7	0.0		−8.9		91b
Ir	(Cp)(PH_3)	C_2H_5	0.0	0.7	−12.2	28.6	125
	(PCP′)	C_2H_5	0.0	3.6	−10.2	12.2	125

[a] No transition state. [b] MO//IMOMM. [c] BSI of ref 89c. [d] BSII of ref 89c.

Focused on the catalytic properties of the late-transition-metal complexes, Morokuma, Ziegler, Siegbahn, Hall, and co-workers have studied several hydrogen-transfer processes along the β-H-transfer pathway for the d^6 and d^8 complexes.[89−91,95,125] The calculated relative energies at different levels of theory for β-agostic complex (**36**), β-H-transfer transition state (**37**), π complex (**38**), and metal−hydride product (**39**) are summarized in Table 16. The calculations show that β-H transfer from the β-agostic complex is more facile for a late-transition-metal complex than it is for an early-transition-metal complex. Although the olefin elimination (dissociation) from the π complex is about 20−40 kcal/mol endothermic, the β-H-transfer step has a low activation barrier of 1−15 kcal/mol. For third-row transition metals, Pt and Ir, the β-H-transfer step is exothermic by 10 kcal/mol (Tables 10 and 16). The origin of the differences between second- and third-row transition metals has been attributed to relativistic effects[18] which stabilize the $(n + 1)$s orbitals and destabilize the *n*d orbitals more for the heavier third-row transition metals. Thus, the higher energy d orbitals stabilize the π complex and the β-H-transfer transition state by contributing to a stronger back-donating interaction. However, as discussed above, the *trans*-influence of the spectator ligand also plays an important role in the β-H-transfer step. Thus, facile β-H transfer is also responsible for branching in the palladium-catalyzed polymerization of olefin and for the deuterium exchange reaction of olefin.

In comparison to the β-H transfer of metal−alkyl complexes, the β-H transfer of metal−alkenyl complexes usually has a higher activation barrier due to the stronger M−C and C−H bonds. A study by Endo, Koga, and Morokuma shows that the β-H-transfer barrier of $Cp_2Zr(Cl)C_2H_3$ is about 13 kcal/mol higher than that of $Cp_2Zr(Cl)C_2H_5$.[66f] From calculations on a model system, Hyla-Kryspin, Niu, and Gleiter suggest that $(Cl)_2ZrC_2H_3^+$ cannot reversibly form a hydride−acetylene complex due to a very high β-H-transfer barrier.[70] In a recent publication, Niu et al. investigated the β-H-transfer process of CpIr(vinyl)$^+$.[95] In the CpIr(vinyl)$^+$ complex, the expected β-agostic interaction is missing and is replaced by a stronger π-back-bonding interaction between the vinyl ligand and the metal center. This effect leads to very different behavior for CpIr(vinyl)$^+$ where the β-H-transfer process is kinetically and thermodynamically unfavorable compared to that in CpIr(ethyl)$^+$.

B. Hydrogen Exchange

Hydrogen-exchange reactions between the alkyl and olefin fragments in the metal−alkyl−olefin complex are another possible chain isomerization and termination mechanism in metal-catalyzed olefin polymerization and olefin/CO copolymerization processes.[84] As shown in Scheme 9, in addition to β-H transfer, hydrogen transfer from the β-agostic alkyl ligand to the olefin ligand can proceed via either a metathesis-like transition state (direct transfer) or a five-coordinate oxidative-addition-like intermediate (indirect or metal-mediated transfer).

In early work using the MP2 method,[126] Lin et al. investigated the hydrogen-exchange mechanism for the β-agostic ethylene complex of cyclopentadienyl rhodium. NMR spectroscopic studies suggested that several Rh and Co agostic ethyl species **40** are in rapid equilibrium with the olefin−hydride species **42**. By NMR spectroscopy, the lowest energy process, which has a ΔG value <7 kcal/mol for both Co and Rh complexes, involves a scrambling of hydrogens that could be explained by a rapid equilibrium between a β-agostic complex (**40**) and an olefin−hydride intermediate (**42**).[127] The calculations show that the four-coordinate mirror-symmetric olefin−hydride species (**42**) is an intermediate (3.4 kcal/mol higher in energy than the β-agostic complex) rather than a transition state (∼5 kcal/mol) in the interconversion process of the two enantiomeric forms as illustrated in Figure 20. Since a stronger M−H−C agostic interaction produces a weaker C−H bond, the initial step (β-H transfer) will have a lower activation barrier for Rh. This argument is supported by the experimentally observed interconversion process, where the activation energy for Rh and Co complexes is reported to be 3.7 and 7.2 kcal/mol, respectively.

This process, a β-transfer step followed by a hydrogen migration, has also been found in studies of ethylene oligomerization and polymerization by organometallic catalysts (M = Ni, Pd).[89−91,128] The calculated results of Fan et al. show that chain termination by β-hydrogen-transfer olefin elimination is energetically unfavorable (44.7 kcal/mol).[128] Instead, β-hydrogen transfer to the incoming ethylene unit, a hydrogen-exchange process, seems to be operative. As shown in Table 17, the reaction proceeds along the metal-mediated mechanism from β-agostic complex (**36**) and a free olefin through the π complex (**40**) and intermediate (**42**) to a new π complex (**44**). The β-H-transfer and hydrogen-migration barriers for the H-exchange reaction are 6.5 and 8.3 kcal/mol, while the olefin insertion into the Ni−R bond has a barrier of 5.7 kcal/mol. Experimentally, Keim and co-workers have identified a hydride

Scheme 9

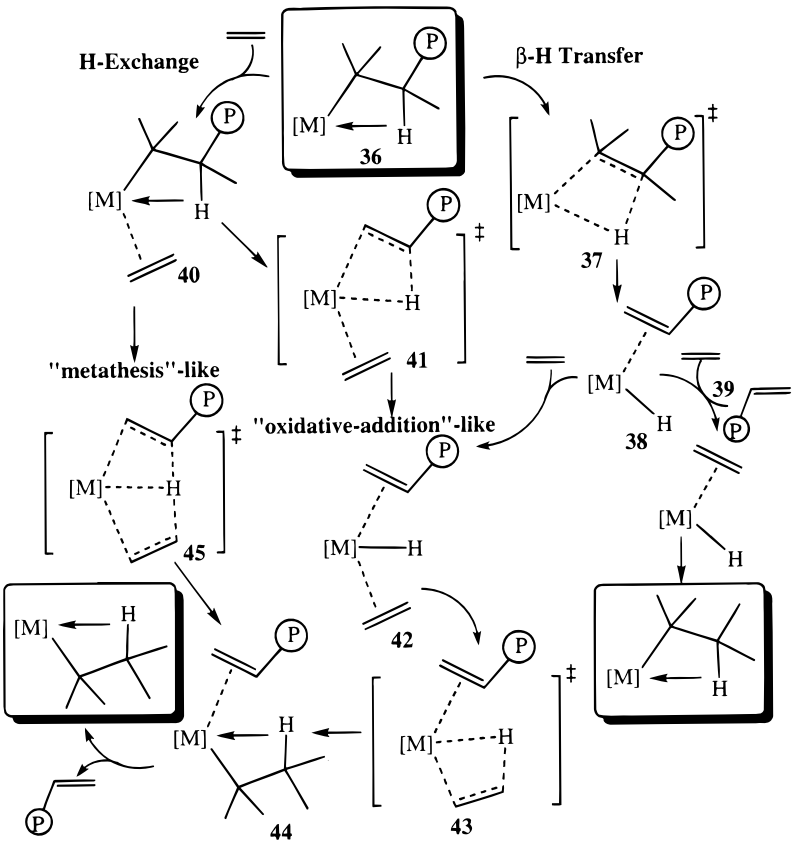

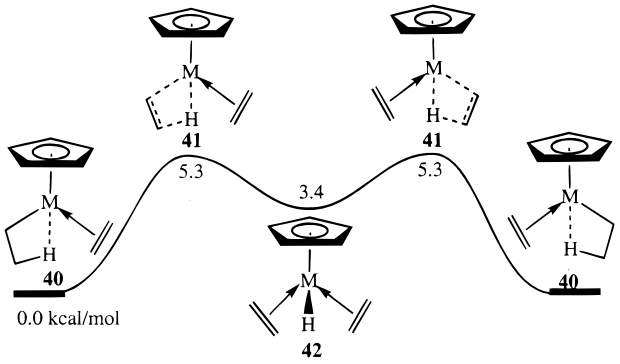

Figure 20. Hydrogen transfer along hydrogen-exchange mechanism involving a five-coordinated intermediate for $CpM(C_2H_5)(C_2H_4)$.

system in the oligomerization mixture. Fan et al. suggest that this hydride complex might be the olefin−hydride intermediate rather than the (acac)-NiH species.[129]

From Scheme 9, one can see that the olefin−hydride intermediate **42** might be formed via two different pathways: (i) ethylene association followed by the β-H transfer (**36** → **40** → **41** → **42**) or (ii) β-H transfer followed by ethylene association (**36** → **37** → **38** → **42**). Musaev et al. have investigated the chain termination via the latter pathway for the diimine−metal-catalyzed (M = Ni, Pd) ethylene polymerization reaction.[89f] In this case, the β-H transfer has a lower barrier before ethylene association, **36** to **38** (Table 16), than after it, **40** to **42** (Table 17). Along the H-exchange pathway, **36** → **37** → **38** → **42** → **43** → **44**, the calculated results of Musaev et al. show that (i) the rate-determining step of the hydrogen-exchange process is the β-H transfer (**36** to **38**) for M = Ni and the incoming ethylene insertion (**42** to **44**) for M = Pd, which have barriers of 14−15 and 7.5 kcal/mol, respectively, (ii) the H-exchange chain termination mechanism is the most favorable chain termination process for the unsubstituted diimine−M-catalyzed ethylene polymerization reaction, and (iii) it occurs more easily for Pd than for Ni.

For the same catalytic system, Deng et al. examined the role of the bulky ligands in Ni(II) diimine-catalyzed ethylene polymerization with a combined quantum mechanical (DFT) and molecular mechanical (QM/MM) model.[90b] Unlike the H-exchange process for the pure QM model, no discernible intermediate hydride−olefin complex (**42**) could be located for the QM/MM model. Thus, in the QM/MM calculation, the β-hydrogen is transferred directly from the alkyl chain to the incoming monomer in a mechanism similar to a metathesis reaction. The QM/MM H-exchange barriers of ~19 kcal/mol for chain termination are roughly double those of their pure QM counterparts. Thus, the substituents on the diimine ligand play an important role in destabilizing the H-exchange transition state for chain termination. It has been observed experimentally that if the diimine methyl groups are replaced by hydrogen atoms, the molecular weight of the polymer decreases dramatically from 8.1×10^5 to 2.8×10^5 g/mol.[84a]

In studies of the chain termination mechanism for the diimine−metal-catalyzed (M = Ni, Pd) ethylene polymerization reaction,[89c,d] Musaev et al. also in-

Table 17. Calculated Relative Energetic Parameters[a] (kcal/mol) of H-Exchange Reactions via "Oxidative-Addition"-Like Pathway of Late-Transition-Metal Complexes

metal	L_2	**40**	**41**	**42**	**43**	**44**	ref
Ni	O=CHCHCH=O	−1.8	4.7	−3.6	4.7	−1.8	128a
	NH=CHCH=NH	−19.4	−9.7	−10.9	−9.2	−20.1	90a
	NH=CHCH=NH	−11.6	8.0	5.8	8.1	−16.6	89f
	NAr=CMeCMe=NAr	−13.3	5.8			−14.9	90b
Pd	NH=CHCH=NH	−18.0	8.7	1.1	8.5	−22.6	89f
	NH=CHCH=NH	−16.3	8.0	3.8			91b
Rh	(Cp)	0.0[b]	5.3	3.4	5.3	0.0	126

[a] Relative to the β-agostic complex and free ethylene. [b] Relative to ethylene π complex.

vestigated the H-exchange process along the direct pathway. They found that the H-exchange process between the alkyl and olefin fragments on the olefin-associated metal−alkyl complex (**40**) via this pathway is inefficient as a chain termination process due to very high activation barriers, 41−47 kcal/mol, from **40** through **45** to **44**. In comparison, the metal-mediated pathway for the H-exchange process seems more favorable. However, this conclusion apparently does not hold true for early transition-metal systems.

In investigations of chain termination processes for a number of d^0 [L]M−R^n fragments (M = Sc(III), Y(III), La(III), Ti(IV), Zr(IV), Hf(IV), Ce(IV), Th(IV), and V(V); L = $NH-(CH)_2-NH^{2-}$, $N(BH_2)-(CH)_2-(BH_2)N^{2-}$, $O-(CH)_3-O^-$, Cp_2^{2-}, $NH-Si(H)_2-C_5H_4^{2-}$, $[(oxo)(O-(CH)_3-O)]^{3-}$, $(NH_2)_2^{2-}$, $(OH)_2^{2-}$, $(CH3)_2^{2-}$, $NH-(CH_2)_3-NH^{2-}$, $O-(CH_2)_3-O^{2-}$, and DPZ; R = H, CH_3, and C_2H_5; n = 0, +1, and +2),[124] Margl, Deng, and Ziegler also studied the direct pathway, where β-hydrogen transfer proceeds from the β-agostic front-side (FS) π complex through a pseudo-mirror-symmetric transition state as shown in **45** of Scheme 9. From Table 18, one can see several systematic trends: (i) the β-H-exchange barrier is always lower than the β-H-transfer barrier, (ii) the β-H-exchange barriers of the group-3 d^0 systems are slightly higher than those of group 4, (iii) for both the group-3 and -4 triads, the barrier increases when going from lighter metals to heavier metals, and (iv) steric congestion around the metal center tends to increase the β-H-exchange barriers. Since the β-H-exchange barriers show little dependence on the metal, the steric encumbrance imposed by bulky spectator ligands, as shown in Scheme 10, is an efficient method for lowering insertion barriers and simultaneously increasing the β-H-exchange barrier for early-transition-metal d^0 catalysts.

Table 18. Barriers (kcal/mol) for the Chain Termination Processes "β-H Exchange" and "β-H Transfer" for the d^0 Early-Transition-Metal Complexes

metal	spectator ligand [L][a]	termination barrier	
		β-H exchange[b]	β-H transfer[c]
Sc(III)	[1]-exo	9.32	15.06
	[2]	13.86	26.29
	[3]	10.04	17.93
	[4]	9.80	16.73
	[5]	8.84	18.40
Y(III)	[1]-exo	9.80	16.49
	[3]	10.99	16.73
	[4]	10.52	17.21
	[5]	9.80	18.16
La(III)	[1]-exo	11.23	18.16
	[3]	12.19	20.08
	[4]	11.47	20.08
	[5]	12.67	21.51
Ti(III)	[1]-exo	7.41	19.60
	[2]	8.37	33.70
	[3]	7.17	14.10
	[4]	7.17	16.01
	[5]	3.35	18.64
Zr(III)	[1]-exo	8.37	17.45
	[2]	7.17	10.76
	[3]	8.37	16.25
	[4]	8.60	16.49
	[5]	7.89	16.97
Hf(III)	[1]-exo	9.08	19.84
	[2]	8.60	10.28
	[3]	9.56	23.90
	[4]	9.56	24.38
	[5]	9.56	26.53

[a] [1] = $NH-(CH)_2-NH^{2-}$, [2] = Cp_2^{2-}, [3] = $(NH_2)_2^{2-}$, [4] = $(OH)_2^{2-}$, [5] = $(CH3)_2^{2-}$. [b] Relative to the π complex [L]$MC_2H_5(C_2H_4)^{n+}$. [c] Relative to the agostic precusor [L]$MC_3H_7^{n+}$.

Scheme 10

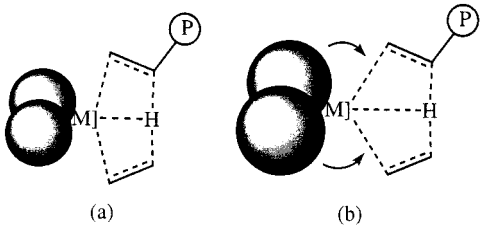

"metathesis"-like H-exchange transition state

C. Oxidative Addition and Reductive Elimination

Oxidative-addition and reductive-elimination reactions (reaction 17) are among the most important fundamental steps in metal-centered reactions of inorganic and organometallic complexes.[1−3]

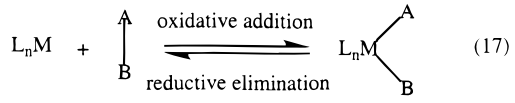

(17)

In the former reaction, a single A−B bond is activated by oxidative addition to a transition-metal center, and in the reverse, a new compound is produced by the reductive elimination, which couples ligands A and B. In catalytic hydrogenation, dehydrogenation, and hydroformylation, the generally accepted mechanism involves the concerted addition of H_2 and RH to form metal hydride complexes. There have been numerous experimental and theoretical studies on these processes.[1−3] In general, the hydrogen transfer from H_2 and RH to the metal center via oxidative

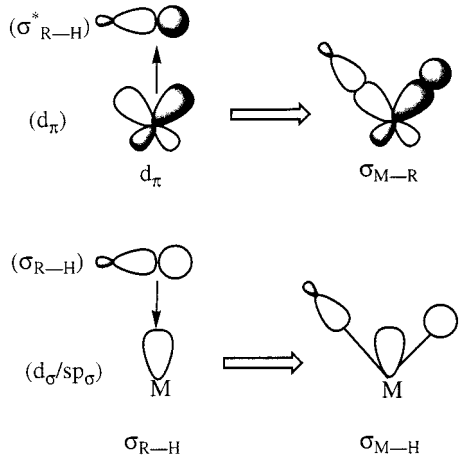

Figure 21. Schematic bonding interactions for RH oxidative addition to metal complex.

Scheme 11

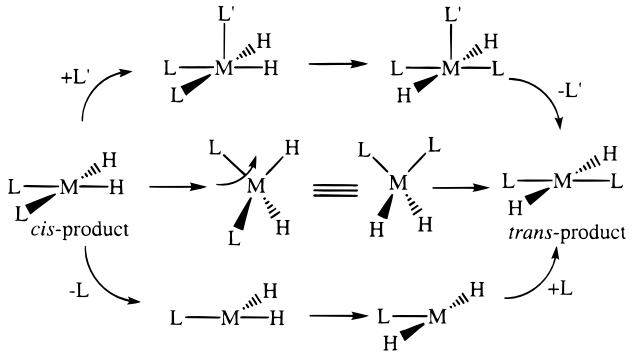

addition occurs through a three-center transition state. As illustrated in Figure 21, there is an interaction between the filled σ_{R-H} orbital of RH and the empty σ-type orbital (d_σ or sp_σ) of the metal, leading to electron donation from RH to the metal center. There is a second interaction between the filled d_π orbital of metal and the σ^*_{R-H} orbital, leading to electron transfer from the metal to the ligand. Thus, we can expect that strong back-donation will lead to fission of the H−H or R−H bond and the generation of the metal hydride complex.

The oxidative addition of H_2 to **d^{10} ML_2 complexes** has been observed for the case of $Pt(PR_3)_2$ complexes, in which most d^8 $L_2Pt(H)_2$ complexes are found in the trans geometry except where the ligands, L_2, are chelating diphosphine groups.[130] However, for the complex with trimethylphosphine ligands ($L = PMe_3$), both cis and trans $Pt(PMe_3)_2(H)_2$ species are in equilibrium in solution.[130d] In contrast to these experimental facts, the concerted H_2 trans addition to ML_2 with a d^{10} configuration is unfavorable under thermal conditions while the coplanar H_2 cis addition is more favorable.[85c] In general, there are at least three alternative paths that could be involved in a cis−trans isomerization process as illustrated in Scheme 11. Since the cis to trans interconversion via a tetrahedron is symmetry-forbidden under thermal conditions, it should be a high-energy process. Thus, dissociative and associative paths represent the most viable alternatives. In addition, due to the much stronger M−SiR_3 and M−H bond strengths (60 kcal/mol) compared to M−CR_3 bond strengths (30 kcal/mol), the reductive-elimination process has been observed more frequently in metal−alkyl complexes than the oxidative-addition process.[131]

Table 19. Energy of Reaction (ΔE)[a] and Activation Energy ($\Delta E^{\ddagger}$)[b] (kcal/mol) of R−H Oxidative Addition to d^{10} Species (R = H, CH_3, SiH_3)

[M]	activated molecule	activation barrier $\Delta E^{\ddagger}$	reaction energy ΔE	ref
Ni(^{1}D)	H−H	2.0	−9.0	133a,b
Pd	H−H	5.2	3.6	132b
$Pd(PH_3)_2$	H−H	uphill	22	132
Pt	H−H	downhill	−33.6	132b
$Pt(PH_3)_2$	H−H	2.3	−15.9	132b
	H−H	7.3	−27.0	134a
	H−H	16.6	−5.0	135a
	H−H	9.2	−10.9	135c
	H−H	3.8	−16.4	134c
$Pt(PMe_3)_2$	H−H	3.8	−16.6	134c
$Pt(PPh_3)_2$	H−H	1.3	−18.2	134c
$Pt(P(t\text{-}Bu)_3)_2$	H−H	14.5	6.0	134c
	H−H	18.3	10.5	134d
	H−H	19.1	14.9	134d
	H−H	16.8	7.0	134d
	H−H	14.2	4.1	134d
Ni(^{1}D)	H−CH_3	54.1	20.7	133a,b
	H−CH_3	14.1	−1.4	133g
Pd	H−CH_3	30.3	20.1	132b
	H−CH_3	3.6	−2.3	133g
$Pd(PH_3)_2$	H−CH_3	uphill	44	132
	H−CH_3	27.1	30.6	137
$Pd(CO)_2$	H−CH_3	35.2	37.1	137
Pt	H−CH_3	12.9	−16.1	132b
	H−CH_3	2.1	−26.6	133g
$Pt(PH_3)_2$	H−CH_3	25.5	7.2	133c
	H−CH_3	35.3	1.2	134a
	H−CH_3	29.6	4.7	134a
	H−CH_3	28.7	6.5	136a,b
	H−CH_3	27.9	9.4	136f
	H−CH_3	24.4	9.8	137
$Pt(CO)_2$	H−CH_3	23.7	15.3	137
$Pd(PH_3)_2$	H−SiH_3	1.1	−8.1	136a,b
$Pt(PH_3)_2$	H−SiH_3	0.7	−25.6	136a,b
	H−SiH_3	2.9	−19.3	136f
	H−$SiCl_3$	3.0	−16.8	136f
	H−$SiMe_3$	2.8	−32.3	136f

[a] Relative to the reactants. [b] Relative to the precursor.

As mentioned in earlier reviews[3a,b,135b] the oxidative addition of H_2, SiH_4, and CH_4 to d^{10} PdL_2 complexes is less favorable than that to d^{10} PtL_2 complexes because of the high energy of the Pd d^9s^1 state (see Table 19). Calculations by Low and Goddard[132] and by Siegbahn et al.[133] emphasize the importance of the competition between the d^9s^1 and d^{10} states of the metal atom in influencing the course of the reaction. In the d^{10} ML_2 fragment, the metal can be described qualitatively by a d^{10} configuration with the dative bonding of the spectator ligands primarily involving donation of the ligand lone pairs to s and p metal orbitals. To form two more covalent bonds, promotion of the metal to the d^9s^1 state is required. As the H_2 approaches the bending ML_2 fragment, sd hybridization from this d^9s^1 state serves to form the two new M−H bonds. Therefore, a d^9s^1 ground state (or low-lying d^9s^1 excited state) leads to stronger bonding interactions between the hydrogen 1s orbitals and the M sd hybrid orbitals. In a comparison of the addition of H_2 to Pt (which has a d^9s^1 ground state) and Pd (which has the d^{10} ground state and a high-lying d^9s^1 excited state), the reaction is exothermic for Pt by

34 kcal/mol but is endothermic for Pd by 4 kcal/mol.[135c] As in the β-H transfer, the origin of the atomic differences have been attributed to relativistic effects,[18] which stabilize the $(n + 1)$s orbitals and destabilize the nd orbitals more for the heavier third-row transition metals.[132]

Recently, Sakaki et al. presented a series of theoretical studies on oxidative addition of $H-CH_3$, $H-CH_2CN$, $H-CH(CN)_2$, CH_3-CH_3, $H-SiR_3$, and SiR_3-SiR_3 (R = H, Cl, or Me) to d^{10} $M(PH_3)_2$ (M = Pd or Pt) using ab initio MO/MP2-MP4SDQ, CCD, and CCSD methods.[136e−g] To investigate the chelate effect,[136e] they compared model calculations for the oxidative additions of $H-CH_3$ to d^{10} $M(PH_3)_2$ and to the same complex with the phosphine ligands bent back to mimic a chelating phosphine. The unconstrained reaction requires a high activation energy, 30 and 37 kcal/mol for M = Pt and Pd (MP4SDQ values), respectively, while the constrained reaction requires a much lower activation energy, 3.8 and 20.0 kcal/mol for M = Pt and Pd, respectively. The enhanced reactivity predicted for this model and seen in M(dipe) (dipe = diphosphinoethane) and M(dipm) (dipm = diphosphinomethane) arises from the higher lying d_π orbital and lower lying sp_σ orbital found in the chelating phosphine complexes.

Recently, Su and Chu reported similar studies on oxidative addition of $H-CH_3$ to the 14-electron d^{10} $M(L)_2$ (M = Pd, Pt; L = CO, PH_3, $L_2 = PH_2CH_2CH_2PH_2$) at the MP2 and MP4SDTQ levels of theory.[137] Since the triplet state of the d^{10} $M(L)_2$ system should be more bent than its singlet analogue and since a smaller ΔE_{st} of 14-electron d^{10} $M(L)_2$ results in a lower barrier, the more strongly bent $M(L)_2$ systems should react more rapidly. In addition, the calculations show that more strongly electron-donating ligands, L, and third-row transition metals also favor the oxidative addition of saturated C−H bonds.

In a related study,[136f] Sakaki et al. examined the effects of electron-withdrawing substituents on the activated methane derivatives. Although introduction of an electron-withdrawing CN group lowers the activation energy (to 25 kcal/mol) and decreases the endothermicity (to 11 kcal/mol) for the C−H oxidative addition by a d^{10} Pd complex, the reaction still proceeds only at high temperature. The C−H activation of $CH_2(CN)_2$ with a palladium bidentate phosphine model complex, Pd(dipe) or Pd(dipm), becomes much easier; the reaction is exothermic by 6−11 kcal/mol with an activation barrier of 18−19 kcal/mol. The acceleration by the CN group is interpreted in terms of the charge-transfer interaction from Pd through the π^* orbital of $CH_2(CN)_2$ into the C−H σ^* orbital. These computational results suggest that the C−H activation by a d^{10} Pd complex occurs more easily when electron-withdrawing groups are introduced on the sp^3 carbon atom and a chelating phosphine is used as a ligand.

The steric effects of the spectator phosphine ligands on the transition state and reactivity were also investigated by Sakaki et al.[136g] The calculations show that the TS structures for the oxidative addition of $H-CH_3$ and $H-SiR_3$ to $Pt(PH_3)_2$ are coplanar, as expected from the orbital interaction diagram, while unexpectedly the TS structures for the oxidative addition of CH_3-CH_3 and SiR_3-SiR_3 to $Pt(PH_3)_2$ are nonplanar. Frequency analysis and IRC calculations clearly indicate that these nonplanar transition states are real transition states and that they are smoothly connected to the planar precursor complex and product. Since the electron distributions show stronger charge-transfer interactions from Pt d orbital to the σ^*_{Si-C} or σ^*_{C-C} orbital in the coplanar structure than in the nonplanar structure, this electronic factor is not responsible for the twisted transition state. Moreover, the dihedral angle (δ) between the PtP_2 and the PtXC planes (X = C or Si) increases in the order SiH_3-CH_3 < $SiMe_3-CH_3$ < $SiCl_3-CH_3$, and the $Pt-SiR_3$ distance at the TS increases in the same order. Thus, Sakaki et al. concluded that the steric factors between the activation substrate, particularly the greater steric repulsion by the SiR_3 group, and the spectator phosphine group is responsible for the nonplanar TS structure.

In another recent theoretical study of H_2 oxidative addition, Morokuma et al. investigated the oxidative addition of H−H to $Pt(PR_3)_2$ (R = H, Me, *t*-Bu, and Ph) using mixed methods (IMOMM and ONIOM).[134c,d] The calculated results at the IMOMM(MP2:MM3) level show that the reactivity of PtL_2 toward H_2 increases in the following order: $P(t\text{-}Bu)_3$ < $PPh(t\text{-}Bu)_2$ < $P(c\text{-}C_6H_{11})_3$ < $P(i\text{-}Pr)_3$, an order that is consistent with the experimental facts. The $Pt[P(t\text{-}Bu)_3]_2$ complex has a high calculated barrier (15 kcal/mol) for oxidative addition of H_2, while $Pt(Ph_3)_2$, $Pt(PMe_3)_2$, and $Pt(PH_3)_2$ all have low barriers (<4 kcal/mol). These energetic differences are paralleled by differences in the transition-state structure for the sterically congested vs the uncongested system. The calculated energy barrier for reductive elimination of H_2 from $Pt(PMe_3)_2(H)_2$ is 20.4 kcal/mol and agrees well with the experimental activation enthalpy $\Delta H^{\ddagger}$ of 20.0 kcal/mol. The energetics at the more reliable IMOMM(MP2:MM3) level show that while complexes with R = H, Me, and Ph have early coplanar transition states and low barriers, the complex with R = *t*-Bu has a relatively late nonplanar transition state and a high barrier.

The successful activation of H−H and R−H by **d^8 ML_n (n = 3 or 4) complexes** has prompted extensive experimental and theoretical studies for more than 10 years.[1−3] These complexes have the general formula MXL_2 (L = PPh_3; X = Cl) or CpML (L = CO, PR_3). Complexes containing the MXL_2 moiety, such as Vaska's complex $IrCl(CO)(PPh_3)_2$ and Wilkinson's catalyst $RhCl(PPh_3)_3$, are among the most important and widely used catalysts, promoting a diverse array of organic transformations.[138] The first activation of a simple alkane by a transition-metal complex was reported in 1982.[139] The active species are generated by photolysis of CpMLL′ (M = Rh, Ir; L = CO, PPh_3, PMe_3; L′ = CO, $(H)_2$); the resulting d^8 CpML fragments are unique in that they are among only a few late transition-metal complexes capable of activating H−H and C−H bonds. These coordinatively unsaturated d^8 ML_n complexes differ from the d^{10} ML_2 complexes because the former have a low-lying vacant d_σ orbital which can accept an electron from

Table 20. Energy of Reaction (ΔE)[a] and Activation Energy ($\Delta E^{\ddagger}$)[b] (kcal/mol) of R−H Oxidative Addition to d^8 Three-Coordinated ML_2X Species (R = H, CH_3, SiH_3)

[M][c]	activated molecule	method	activation barrier $\Delta E^{\ddagger}$	reaction energy ΔE	ref
$Rh(PH_3)_2Cl$	H−CH_3	MP2	3.3	−22.6	140b
		MP4	2.8	−19.3	140b
		QCISD(T)	7.7	−10.0	140b
	H−SiH_3	MP2	downhill	−58.4	140b
		MP4	downhill	−55.1	140b
		QCISD(T)	downhill	−44.6	140b
	H−CH_3	BP86	3.3	−15.1	141
cis-$Rh(PH_3)_2Cl$	H−CH_3	BP86	15.3	3.6	141
$Ir(PH_3)_2H$	H−H	B3LYP		−21.6	142
	H−CH_3	B3LYP	11.8	−2.9	143
		B3LYP	1	−12.8	143
	H−CF_3	B3LYP	8.0	−12.8	142
$Ir(PH_3)_2Ph$	H−H	B3LYP		−23.0	142
	H−CH_3	B3LYP	14.6	4.4	142
$Ir(PH_3)_2Cl$	H−H	B3LYP		−54.1	142
	H−CH_3	B3LYP	0.25	−27.2	142
		MP2		−41.6	143
	H−CF_3	B3LYP		−42.7	142
$Ir(PH_3)_2F$	H−H	B3LYP		−47.0	142
$Pt(PH_3)(Cl)_2$	H−CH_3	MP2	24.8	4.3	145
$Pt(NH_3)_2(Me)^+$	H−CH_3	B3LYP	29	26[b]	144
$Pt(PH_3)_2(Me)^+$	H−CH_3	B3LYP	30	26[b]	144

[a] Relative to the reactants. [b] Relative to the precursor. [c] *trans* structure.

the σ_{C-H} orbital. This donating interaction leads to a stronger agostic interaction for the precursor complex and to a lower activation barrier for the oxidative-addition reaction, when compared to the d^{10} ML_2 complexes.

Koga and Morokuma investigated the oxidative addition of the C−H, Si−H, and Si−Si bonds to the T-shaped **three-coordinate** d^8 complex $RhCl(PH_3)_2$ with MP2, MP4, and QCISD(T) methods.[140a,b] Methane C−H activation by $RhCl(PH_3)_2$ proceeds through the η^2-CH_4 precursor complex and a three-centered transition state. The overall reaction is exothermic by 23, 19, and 10 kcal/mol at the MP2, MP4, and QCISD(T) levels, respectively, with a low, 3−8 kcal/mol, activation barrier (Table 20). Thus, the C−H activation by this coordinatively unsaturated complex will occur at relatively low temperatures. The potential energy profile for the Si−H bond activation is quite different (see Figure 22). The Si−H bond activation is nearly barrierless; the η^2-SiH_4 complex is found to be the transition state instead of an intermediate. This difference, between SiH_4 and CH_4, originates from the strong Rh−Si bond and the weak Si−H bond and results in a much larger exothermicity for Si−H bond activation than that for C−H bond activation. Koga, Morokuma, and co-workers also studied the oxidative addition of acetylene to the T-shaped d^8 complex $RhCl(PH_3)_2$ with the MP2 method.[140c] The calculations show that the reaction from an η^2-alkyne complex to an alkynyl−hydrido complex is endothermic by 9.4 kcal/mol with a high activation barrier of 36.3 kcal/mol. In the actual reaction, where a bulky phosphine like P^iPr_3 and a bulk substituent on the alkyne are employed, the η^2-alkyne complex should be less stable than it is in the present model system. Furthermore, the more basic nature of the central metal with P^iPr_3 ligands, as compared with PH_3, should favor the alkynyl−hydrido complex. In this work the authors also investigated the intra- and intermolecular hydride-transfer mechanism from the alkynyl−hydrido complex to the vinylidene complex with the QM and QM/MM methods.

Margl, Ziegler, and Blöchl also studied the electronic and molecular structures of the oxidative addition of the H−CH_3 to the d^8 *trans*- and *cis*-$RhCl(PH_3)_2$ complexes.[141] The calculations show that the three-coordinate d^8 *trans*-$RhCl(PH_3)_2$ species formed by CO photoejection from *trans*-$RhCl(CO)(PH_3)_2$ has a preferred *cis*-geometry and that the *trans*-isomer

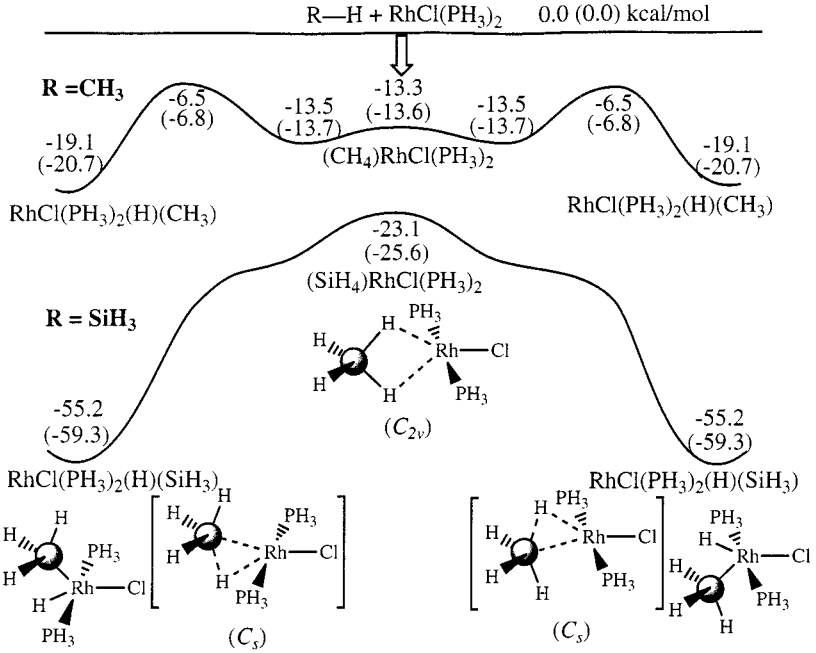

Figure 22. MP2/BS1 potential energy profile for the Si−H and C−H bond activation to $Rh(PH_3)_2(Cl)$. Numbers in parentheses are at the MP2/BS2 level.

is 16.5 kcal/mol higher in energy. The more stable *cis*-isomer is formed by a trans to cis isomerization process through an Y-shaped transition state with a calculated barrier of 9.8 kcal/mol. Because of the *trans*-influence of the spectator ligands, the *trans*-$RhCl(PH_3)_2$ isomer is more reactive toward the methane C−H bond than the *cis*-isomer. The *trans*-isomer forms a stronger η^2-methane complex and has a lower activation barrier and a more stable product (see Table 20).

In previous studies of methane activation by 14-electron $Ir(PH_3)_2(X)$ complexes (X = H, Cl),[143a] Cundari and co-workers found that a more strongly bound adduct (larger agostic interaction) occurs when X = Cl than when X = H. Methane addition to $Ir(PH_3)_2$-(H) and $Ir(PH_3)_2(Cl)$ from the adduct precursor to the metal methyl hydride complex is exothermic by 6 and 26 kcal/mol with an activation barrier of 20 and 9 kcal/mol, respectively. Analysis of the wave function along the intrinsic reaction coordinate (IRC) suggested that although donation of electron density from methane to metal is essential for adduct formation, it is not until the back-donation to σ^*_{CH} increases that the C−H bond is activated and cleaved. The calculated electronic and molecular structures along the IRC suggested a two-stage mechanism: substrate to complex donation is important in the early part of the reaction (electrophilic stage) while complex to substrate back-donation is necessary later for C−H scission (nucleophilic stage). Recently, Benson and Cundari presented a study of ethane dehydrogenation by the 14-electron complex $Ir(PH_3)_2H$ with the MP2 method.[143b] The IRCs for ethane C−H oxidative addition are consistent with an experimental trajectory derived from analysis of the crystal structures of agostic complexes. Although ethane binds to $Ir(PH_3)_2H$ as strongly as, if not stronger than, methane, calculation of the IRC suggests that for ethane, unlike methane, an alkane adduct complex does not lie along the path to C−H oxidative addition. The product of oxidative addition is a nonagostic Ir(III)−ethyl complex.

Recently, Krogh-Jespersen and Goldman examined oxidative addition of dihydrogen (H_2), methane (CH_4), and fluoromethanes (CH_3F, CHF_3, CF_4) to $Ir(PH_3)_2X$ (X = H, Li, Cl, F, BH_2, NH_2, Ph) with hybrid DFT method.[142a] Exothermicity of H_2 addition to $Ir(PH_3)_2X$ increases as follows for various X: $BH_{2(vert)} \approx Li < BH_{2(eq)} \ll H \approx Ph_{(vert)} < NH_{2(eq)} < F < NH_{2(vert)} \approx Cl$. Clearly, the *trans*-influence of the X ligand, both π and σ effects, plays an important role in the order above. As shown in Scheme 12, the addition of H_2 to $Ir(PH_3)_2(NH_2)$ with the NH_2 coplanar to the equatorial plane (**46a** to **47a**) is exothermic by 37 kcal/mol, while with the NH_2 plane perpendicular to the equatorial plane (**46b** to **47b**) the exothermicity increases to 52 kcal/mol. In contrast, the addition of H_2 to $Ir(PH_3)_2(BH_2)$ with BH_2 perpendicular to the equatorial plane (**46b** to **47b**) is endothermic and no dihydride complex is observed, while with BH_2 in the equatorial plane (**46a** to **47a**) the reaction is exothermic by 7 kcal/mol. Thus, π-donation from the spectator ligand X favors the addition reaction. From Table 20, one can also see that increased σ-donation by X

Scheme 12

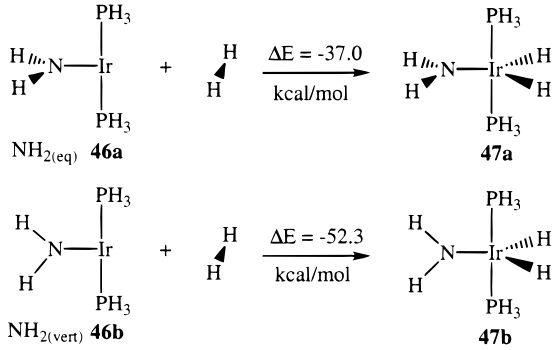

Scheme 13

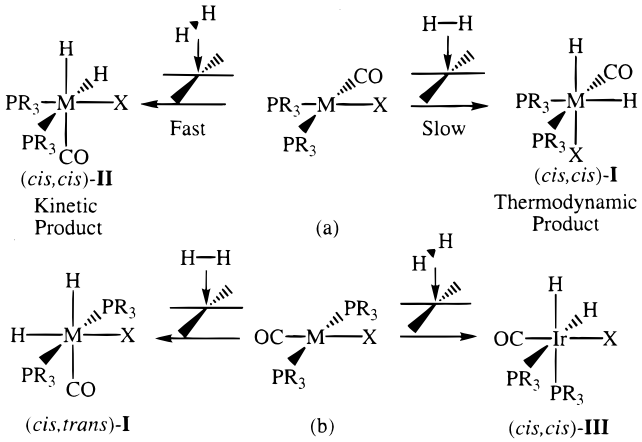

disfavors addition of H_2 to $Ir(PH_3)_2X$. These results can be explained in terms of the *trans*-influence of the X ligand. In the T-shaped $Ir(PH_3)_2X$ fragment, the trans spectator X ligand (trans to the vacant position) influences the metal d_σ orbital (LUMO) as illustrated in Scheme 6;[85c] increased σ-donation by X leads to a higher-lying d_σ orbital and a decrease in the interaction between the metal d_σ orbital and the σ_{R-H} orbital. In contrast, increased π-donation by X leads to a higher-lying d_π orbital and an increase in the interaction between the metal d_π orbital and the σ^*_{R-H} orbital. The methane C−H activation by other T-shaped ML_2X such as $Pt(PH_3)(Cl)_2$, $Pt(NH_3)_2(Me)^+$, and $Pt(PH_3)_2(Me)^+$ has also been studied recently.[144,145]

The oxidative addition of H_2 to square-planar d^8 **four-coordinate** complexes, such as Vaska's complex and $RhCl(CO)(PPh_3)_2$, has been extensively studied. The generally accepted mechanism for the reaction involves the concerted addition of H_2 to form pseudooctahedral products with a cis disposition of the hydride ligands as shown in Scheme 13, where concerted cis addition of H_2 to each isomer, either *cis*-$MCl(CO)(PR_3)_2$ or *trans*-$MCl(CO)(PR_3)_2$, yields two possible isomeric products. Experimentally, IrCl(CO)-(dppe) (dppe = 1,2-bis(diphenylphosphino)ethane) oxidatively adds H_2 along the P−Ir−CO axis to generate (*cis*,*cis*)-**II** isomer with a >99% stereoselectivity at low temperature, while the other (*cis*,*cis*)-**I** isomer, formed from the addition along the P−Ir−Cl axis, appears at higher temperatures and eventually dominates the final equilibrium (Scheme 13a).[146] However, for Vaska's complex, *trans*-$IrCl(CO)(PPh_3)_2$,

only the (*cis*,*trans*)-**I** isomer is observed (Scheme 13b).[138a−f]

Sargent, Hall, and Guest investigated the oxidative addition of H_2 to *cis*- and *trans*-$IrX(CO)(PPh_3)_2$ (X = Cl, H, Me, and Ph) with ab initio MO techniques.[147] The calculations show that (i) as the square-planar complex evolves to a six-coordinate species during the course of the reaction, the ligands in the addition plane move past regions of charge concentration from the metal lone-pair electrons; (ii) strong σ- and π-donor ligands destabilize the five-coordinate transition state by contributing to the repulsion between the electronic charge density of the ligands and the metal concentrations; (iii) electron-withdrawing ligands stabilize the five-coordinate transition state by delocalizing some of the charge density contributing to this repulsive interaction; (iv) the electronic contribution to the relative stabilities of the six-coordinate d^6 final product can be predicted based on the relative orientations of the ligands with the strongest *trans*-influence; and (v) additional stability in the final product is gained by orienting a strong *trans*-influencing ligand trans to a strong π-donor ligand. For the oxidative addition of H_2 to *cis*-$IrCl(CO)(PH_3)_2$, addition along the P−Ir−CO axis to generate a (*cis*,*cis*)-**II** product is kinetically favored due to the electron-withdrawing nature of the CO ligand, which provides additional stabilization to the five-coordinate transition state by a back-bonding interaction between the filled metal d_{z^2} orbital and the unoccupied CO π^* orbital. The (*cis*,*cis*)-**I** product is thermodynamically favored because the two strongest *trans*-influencing ligands are trans to a phosphine ligand and a relatively weak *trans*-influencing Cl^- ligand. In the oxidative addition of H_2 to Vaska-type complexes, *trans*-$IrX(CO)(PR_3)_2$ (X = Cl, H, Me, and Ph), the nature of the X ligand is crucial to determining the direction of addition. Weak electron-donor ligands, such as Cl^-, favor addition along the X−Ir−CO axis, whereas for stronger electron-donor ligands, such as Ph^-, Me^-, and H^-, addition is preferred along the P−Ir−P axis. For Ph^- and Me^-, the more stable isomer of the final products corresponds to the species formed ((*cis*,*trans*)-**I**) from addition along the X−Ir−CO axis. This isomer gains stability by orienting a weaker σ-donor and/or stronger π-donor ligand trans to a hydride ligand. The weaker σ-donor character strengthens the strong Ir−H σ bond to which it is trans, while the strong π-donor character, which results in an antibonding interaction of π symmetry, is able to minimize the impact of antibonding interaction by being trans to the strongly *trans*-influencing hydride ligand.

Abu-Hasanayn, Goldman, and Krogh-Jespersen also studied the oxidative addition of H_2 to Vaska-type complexes, *trans*-$IrX(CO)(L)_2$ (L = NH_3, PH_3, AsH_3; X = F, Cl, Br, I, CN, H, CH_3, SiH_3, OH, SH, BH_4), to generate (*cis*,*trans*)-**I** addition products.[148] The calculations show that the activation barrier height of the oxidative-addition reaction decreases and its exothermicity increases via the trend F < Cl < Br < I < CN < H. This trend parallels the π-donor capability of the halides, which decreases in strength going down a group in the periodic table. Abu-Hasanayn et al. emphasize how the π-orbital properties of the substituents play an important role in determining the thermodynamics of the addition reaction; the presence of an occupied π orbital on the substituents strongly disfavors the reaction. In other words, increased π-donation from the X ligand contributes to the activation barrier to H_2 addition. Strong π-donation from X increases the four-electron−three-center π interaction in the X−Ir−CO moiety and increases the barrier to addition by increasing the resistance of the X−Ir−CO moiety to bending. In addition, increased π-halide donation to metal raises the energy of the metal unoccupied sp_σ (p_z) orbital and decreases the bonding interaction between the metal sp_σ orbital and the H−H σ orbital. Similar reasoning can explain the trend in the exothermicity of the addition, which increases in the order L = NH_3 < PH_3 < AsH_3 for X = Cl.[149]

Focusing on the catalytic mechanism of Wilkinson's catalyst, $RhCl(PPh_3)_3$, Morokuma and co-workers studied the structure and reactivity of the oxidative addition of H_2 and CH_4 to *trans*- and *cis*-$RhCl(CO)(PH_3)_2$ using the HF and MP2 methods.[86d,150] The recent calculations of Musaev and Morokuma show that (i) *trans*-$RhCl(CO)(PH_3)_2$ is about 13 kcal/mol more stable than *cis*-$RhCl(CO)(PH_3)_2$, (ii) the stability of the H_2 addition products, $RhCl(PPh_3)_3(H)_2$, decreases in the order (*cis*,*trans*)-**I** (0.0 kcal/mol) ≈ (*cis*,*cis*)-**III** (0.4 kcal/mol) > (*cis*,*cis*)-**I** (3.5 kcal/mol) > (*cis*,*cis*)-**II** (10.3 kcal/mol), (iii) the oxidative addition of H_2 to *trans*- and *cis*-$RhCl(CO)(PH_3)_2$ is exothermic by 2 and 11 kcal/mol with an activation barrier of 16 and 18 kcal/mol, respectively, (iv) the oxidative addition of CH_4 to *trans*- and *cis*-$RhCl(CO)(PH_3)_2$ is endothermic by 20 and 9 kcal/mol with an activation barrier of 27 and 31 kcal/mol, respectively, and (v) among CO, PH_3, and Cl^-, the trans influence seems to decrease in the order CO > PH_3 ≥ Cl^-. The Musaev and Morokuma results for the addition reaction of H_2 to *trans*- and *cis*-$RhCl(CO)(PH_3)_2$ are consistent with those obtained for *trans*- and *cis*-$IrCl(CO)(PH_3)_2$ by Hall and co-workers.[147] In agreement with experiment,[151] the oxidative-addition reactions of four-coordinate d^8 $RhCl(CO)(PH_3)_2$ complexes are substantially more difficult than the corresponding reactions of three-coordinate d^8 $RhCl(PH_3)_2$ complexes.[140]

In their study, Ziegler and co-workers also investigated the oxidative addition of methane to *trans*- and *cis*-$RhCl(CO)(PH_3)_2$ using DFT method.[141] Again, the calculated results show that (i) *trans*-$RhCl(CO)(PH_3)_2$ is about 9 kcal/mol more stable than *cis*-$RhCl(CO)(PH_3)_2$ and (ii) the oxidative addition of CH_4 to *trans*- and *cis*-$RhCl(CO)(PH_3)_2$ is endothermic by 28 and 21 kcal/mol with an activation barrier of 45 and 35 kcal/mol, respectively, while the reverse reaction, reductive elimination of methane, is relatively facile with kinetic barriers of 17 (trans) and 14 (cis) kcal/mol, respectively.

More recently, Wang and Weitz studied the oxidative addition of H_2 to $Fe(CO)_4$ using DFT methods (BP86, BLYP, and B3LYP).[152] The BP86 functional gives good agreement with the experimental data for the dissociation enthalpy of H_2 from $Fe(CO)_4(H)_2$. The

reaction is expected to involve a curve crossing from the singlet potential energy surface to the triplet surface. The reverse reaction, oxidative addition of H_2 to $Fe(CO)_4$ to form $Fe(CO)_4(H)_2$, involves an (η^2-H_2)$Fe(CO)_4$ intermediate which continues to the product with a low activation barrier (0.4 kcal/mol). If the reference state for dissociation of $Fe(CO)_4(H)_2$ is the triplet state of $Fe(CO)_4$, then calculations with the B3LYP functional lead to a value for the bond dissociation enthalpy that is too small. However, if the dissociation process actually should be referenced to the singlet state of $Fe(CO)_4$, then calculations with the B3LYP functional agree with experimental data. In both cases the BLYP functional gives poor agreement with experimental data for the bond dissociation enthalpy of $Fe(CO)_4(H)_2$. Overall, the calculated reaction enthalpy at BP86 is 23 kcal/mol, a value that compares favorably with the experimental value of 21 ± 2 kcal/mol.[153] These results by Wang and Weitz are consistent with previous work by Ziegler and coworkers. In their study,[41a] Ziegler et al. investigated the electronic and molecular structures of $M(CO)_4$ (M = Fe, Ru, Os) and the oxidative addition of H_2 and CH_4 to $M(CO)_4$ (M = Ru, Os) using DFT method. The optimized geometries show that the $M(CO)_4$ fragment in the $^1A_1$ singlet state is C_{2v} symmetry, while the $M(CO)_4$ fragment in the $^3B_2$ triplet state is nearly T_d symmetry. The $^1A_1$ singlet state is calculated to be the ground state for $Ru(CO)_4$ and $Os(CO)_4$ by 8.8 and 10.0 kcal/mol, respectively. However, the calculated $^1A_1$ and $^3B_2$ states for $Fe(CO)_4$ are very close in energy ($\Delta E_{T-S} < 1$ kcal/mol). The calculations show that (i) the oxidative addition of H_2 to $M(CO)_4$ (M = Ru, Os) has a low activation barrier of 0.7 and 2.6 kcal/mol and is exothermic by 5.3 and 18.2 kcal/mol, respectively, and (ii) the oxidative addition of the CH_4 is much more difficult with an activation barrier of 18.9 and 24.1 kcal/mol and a total reaction enthalpy of 6.7 and −1.4 kcal/mol, respectively. Thus, the CH_4 addition to $Ru(CO)_4$ and $Os(CO)_4$ is unfavorable and unlikely to be observed.

A now common alkyl C−H activation procedure has been the irradiation of $Cp^*ML(H)_2$ and $Cp^*ML(CO)$, where $Cp^* = \eta^5$-C_5Me_5, L = PMe_3, PPh_3, or CO, and M = Rh or Ir, to produce a postulated unsaturated d^8 **Cp*ML precursor**. A hydrocarbon R−H used as solvent during the irradiation undergoes oxidative addition to the precursor with the production of $Cp^*ML(H)(R)$.[139,154a−c] The electronic structure of the coordinatively unsaturated 16-electron d^8 fragment CpML has been studied by Hofmann and Padmanabhan for various ligands, L, and M = Co, Rh, and Ir.[155a] The CpML fragment of C_s point group symmetry has two low-lying metal-based $d_{x^2-y^2}$ and d_{xz} orbitals, 1a′ and 1a″, stabilized by interaction with the π^* orbitals on L (see Figure 23). At somewhat higher energy is the occupied metal-based d_{z^2} orbital, 2a′, with a weak M−L antibonding σ interaction. Highest in energy are two metal-based orbitals, 2a″ and 3a′, primarily d_{yz} and d_{xy} in character, respectively. The 2a″ and 3a′ orbitals are destabilized by out-of-phase interactions with occupied π orbitals on the Cp ring, and 3a′, the highest in energy, is in addition destabilized by out-of-phase interaction with the σ orbital on L.

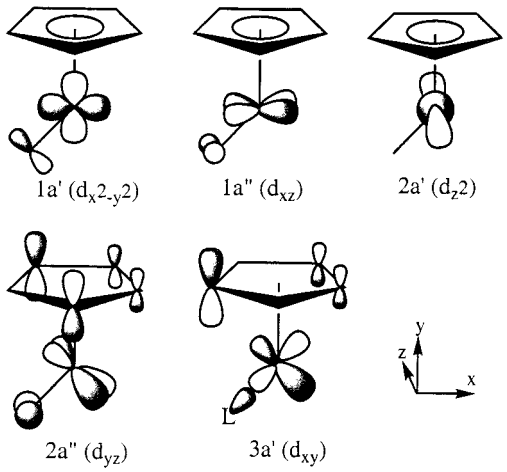

Figure 23. Valence molecular orbitals of CpML complex.

Scheme 14

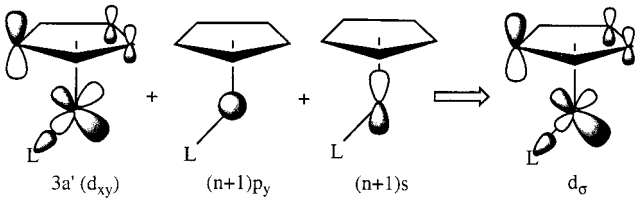

A strong π-acceptor ligand such as CO seems to stabilize the 2a″ (d_π) orbital.[85,155] Although the strong σ-donor ligand (L) seems to destabilize the 3a′ (d_σ) orbital, a hybridization of 3a′ with the $(n + 1)p_y$ and $(n + 1)$s orbitals still leads to the d_σ orbital remaining in a low-lying position as illustrated in Scheme 14.

There are several theoretical studies in the literature on the oxidative-addition reaction between R−H (R = H, CH_3, NH_2, OH, and SiH_3) and the d^8 CpML (M = Co, Rh, Ir, Ru^-, Os^-, Pd^+, and Pt^+; L = CO, PH_3) complexes.[41,156] We summarized the calculated energetic parameters in Table 21. Stoutland et al. carried out a detailed experimental analysis of the energetics involved in the C−H activation by $Cp^*Ir(PMe_3)$.[154c] They infer a small barrier of 2−10 kcal/mol and a reaction enthalpy of −26 to −29 kcal/mol. Jones and Feher have investigated the energetics for the addition of CH_4 to the corresponding Rh system, $Cp^*Rh(PMe_3)$.[139d] Their data are consistent with a reaction enthalpy of −7 to −10 kcal/mol and an upper limit of 5 kcal/mol for the activation energy.[41a,139d]

In early theoretical work, Ziegler et al.[41a] studied the oxidative addition of CH_4 to CpML (M = Rh, Ir; L = CO, PH_3) using DFT method. They found that for M = Ir, the reaction has a modest activation barrier of 2 kcal/mol with a reaction enthalpy of −34 to −36 kcal/mol. The activation barrier for M = Rh is somewhat higher at 9 kcal/mol, and the reaction enthalpy is less favorable at −17 to −15 kcal/mol. These findings are in agreement with the general experimental observation that the 5d species CpIrL activates alkylic C−H bonds more readily than 4d homologues. The differential is due to relativistic effects,[18] which stabilize the 6s orbitals and destabilize the 5d orbitals for the heavier third-row transition metals.

The C−H oxidative addition of CH_4 to CpML (M = Rh, Ir; L = CO, PR_3) was also studied by Hall and

Table 21. Energy of Association Energy (ΔE_{Prec}),[a] Reaction (ΔE_{Prod}),[a] and Activation Energy ($\Delta E^{\ddagger}$)[b] (kcal/mol) of R−H Oxidative Addition to d^8 CpML

system	method	ΔE_{Prec}	$\Delta E^{\ddagger}$	ΔE_{Prod}	ref
$CpCo(CO) + CH_4$	B3LYP	−9.0		−7.7	41d
	B3P86	−11.5		−11.8	41d
	MP2	−19.5		−35.7	41d
	PCI-80	−17.1	−6.0	−34.1	41d
	MCPF	−13.3		−22.0	41d
	CASPT2	−15.4		−23.0	41d
$CpRu(CO)^- + CH_4$	B3LYP	−6.9	3.2	−27.2	41e
	MP2	−13.2	3.3	−30.2	41e
	MP4SDTQ	−14.0	4.6	−26.1	41e
$CpRh(CO) + CH_4$	LDA	−6.9	∼8.8	−14.8	41a
	B3LYP	−6.4	12.9	−4.2	41e
	B3LYP	−5.6	8.7	−5.8	41d
	B3P86	−8.0	6.0	−9.9	41d
	MP2	−12.3	6.1	−18.8	41d
	MP2	−14.8	4.1	−30.6	41b
	MP2	−13.6	23.5	−19.2	41e
	MP2	−7.7	5.5	−16.4	41c
	MP4SDTQ	−13.8	10.4	−13.3	41e
	PCI-80	−12.5	5.9	−17.2	41d
	MCPF	−10.1	8.4	−11.5	41d
	CASPT2	−11.7	2.1	−21.9	41d
$CpRh(CO) + NH_3$	MP2	−36.8	41.9	−3.2	41c
$CpRh(CO) + H_2O$	MP2	−20.5	25.9	−2.4	41c
$CpRh(CO) + SiH_4$	MP2	none	none	−49.4	41c
$CpRh(PH_3) + CH_4$	LDA	−5.7	∼8.8	−17.2	41a
	MP2			−40.0	155
$CpPd(CO)^+ + CH_4$	B3LYP	−10.0	29.4	19.3	41e
	MP2	−16.2	28.4	9.1	41e
	MP4SDTQ	−15.0	29.3	13.2	41e
$CpOs(CO)^- + CH_4$	B3LYP	−10.1	0.6	−49.1	41e
	MP2	−19.4	1.8	−50.4	41e
	MP4SDTQ	−18.2	2.7	−46.7	41e
$CpIr(CO) + CH_4$	LDA	−14.1	∼2.4	−33.5	41a
	B3LYP	−9.6	1.9	−31.8	41e
	B3LYP	−9.8	−1.9	−33.7	41d
	B3P86	−13.7	−2.9	−38.8	41d
	MP2	−17.6	−3.1	−46.3	41d
	MP2	−16.4	15.5	−32.8	41e
	MP4SDTQ	−15.8	7.1	−27.8	41e
	PCI-80	−6.5	−1.8	−29.2	41d
	MCPF	−4.5	−1.2	−26.4	41d
$CpIr(PH_3) + CH_4$	LDA	−12.2	∼2.4	−36.3	41a
	MP2			68.6	155
$CpPt(CO)^+ + CH_4$	B3LYP	−10.9	14.5	−6.3	41e
	MP2	−17.4	17.5	−11.5	41e
	MP4SDTQ	−16.5	18.3	−7.2	41e

[a] Relative to the reactants. [b] Relative to the precursor.

co-workers at the HF and MP2 levels of theory.[41b,156] The shape of the potential energy surface obtained in these papers is similar to that obtained by Ziegler et al. For M = Rh, the whole reaction is calculated to be exothermic by 31−40 kcal/mol with a low activation barrier of 4 kcal/mol, while the reaction enthalpy for M = Ir is −69 kcal/mol. The studies on the behavior of intermolecular versus intramolecular C−H bond activation in rhodium and iridium complexes (Scheme 15) show that the thermodynamic exothermicity follows the sequence *inter* > *intra-P* > *intra-Cp* with decreasing differences as the ring size increases.

Musaev and Morokuma studied the oxidative addition of the H−H, C−H, N−H, O−H, and Si−H bonds of the H_2, CH_4, NH_3, H_2O, and SiH_4 molecules to CpRh(CO) at the MP2 level using polarized basis sets.[41c] The calculations show that along the CH_4 addition pathway a molecular precursor was found

Scheme 15

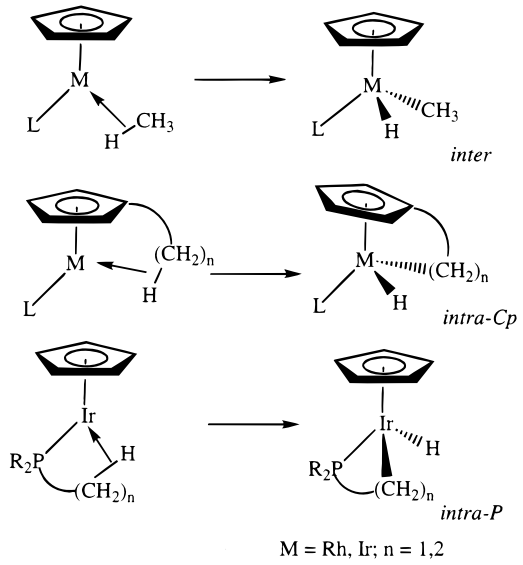

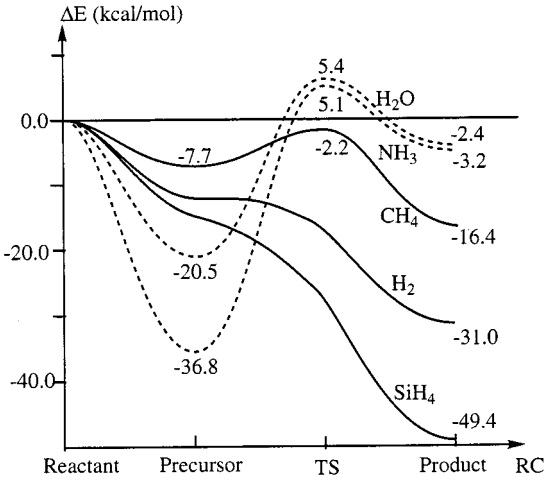

Figure 24. Potential energy profiles of the reaction of CpRh(CO) with H_2, CH_4, H_2O, NH_3, and SiH_4.[41c]

to be bound by 7.7 kcal/mol, the barrier was found to be 5.5 kcal/mol above the precursor, and the exothermicity was 16.4 kcal/mol. The reaction energy profile for CH_4 addition is in good agreement with the one suggested by experiment. As shown in Table 21 and Figure 24, at gas-phase collisionless conditions, the oxidative-addition reaction of $H-SiH_3$, H−H, and $H-CH_3$ to CpRh(CO) should take place without an activation barrier while the reaction of $H-NH_2$ and H−OH goes over a barrier about 5 kcal/mol relative to the reactants. The differences in the reactivity of the substrates considered here can be correlated to the H−R bond strength and the Rh−R bond strength. Going from SiH_4 to H_2, CH_4, NH_3, and H_2O, the H−R bond becomes stronger (88, 99, 108, 109, and 118 kcal/mol, respectively), the Rh−R bond becomes weaker (73, 65, 59, 47, and 55 kcal/mol, respectively), and, thus, the exothermicity becomes smaller (49, 31, 16, 3, and 2 kcal/mol). In solution or in the gas phase when the collisional energy equilibrium is faster than the reaction itself and reaction should be considered to start from the prereaction molecular complex CpRh(CO)·(HR), the oxidative-addition reaction of CH_4 requires a small barrier (5

kcal/mol) while that of NH_3 and H_2O, which have a strong Lewis-base character, requires a large barrier (42 and 26 kcal/mol, respectively) and would not take place easily under normal conditions.

Using a variety of methods, including a recently developed scaling scheme (PCI-80 and MCPF), different perturbation methods (MP2 and CASPT2), and hybrid density functional methods (B3LYP and B3P86), Siegbahn also studied the C−H activation reactions of methane by CpM(CO) (M = Co, Rh, and Ir).[41d] This work concentrated on the recent finding that CpCo(CO) is entirely inert toward alkanes in contrast to the corresponding rhodium and iridium system.[154d] Several commonly used methods produced surprisingly different results when applied to the CpM(CO) reactions. The differences were largest for the cobalt reaction, mainly because of near-degeneracies but also because of an intricate balance of exchange and promotion effects which change as the bonds formed. Compared to the PCI-80 results, which are highly satisfactory in comparison to the experimental estimates for CH_4 addition to CpRh(CO), the B3LYP method somewhat underestimates the association energy (ΔE_{Prec}) and the reaction energy (ΔE_{Prod}). Overall, the B3LYP gives a satisfactory description of the geometries and relative energies, especially for the cobalt reaction. The calculations of the singlet−triplet splittings of the CpM(CO) reactants show that for rhodium the singlet state is the ground state and for iridium the singlet and triplet states are almost degenerate. However, the CpCo(CO) reactant is definitely a triplet state with an excitation energy to the singlet state as high as 11−28 kcal/mol. Clearly, the required high-energy spin crossing explains why CpCo(CO) is unreactive toward alkanes.

Recently, Bosque et al. studied the reactivity of aryl−H and aryl−F bonds toward oxidative addition to $CpRh(PH_3)$ with the B3LYP method.[157] The calculations reveal that both C−H and C−F oxidative additions are exothermic and that the C−F oxidative addition is thermodynamically preferred. However, the activation energy (33.3 kcal/mol) for C−F activation is considerably higher than that for C−H activation (9.4 kcal/mol). These results clearly show that the inertness of the C−F bond has a kinetic origin.

More recently, Su and Chu investigated the potential energy surfaces corresponding to the reaction of d^8 CpM(CO) (M = Ru^-, Os^-, Rh, Ir, Pd^+, Pt^+) with methane at MP2, MP4SDTQ, and B3LYP levels of theory.[158] As shown in Table 21, the activation barriers from the precursor complex to the transition state at the MP4SDTQ level increase in the order $Os^- < Ru^- < Ir < Rh < Pt^+ < Pd^+$ (2.7, 4.6, 7.1, 10.4, 18.3, and 29.3 kcal/mol, respectively) and the reaction enthalpies decrease in the order $Pd^+ > Pt^+ > Rh > Ru^- > Ir > Os^-$ (13.2, −7.2, −13.3, −26.1, −27.8, and −46.7 kcal/mol, respectively). These model calculations predict that the facility of oxidative addition is in the order $Os^- > Ru^- \approx Ir > Rh \approx Pt^+ > Pd^+$. On the basis of these results, Su and Chu conclude that a more electron-rich as well as heavier transition-metal center (i.e., the third row) will facilitate the oxidative-addition reactions with alkane C−H bonds. In contrast, a very electron-deficient and lighter transition-metal center (i.e., the second row) will tend to undergo reductive-elimination reactions, favor C−H bond formation. Su and Chu have also studied the C−H bond activation of propane and cyclopropane by coordinatively unsaturated d^8 $CpM(PH_3)$ (M = Rh, Ir) complexes using the B3LYP method. For both $CpRh(PH_3)$ and $CpIr(PH_3)$, the ease of oxidative addition is in the order secondary C in cyclopropane > primary C in propane > secondary C in propane and the less reactive $CpRh(PH_3)$ complex is more highly selective. Again, these preferences emphasize the importance of forming a sd hybrid for the two new covalent bonds in the addition product. Previous theoretical work[132] has shown that the third-row transition-metal complexes undergo oxidative addition, $M^I + A-B \rightarrow M^{III}(A)(B)$, more easily than their second-row transition-metal congeners since late third-row transition metals have either $d^n s^1$ ground states or $d^n s^1$ low-lying excited states while late second-row transition metals have d^{n+1} ground states with high-lying $d^n s^1$ excited states.

The C−H oxidative addition of alkene and alkane to the d^8 **TpML precursor** (Tp = HB(pyrazolyl)$_3$; M = Rh and Ir) experimentally shows different reactivities with respect to the isolobal CpML system. Compared to the η^2-ethene complexes, the metal vinyl hydride complexes such as CpM(H)(vinyl) are usually thermally unstable (reaction 18).[159a,b] However, in the

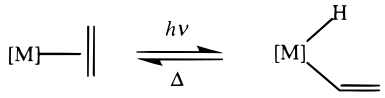

(18)

case of reaction 19, Ghosh et al.[159c] showed that the hydridovinyl isomer (**48**) is favored over the η^2-ethylene isomer (**49**) in the pyrazolylborate iridium system. According to Ghosh et al., reaction 19 proceeds with a half-life of 4.5 h at 100 °C in the dark and the only product besides **49** is a small amount (<5%) of $HB(fmpz)_3Ir(CO)_2$.

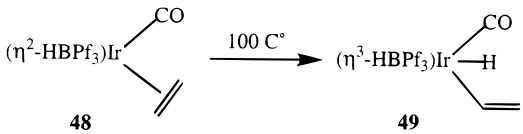

48 49 (19)

It is clearly different from an analogous pyrazolylborate rhodium system, in which the η^2-ethylene complex (**51**) is produced from the hydridovinyl complex (**50**) at 25 °C in the dark with a half-life of 3.2 min, as shown in reaction 20.

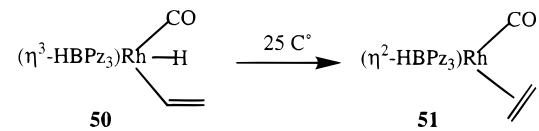

50 51 (20)

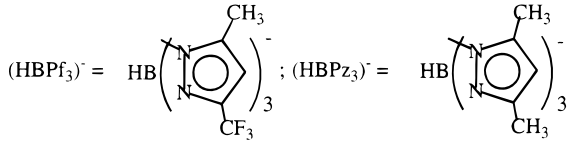

Scheme 16

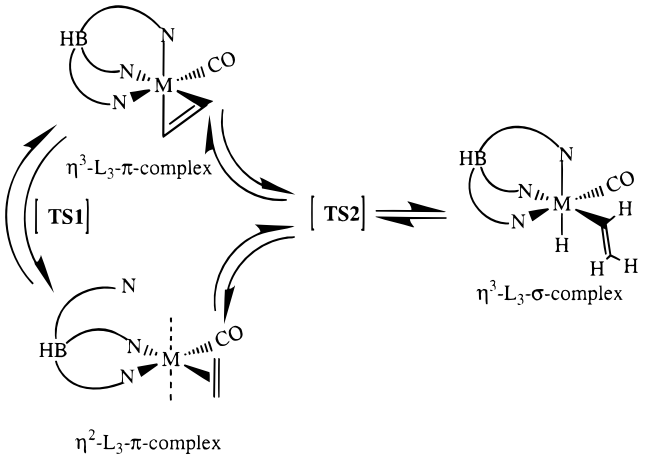

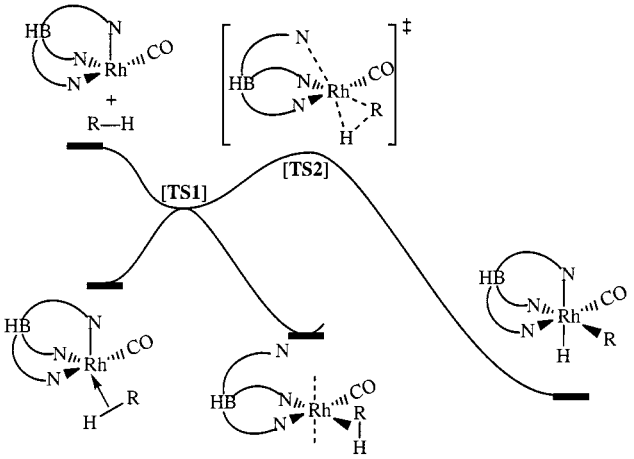

Figure 25. Potential energy profiles of the alkane oxidative addition to Tp*Rh(CO).

Recently, Hall and co-workers investigated the C−H activation reactions of methane and ethylene by model TpM(CO) (M = Rh and Ir) complexes using the RHF, MP2, and DFT methods.[160] It was found that (i) both (η^3-Tp)M(CO)(η^2-C_2H_4) and (η^2-Tp)M(CO)(η^2-C_2H_4) isomers are stable species connected by a small barrier and (ii) the subsequent reaction of these species to the oxidative-addition product (η^3-Tp)M(CO)(H)($CHCH_2$) proceeds through a single transition state from both of the ethylene isomers as shown in Scheme 16.[160a] Generally, the (η^3-Tp)M(CO)(η^2-C_2H_4) species shows d^6 octahedral structural features while the (η^2-Tp)M(CO)(η^2-C_2H_4) species shows d^8 square-planar structural features. The optimized geometries show that there are strong back-donating interactions between the metal and ethylene and between the metal and CO and that the ethene complexes are more sensitive to the steric properties of the pyrazolyborate ligands. In comparison to (η^2-Tp)M(CO)(η^2-C_2H_4), the M−(η^2-C_2H_4) back-donating interaction in (η^3-Tp)M(CO)(η^2-C_2H_4) is much stronger and the M−CO back-donating interaction is clearly weaker. In comparison to the Rh complexes, both Ir−(η^2-C_2H_4) and Ir−CO back-donating interactions are much stronger due to a stronger relativistic effects. The calculations show that (i) for M = Rh, TpRh(CO)(η^2-C_2H_4) favors the η^2-Tp form over η^3-Tp by −0.7 to −9.9 kcal/mol, while for M = Ir, TpIr(CO)(η^2-C_2H_4) favors the η^3-Tp form in all complexes; (ii) in complexes without strong steric effects, the ethylene oxidative addition is generally more endothermic for Rh than Ir; and (iii) with an increase of the steric bulk of the pyrazolyl group, the ethylene oxidative addition by the Ir complex becomes exothermic by 0.8 to 6.3 kcal/mol. These results are consistent with those experimentally observed.

Recently, Lian et al. reported time-resolved IR spectra of the photoinitiated alkane activation reaction of Tp*Rh(CO)$_2$ (Tp* = HB(3,5-dimethylpyrazolyl)$_3$).[161a] After initial photolysis and vibrational deactivation (66 ps), the spectrum shows a single intermediate with ν_{CO} of 1972 cm^{-1}. This intermediate decays with a time constant of 200 ps to a second more stable species with ν_{CO} of 1990 cm^{-1}. The latter species decays at a much slower rate to the oxidative-addition product Tp*Rh(CO)(R)(H). This result can be explained in terms of the structural nature of TpRh(CO)·CH_4. On the basis of their theoretical studies,[160] Hall and co-workers predicted that the first observed species is an (η^3-Tp*)Rh(CO)·RH precursor, which subsequently rearranges to an (η^2-Tp*)Rh(CO)·RH species with a strongly bound RH before undergoing oxidative addition to the product Tp*Rh(CO)(R)(H) as shown in Figure 25. This prediction has been confirmed by recent experimental observations.[161b]

In recent years the synthesis and isolation of the first metal complexes containing adducts of molecular hydrogen have been achieved.[162a] In the first prototypical complex studied by Kubas, the stable form of W(CO)$_3$(PR$_3$)$_2$(η^2-H_2) is a **d^6 ML_n complex**. Experimentally the W(CO)$_3$(PR$_3$)$_2$(H_2) complex has been found to be in equilibrium with the dihydride form, with the latter form 1−2 kcal/mol higher in energy for R = *i*-Pr.[162b] Jean et al. have investigated the structure of the W(CO)$_3$(PR$_3$)$_2$(η^2-H_2) complex using extended Hückel method,[163] and Hay has studied the structure and oxidative addition of the model complexes W(CO)$_3$(PR$_3$)$_2$(η^2-H_2) and W(PR$_3$)$_5$(η^2-H_2) using ab initio method.[164] The calculations show that the process of forming the seven-coordinate dihydride W(CO)$_3$(PR$_3$)$_2$(H_2) is symmetry-allowed. In ab initio studies of the model complex W(CO)$_3$(PH_3)$_2$(H_2), the results of Hay show that this oxidative addition is expected to be unfavorable, where the precursor W(CO)$_3$(PR$_3$)$_2$(η^2-H_2) is more stable by 17 and 10 kcal/mol than the reactants and the dihydride product, respectively. However, when the π-accepting CO ligands were replaced by better electron-donating PR$_3$ groups (see Scheme 17), the dihydride species becomes more stable by 14 kcal/mol than the η^2-H_2 species.

Bergman and co-workers recently reported a d^6 Ir(III) system, Cp*Ir(PR$_3$)(CH_3)$^+$ [Cp* = η^5-$C_5(CH_3)_5$], which in the solution phase and at room temperature catalyzes hydrogen exchange in methane and alkanes and generates olefin complexes.[165] Because the behavior of this Ir(III) system, Cp*Ir(PR$_3$)(CH_3)$^+$ [Cp* = η^5-$C_5(CH_3)_5$], is quite different from the now more common Ir(I) systems, Bergman and co-workers suggested two possible reaction mechanisms: (i) one

Scheme 17

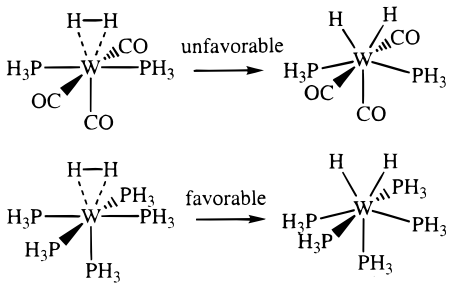

Scheme 18

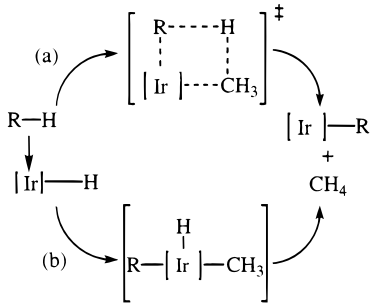

like an early-transition-metal reaction which proceeds through a σ-bond metathesis, as in Scheme 18a, or (ii) one like a late metal, which proceeds through an oxidative-addition/reductive-elimination (OA/RE) pathway, as in Scheme 18b. Although the hydrogen-exchange reaction shows a striking similarity to that reaction in early metals, σ-bond metathesis is unexpected for a late metal. On the other hand, the OA/RE pathway involves Ir(III) going to Ir(V), a fairly high oxidation state for an Ir system without electronegative ligands. Recently, several experimental and theoretical studies have been performed to elucidate the details of this reaction mechanism.[166−168]

Hall and co-workers investigated the oxidative-addition/reductive-elimination (OA/RE) reactions of methane, ethylene, and acetylene with the $CpIr(PH_3)(CH_3)^+$ (**52**) complex at the DFT and CCSD levels of theory.[166a,b] It is found that the OA reaction from $CpIr(PH_3)(CH_3)$(agostic-alkane)$^+$ (**53**) to $CpIr(PH_3)(CH_3)(H)(alkyl)^+$ (**55**) is endothermic by 4.4 and 0.8 kcal/mol with a low barrier of 11.5 and 10.0 kcal/mol at the DFT-B3LYP and CCSD levels of theory, respectively, as shown in Figure 26. The RE reaction from $CpIr(PH_3)(CH_3)(H)(alkyl)^+$ to a β-agostic complex, $CpIr(PH_3)(alkyl)^+$, is exothermic with a low barrier of 7.1 and 9.2 kcal/mol. Thus, the hydrogen-transfer reaction via an oxidative-addition/reductive-elimination (OA/RE) pathway would be a low-temperature process. Despite a careful search for the alternative σ-bond metathesis mechanism along a reaction coordinate (RC) involving both Ir−H and C−H distances, they only found a monotonic increase in energy. Thus, Hall and co-workers conclude that the σ-bond metathesis pathway does not exist for the hydrogen-transfer reaction of the $CpIr(PH_3)(CH_3)^+$ complex.[166] For the OA/RE reaction of ethylene and acetylene, a strong stabilizing interaction between either ethylene or acetylene and $CpIr(PH_3)(CH_3)^+$ leads to a high activation barrier (24−36 kcal/mol) for the OA processes for both. Compared to ethylene, the OA/RE reaction of acetylene with $CpIr(PH_3)(CH_3)^+$ complex is more favorable. Thus, the dimerization of terminal alkynes catalyzed by cationic iridium complexes is plausible.

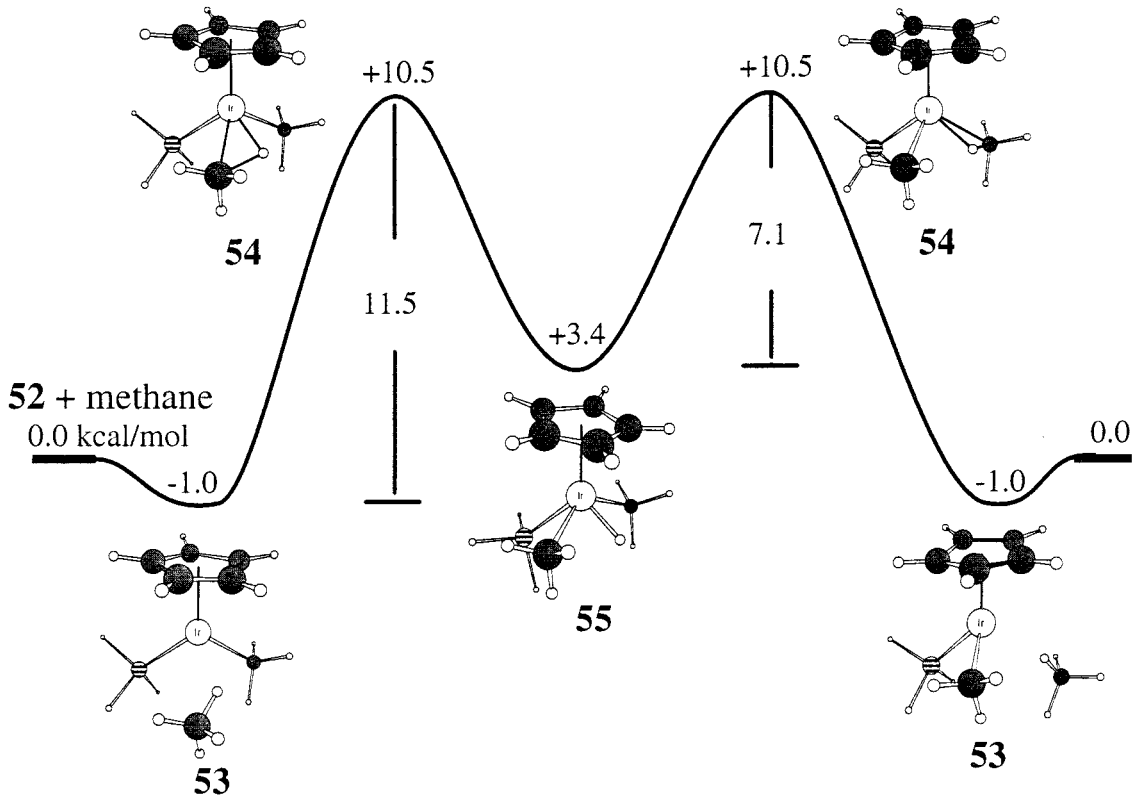

Figure 26. Potential energy profiles and geometries of the oxidative-addition and reductive-elimination reactions of methane with $CpIr(PH_3)(CH_3)^+$.

Scheme 19

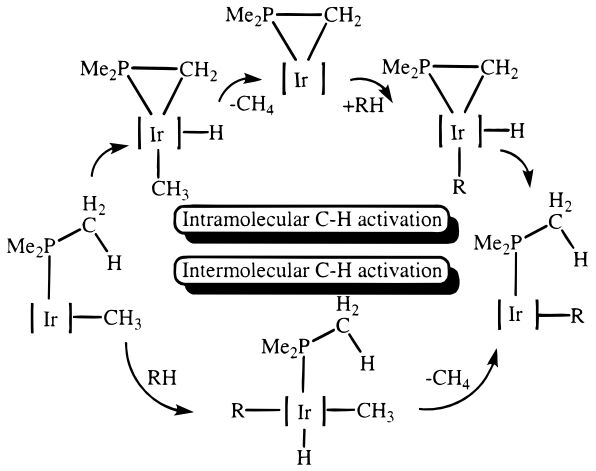

More recently, Hinderling et al. reported a combined gas-phase, solution-phase, and computational study on similar cationic iridium(III) complexes, $CpIr(PMe_3)(CH_3)^+$ [Cp = η^5-C_5H_5] (**56**) and Cp*Ir-$(PMe_3)(CH_3)^+$ (**57**).[167] They showed that intramolecular C−H activation through a cyclometalated intermediate operates in the gas phase and suggested that a similar reaction may operate in solution. Furthermore, after performing density functional theory (DFT) calculations on this system, they concluded that the C−H activation through the oxidative-addition/reductive-elimination mechanism was not operative because the calculated energy difference between the reactant, **56**, and the oxidative-addition intermediate, $CpIr(\eta^2$-$PMe_2CH_2)(H)(CH_3)^+$ (**59**), was higher than the experimentally determined activation energy for the loss of methane from **56**. Hinderling et al. suggested that the system reacts through the four-center σ-bond metathesis mechanism although they did not investigate this mechanism. Following this report, Bergman and co-workers have shown that cyclometalation can take place with cationic iridium(III) complexes in solution, but this observation depends on the nature of the phosphine ligands.[168] With the trimethylphosphine system, they have shown that **57** does not undergo intramolecular

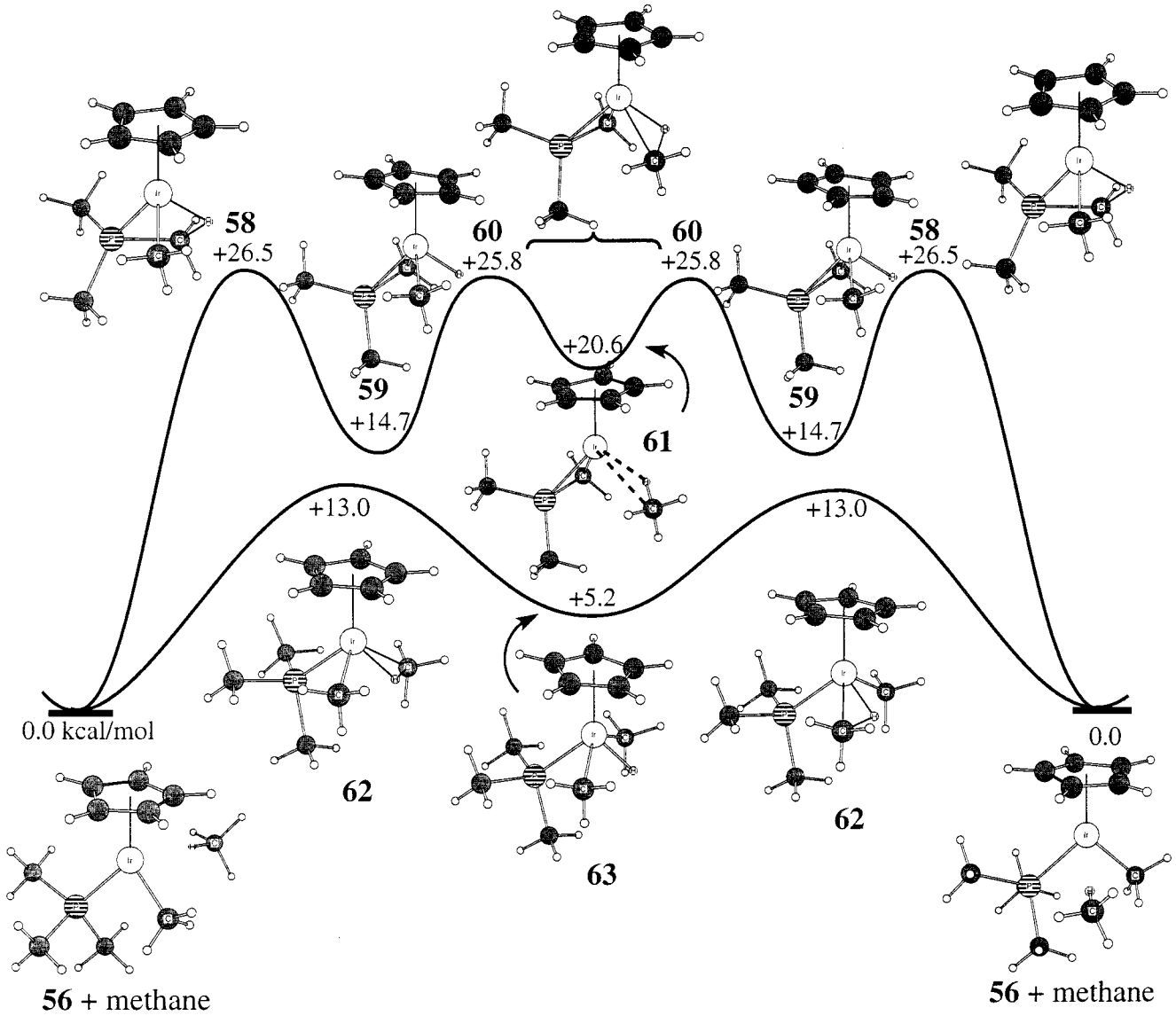

Figure 27. Potential energy profiles and geometries along the intermolecular C−H activation pathway and the intramolecular pathway.[166c]

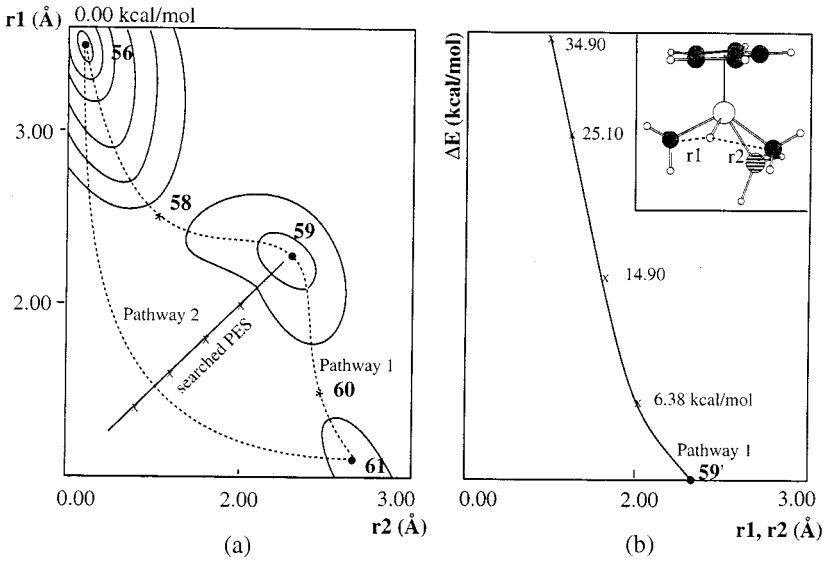

Figure 28. (a) Illustration of the potential energy surface (PES) of the reaction for the intramolecular C−H activation process. Pathway 1 is the oxidative-addition/reductive-elimination pathway, and pathway 2 is the hypothetical σ-bond metathesis pathway. (b) Searched PES along the C−H coordinates (r_1 = CH_3−H and r_2 = $P(H)_2CH_2$−H) from pathway 1 to pathway 2.[166c]

C−H activation in solution via a cyclometalated intermediate.

To elucidate this reaction process, Niu and Hall examined the inter- and intramolecular C−H activation with $CpIr(PMe_3)(CH_3)^+$ [Cp = η^5-C_5H_5] (**56**) and methane (Scheme 19) via both oxidative-addition/reductive-elimination and σ-bond metathesis pathways using the DFT and CCSD methods with the ZPE correction.[166c] From Figure 27, it is clear that along the intermolecular C−H activation process (lower curve in Figure 27), from reactants, $CpIr(PMe_3)(CH_3)^+$ (**56**) and methane, to products, only a single oxidative-addition intermediate, **63**, is found at 5.2 kcal/mol above the reactants. The reaction barrier is only 13.0 kcal/mol at the B3LYP/BS1 level. The reaction along the intramolecular oxidative-addition mechanism from reactant, **56**, to the intermediate, **59**, is endothermic by 14.7 kcal/mol with an activation barrier of 26.5 kcal/mol, while the reductive-elimination reaction from **59** to **61** is endothermic by 5.9 kcal/mol with a barrier of 11.1 kcal/mol at the B3LYP level. Despite a careful search for a σ-bond metathesis pathway for both the inter- and intramolecular C−H activation processes as illustrated in Figure 28, again none was found. To obtain more quantitative results, they reoptimized the geometries of the reactants, intermediates, transition states, and products for both the intra- and intermolecular C−H activation processes using the B3LYP method with the polarized basis sets. The calculations show that the intramolecular oxidative-addition barrier from **56** to **59** is reduced to 21.1 kcal/mol, while the intermolecular oxidative-addition barrier from **56** to **63** is reduced to 9.6 kcal/mol. After the zero-point energy (ZPE) corrections, the intramolecular oxidative-addition barrier is further reduced to 18.4 kcal/mol,[15] a value that compares favorably with the experimental value of 13.6 ± 2 to 16.6 ± 2 kcal/mol at 0 K.[5b,16]

Thus, the theoretical results of Niu and Hall show that the intermolecular C−H activation is a lower-energy process and that both inter- and intramolecular C−H activation proceed only through an oxidative-addition mechanism. Compared to the intramolecular C−H activation process, the intermolecular C−H activation process is a lower energy process. A cyclometalated intermediate for the ligand PMe_3 will be observed under reaction conditions without added hydrocarbon because CH_4 loss in **56** leads to an equilibrium favoring the cyclometalated complex. However, in the presence of added hydrocarbon, an intermolecular C−H activation process is favored over an intramolecular one because of its lower activation barrier.

Su and Chu also studied the C−H bond activation of methane by coordinatively unsaturated d^6 $CpM(PH_3)(CH_3)^+$ (M = Rh, Ir) complexes using the MP2 and QCISD methods.[169] Of the two possible mechanisms (Scheme 18), an OA/RE process and a σ-bond metathesis mechanism, only the former is found for the d^6 Ir cation while the Rh case might adopt the latter. Su and Chu explain the kinetic and thermodynamic differences between the Ir and Rh complexes in terms of singlet−triplet gaps of complexes based on a frontier molecular orbital (FMO) model.

Recently, Niu and Hall expanded their investigation of the C−H bond activation mechanisms of methane by d^6 $CpM(PH_3)(CH_3)^+$ (M = Co, Rh, Ir) complexes with B3LYP and CCSD methods.[166d] For M = Ir, the C−H activation reaction favors an OA/RE process with a low activation barrier, for M = Co, the reaction proceeds along a σ-bond metathesis path with a high activation barrier, and for M = Rh, the reaction adopts a transitional mechanism somewhere between the OA/RE and the metathesis paths as shown in Figure 29. Niu and Hall point out that during the OA/RE process (Scheme 20), the Cp ring of the intermediate $CpIr(PH_3)(CH_3)_2(H)^+$ is clearly slipped with respect to the reactant $CpIr(PH_3)(CH_3)^+$, along the oxidative-addition path, going from the precursor through TS to the OA product, the Ir−Cp and Ir−CH_3 distances are increasing and the Cp ring

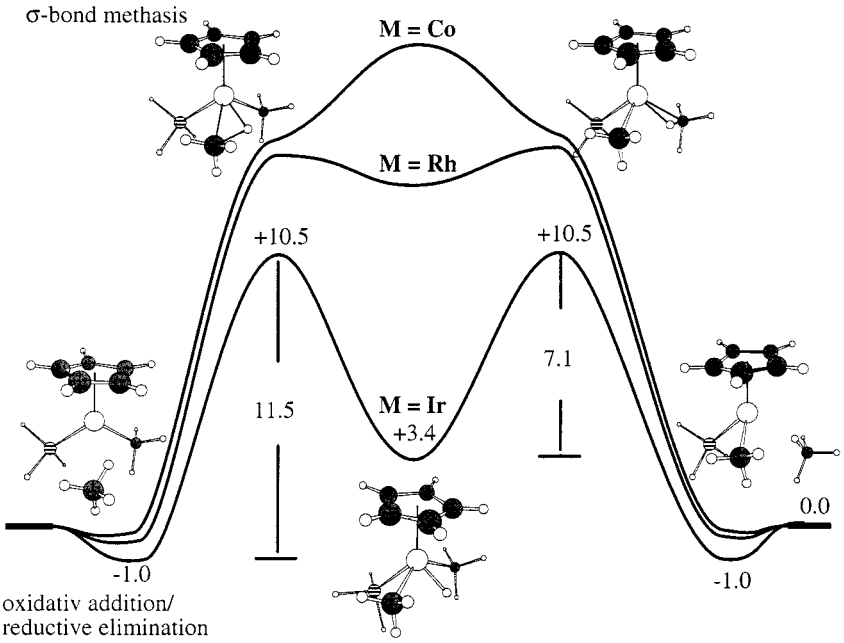

Figure 29. Potential energy profiles of the oxidative-addition and reductive-elimination reactions of methane with $CpM(PH_3)(CH_3)^+$ (M = Co, Rh, Ir).

Scheme 20

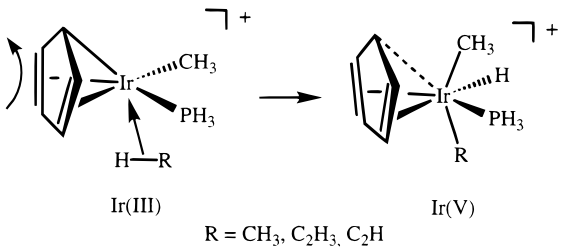

slips more at each step. Thus, both relativistic effects and spectator ligand effects play important roles in the hydrogen-transfer mechanism.

Niu and Hall have also studied the C−H activation process in alkane dehydrogenation catalyzed by the Ir(III) complexes: (PCP′)Ir(H)$_2$ [PCP′ = η^3-$C_6H_3(CH_2PH_2)_2$-1,3] and $CpIr(PH_3)(H)^+$ using the B3LYP method.[125] In the key role played by the spectator ligand systems, PCP′(H) vs $Cp(PH_3)$, the former increases the energy of the metal−ligand fragment's triplet state relative to that of the singlet and thus destabilizes all the Ir(V)-like species.

D. σ-Bond Metathesis Reactions

The σ-bond metathesis reaction between added hydrocarbon and L_nM-R is one of the important reactions in oligomerization and polymerization processes.[1−3] It is well-known that in olefin metathesis alkylidene units are exchanged through a $[2_\pi + 2_\pi]$ cycloaddition pathway (the Chauvin mechanism) as in reaction 21.[170]

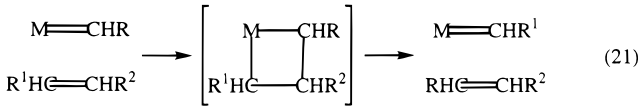
(21)

Hydrogen transfer through σ-bond metathesis involves a $[2_s + 2_s]$ process (reaction 22). Generally,

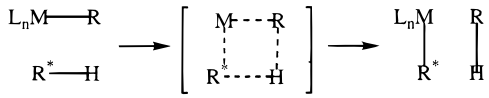
(22)

σ-bond metathesis reactions have been studied for complexes of electron-poor early transition metals and f-block elements. Early theoretical investigations on metathesis reactions have been reviewed.[3]

In the previous theoretical studies with the GVB method, Steigerwald and Goddard showed that the hydrogen transfer between H_2 and Cl_2M-H (M = Ti^+, Ti, Sc) proceeds by a mechanism similar to that shown in reaction 22 with activation barriers of 2, 22, and 17 kcal/mol for Ti^+, Ti, and Sc, respectively.[172] Rappé studied the reaction of a scandium hydride complex with acetylene via two competing pathways, insertion and σ-bond metathesis.[100] His GVB and CI calculations showed that both acetylene insertion into the Sc−H bond and σ-bond metathesis have activation barriers of about 6 kcal/mol.

Ziegler and co-workers presented a systematic study on σ-bond metathesis reactions of R*−H with L_2M-R (M = Sc, Lu; L = Cl, Cp; R = H, CH_3, SiH_3, C≡CH, CH=CH_2; R* = H, CH_3, SiH_3) with DFT methods.[173] They found that all these σ-bond metathesis reactions initially yield adduct complexes (**65**) as shown in Figure 30 and proceed through a four-centered transition state (**66**) to the second adduct complex (**67**), followed by formation of products (**68**). As seen from Table 22, where the calculated energetics for these reactions are summarized, the σ-bond metathesis reaction of H−H with L_2M-R (M = Sc, Lu; L = Cl, Cp; R = H, CH_3, SiH_3) takes place with an activation barrier of 2.1−20.0 kcal/mol and goes easily in the order of Sc > Lu and H > SiH_3 > CH_3. Generally, the reactivity of the σ-bond metathesis between R*−H and L_2M-R are in the order for R* of C≡CH ≫ CH=CH_2 ≈ H > CH_3 for R = H, then C≡CH ≫ H > CH_3 > CH=CH_2 for R = CH_3, and

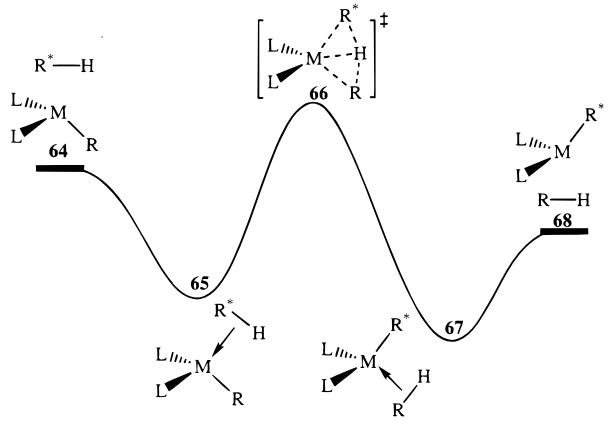

Figure 30. Potential energy profiles of the R−H activation along the σ-bond metathesis mechanism.

Table 22. Calculated Energytic Parameters (kcal/mol)[a] by Ziegler and Co-workers for σ-Bond Metathesis Reactions, $L_2M-R + R^*-H$ to $L_2M-R^* + R-H$

L_2M-R	R^*-H	**65**	**66** (TS)	**67**	**68**	ref
Cp_2Sc-H	H_2	−3.8	−1.7	−3.8	0.0	173a
	CH_4	−4.8	11.9	5.9	10.0	173a
	C_2H_4	−2.9	−4.8	0.7	3.8	173b
	C_2H_2	−8.8	−6.9	−25.8	−20.5	173b
Cp_2Sc-CH_3	H_2	−4.1	1.9	−14.8	−10.0	173a
	CH_4	−6.0	10.8	−6.0	0.0	173a
	C_2H_4	−2.9	9.3	11.5	−6.2	173b
	C_2H_2	−4.3	−0.9	−37.5	−30.6	173b
Cl_2Sc-CH_3	H_2	−6.7	1.0	−11.9	−1.9	173b
	CH_4	−10.8	7.9	−10.8	0.0	173b
$Cl_2Sc-SiH_3$	H_2	−1.9	1.0	−8.4	−0.7	173b
	SiH_4	−7.4	0.2	−7.4	0.0	173b
Cl_2Lu-H	H_2	−1.2	10.6	−1.2	0.0	173c
	CH_4	−1.9	23.7	3.7	4.1	173c
Cl_2Lu-CH_3	H_2	−0.4	19.6	−6.0	−4.1	173c
	CH_4	4.6	25.9	4.6	0.0	173c

[a] Relative to reactants.

SiH_3 > H for R = SiH_3. These trends can be explained in terms of the strength of the Sc−R bonds: C≡CH (−129.6 kcal/mol) ≫ CH=CH_2 (−81.1) ≈ H (−81.6) > CH_3 (−70.8). Although insertion of ethylene and acetylene into Sc−H and Sc−CH_3 bonds are preferred thermodynamically over the alternative alkenylic and alkynylic σ-bond metathesis, the low activation barrier of 1.9 and 3.4 kcal/mol and the exothermicity by 20.5 and 30.6 kcal/mol for the σ-bond metathesis of acetylene with Cp_2ScH and Cp_2ScCH_3 show a kinetically favorable process. Actually, acetylene has been observed to prefer alkynylic C−H activation over insertion for scandium.[174]

Recently, Hyla-Kryspin et al. investigated σ-bond metathesis and insertion reactions of acetylene with Cl_2ZrH^+ and $Cl_2ZrCH_3^+$ based on all-electron HF and MP2 ab initio calculations with split-valence basis sets of double- and triple-ζ quality.[70c] At the MP2//HF level, the acetylide-complex formation reaction by Cl_2ZrH^+ and $Cl_2ZrCH_3^+$ is calculated to have a barrier of 15.8 and 20.8 kcal/mol and to be −44.4 and −18.9 kcal/mol exothermic, respectively. Unlike the scandium system, the agostic adduct complex $Cl_2ZrR(C_2H_2)^+$ cannot be observed, and thus, both σ-bond metathesis and insertion reactions arise from a common adduct complex, $Cl_2ZrR(\eta^2\text{-}C_2H_2)^+$. Thus,

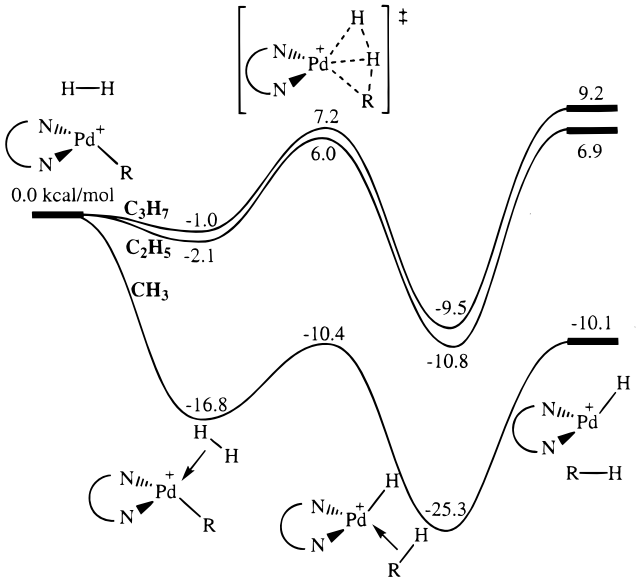

Figure 31. Potential energy profiles of the hydrogenolysis reactions of H_2 to L_2PdR^+ for R = CH_3, C_2H_5, and C_3H_7.

insertion reactions are kinetically and thermodynamically favored over the corresponding σ-bond metathesis reactions for zirconium.

In their studies of the mechanism of the palladium(II)- and nickel(II)-catalyzed ethylene polymerization reaction, Musaev et al. also investigated the chain termination process through the hydrogenolysis reaction with the B3LYP method.[89d,f] Generally, the hydrogenolysis reaction may occur in the presence of hydrogen gas pressure and proceeds via a σ-bond metathesis mechanism to eliminate alkane and to generate a diimine−Pd−hydride complex as shown in Figure 31. It has been found that the coordination energy of H_2 to L_2PdR^+ is 16.8, 2.1, and 1.0 kcal/mol for R = CH_3, C_2H_5, and C_3H_7, respectively. The barrier heights calculated relative to the dihydrogen complexes are 6.4, 8.1, and 8.2 kcal/mol, respectively. The preliminary calculations show that an alternative pathway corresponding to the oxidative addition of H−H to the Pd center followed by reductive elimination of alkane seems to be energetically unfavorable and unlikely to participate. The alkanes dissociation step is calculated to be endothermic by 15.2, 17.7, and 18.7 kcal/mol for RH = CH_4, C_2H_6, and C_3H_8, respectively. Overall, the hydrogenolysis reactions from $L_2PdR^+ + H_2$ to $L_2PdH^+ + RH$ are exothermic by 10.1 kcal/mol for R = CH_3 and endothermic by 6.9 and 9.2 kcal/mol for R = C_2H_5 and C_3H_7, respectively. In a comparison of various chain transfer and termination processes, β-H transfer + dissociation, β-H transfer + associative displacement, H exchange, and hydrogenolysis, hydrogenolysis is found to be an efficient chain termination process. The hydrogenolysis reactions from $L_2NiR^+ + H_2$ to $L_2NiH^+ + RH$ along the σ-bond metathesis mechanism show a similar behavior.[89d]

Das et al. examined the effects of solvation upon the energetics of the chain termination processes through the hydrogenolysis reaction employing continuum and explicit representations of the solvent (toluene).[66i] Relative enthalpies and free energies for

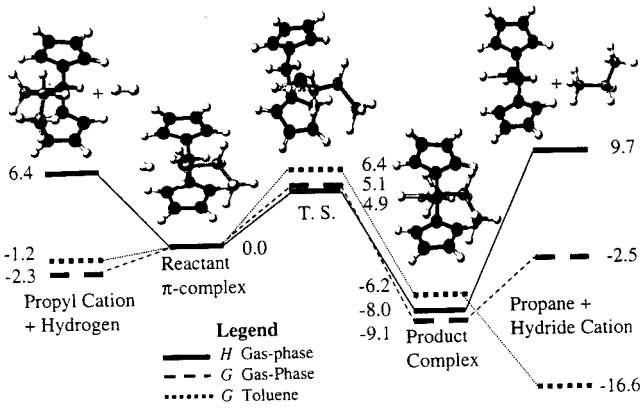

Figure 32. Relative enthalpies (ΔH, kcal/mol) and free energies (ΔG, kcal/mol) in the gas phase (H and G Gas-Phase) and toluene (G Toluene) for the hydrogenolysis reaction from $(CpCH_2Cp)ZrCH_2CH_2CH_3^+ + H_2$ to $(CpCH_2Cp)ZrH^+ + C_3H_8$. (Reprinted with permission from ref 66i. Copyright 1999 Oxford University Press.)

the hydrogenolysis reaction from $(CpCH_2Cp)ZrCH_2CH_2CH_3^+ + H_2$ to $(CpCH_2Cp)ZrH^+ + C_3H_8$ are shown in Figure 32. Again, one can see that solvation effects are also pronounced in the termination reaction steps, where solvation reduces the free energy changes for the alkane separation (dissociation) into products by approximately 17 kcal/mol. Thus, in the solution phase, the hydrogenolysis reaction is exothermic by 16.4 kcal/mol with an activation barrier of 6.4 kcal/mol; the reaction is also an efficient chain termination process in the presence of a hydrogen pressure for zirconocene-based catalytic cycles.

In previous work, Ziegler and co-workers studied metathesis reactions of H_2 and SiH_4 with $Cp_2Ti{=}SiH_2$ using the DFT method.[175] The results of the computations for this type of metathesis indicate that the first reaction can proceed to generate $Cp_2Ti(H)(SiH_3)$ with a low activation barrier of 6.0−7.4 kcal/mol and an enthalpy of −9.6 kcal/mol. The second reaction from $Cp_2Ti{=}SiH_2 + SiH_4$ to $Cp_2Ti(H)(SiH_2SiH_3)$ is found to be exothermic (ca. −11.5 kcal/mol) with an activation barrier of ca. 2.9 kcal/mol.

Recently, using B3LYP method, Siegbahn and Crabtree[176] studied the mechanism of the Shilov reaction,[177] the activation of alkane C−H bonds by Pt salts in aqueous acid solution. The calculated results suggest that the Shilov reaction proceeds via transfer of a hydrogen atom from a methane σ complex, first to a neighboring Cl ligand in what is best described as a σ-bond metathesis and then to the solvent, water. The breaking of a C−H bond in methane occurs in two steps. In the "first step" methane is coordinated to the metal. The energy requirement for this step is 10.5 kcal/mol for the best model used here. In the "second step" the C−H bond is broken with a calculated barrier for the σ-bond metathesis pathway of 16.5 kcal/mol. The sum of these two energies is 27 kcal/mol, a value which is in very good agreement with the experimental estimate of 28 kcal/mol. Although the σ-bond metathesis mechanism seems more likely for Shilov chemistry, the oxidative-addition/reductive-elimination sequence cannot be excluded in this Pt case, where a slightly lower barrier of 24 kcal/mol was obtained. However,

Scheme 21

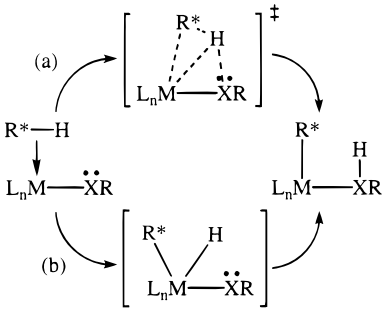

entropy effects were neglected since they cannot be well predicted using the present model.

More recently, Dedieu and co-workers investigated a series of σ-bond metathesis reactions between H_2/CH_4 and late-transition-metal complexes at the MP2 and QCISD(T) levels of theory.[178] In this type of σ-bond metathesis reaction, the hydrogen of R−H directly transfers to the ligand with the additional lone pair through a four-centered TS, giving a metal hydride complex as shown in Scheme 21a, which could be competitive with the OA/RE pathway (Scheme 21b). Generally, this type of reaction is a feasible pathway (at least in the gas phase). The calculations show that any d^8 T-shaped ML_3 or d^6 square-pyramidal ML_5 system which has one ligand with such an additional lone pair not engaged in the bond to the metal should be a good candidate for these [2 + 2] reactions.

E. Nucleophilic Addition and Electrophilic Elimination

Nucleophilic additions to coordinated unsaturated alkene or dihydrogen are important elementary reactions in both organometallic and bioinorganic systems. Early theoretical studies on nucleophilic addition[179] at various levels from semiempirical to ab initio have been previously reviewed.[3] Generally, dihydrogen or an unsaturated ligand such as olefin, carbonyl, and carbene is attacked by a nucleophilic group to form an "ion-pair" (reaction 23 and 24).

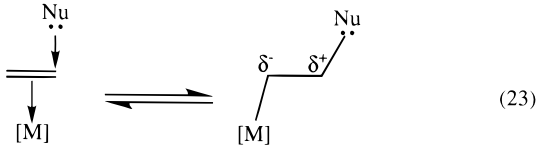

(23)

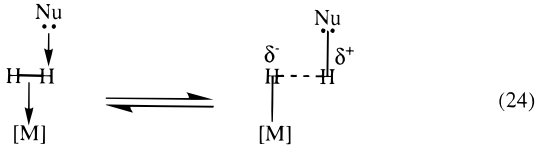

(24)

In recent work, using large basis sets and accounting for solvent effects, Siegbahn investigated the first two steps in the Wacker process, the nucleophilic addition of a hydroxyl group followed by the β-hydrogen transfer to generate a π-coordinated vinyl alcohol complex.[180] The most important new result is found in the nucleophilic addition step, where it is

Scheme 22

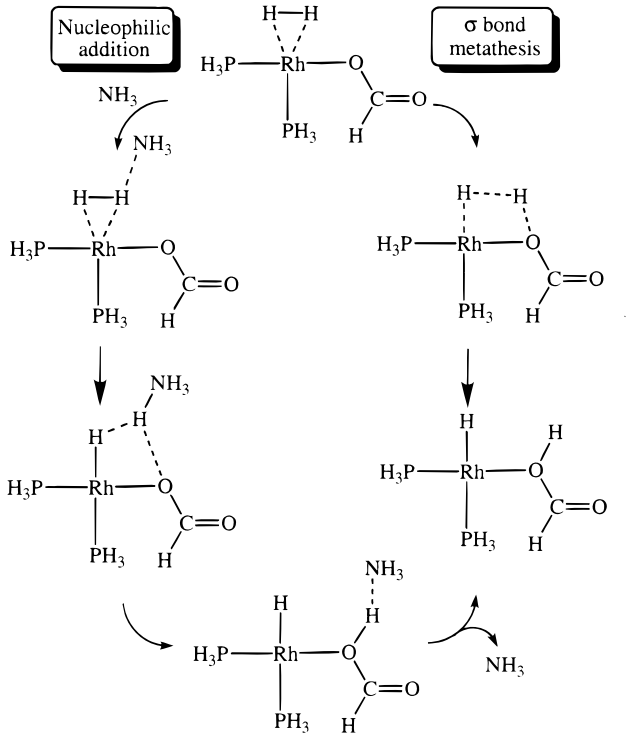

shown that the nucleophile should be modeled by a chain of, at least, three water molecules to bridge from the point of attack on the olefin to the negative chloride ligand. The $H_5O_2^+-Cl^-$ ion pair is formed simultaneously as the nucleophilic addition occurs in a concerted way with a low barrier of 5.7 kcal/mol. The exothermicity for trans and cis attacks is −4.5 and −0.4 kcal/mol, respectively. Since charge separation occurs in this step, solvent effects are quite important.

More recently, Dedieu and co-workers studied the cleavage of H_2 by the nucleophilic addition of an amine to $[Rh(H_2)(PH_3)_2(O_2CH)]$ at the MP2 level.[178d,e] The calculations show that the amine can attack the coordinated H_2 and then relay the proton through the ion-pair intermediate, $[Rh(H)(PH_3)_2(O_2CH)^-\cdots NH_4^+]$ to the formate ligand as shown in Scheme 22. The overall process in the presence of an external amine is exothermic by 13.6 kcal/mol with the two quite low barriers of <2 kcal/mol. At the MP2//MP2 level, the unassisted (no amine) reaction is endothermic by 1 kcal/mol with a barrier of 11 kcal/mol. Thus, both the kinetics and thermodynamics of the heterolytic splitting of H_2 are favored in the presence of an external nucleophilic group. Dedieu and co-workers also investigated the reverse process of reaction 24, which generates dihydrogen from a system having a Rh−H···H−N "dihydrogen bond".[178d,e] This term, coined by Crabtree, refers to an intra- or intermolecular interaction M−H···H−X between a conventional hydrogen-bond donor as the weak acid component and a metal hydride bond as the weak base component.[181] The calculated results by Dedieu et al. showed that the corresponding energy barrier, $[Rh(H)(PH_3)_2(O_2CH)^-\cdots NH_4^+]$ to $[Rh(H_2)(PH_3)_2(O_2CH)\cdots NH_3]$, is very low, 1.4 kcal/mol.

Scheme 23

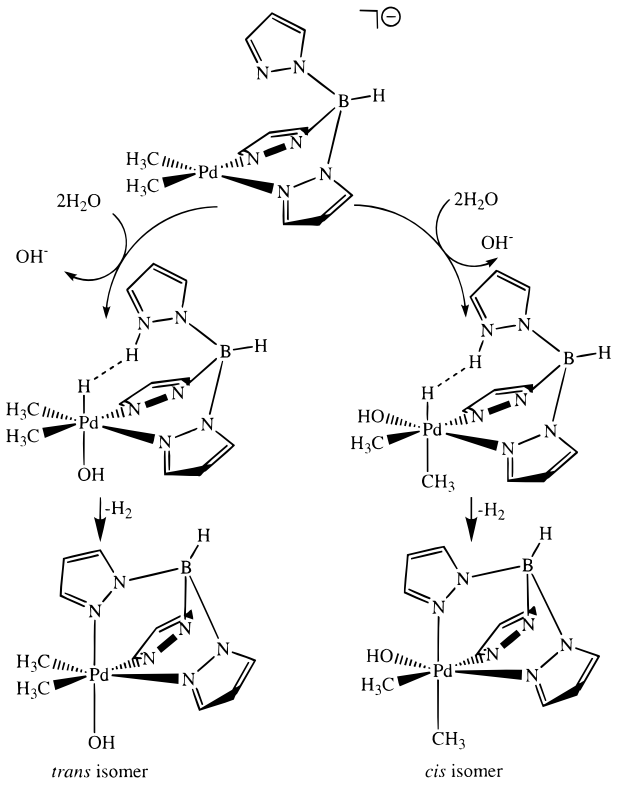

In early theoretical investigations of NH_3 to ethylene coordinated to $Pd(II)(F)_m(NH_3)_{3-m}^n$ with $(m, n) = (1, +1)$, $(2, 0)$, or $(3, -1)$ and $Pd(II)F(PH_3)_2$, Sakaki et al. have found that nucleophilic addition to the cationic complex was easier than that to the neutral and anionic complexes because of the favorable electrostatic interaction, large charge transfer, and small exchange repulsion.[179f] The analysis of electron reorganization upon nucleophile attack shows a strong trans effect. In a similar study, Fujimoto and Yamasaki found that the low-lying vacant d orbital of $PdCl_2(H_2O)$ is more effectively used for charge transfer, polarization, and reduction of exchange repulsion in nucleophilic addition than that of $Pd(Cl)_3^-$.[179e] In an experimental and theoretical study, Peris et al. showed that the magnitude of the Ir−H···H−N interaction can be as great as 5.8 kcal/mol.[182] In their study of the reduction of water to H_2 mediated by bis-alkyl tris(pyrazolyl)borate Pd(II) complexes (Scheme 23),[178d,f] Dedieu and co-workers showed that the energy barrier for this elimination depends on the nature of the Pd−H bond. More recently, Siegbahn,[183] Hall,[184] and co-workers have investigated H_2 oxidative in [NiFe] *D. gigas* hydrogenase using the B3LYP method. Here, dihydrogen activation may involve proton transfer to a cysteine residue and is more exothermic on the Ni(III) species than on the corresponding Ni(II) or Ni(I) species.

VI. Other Catalytic Processes

Because sequences of elementary organometallic reactions can be combined to form catalytic cycles, complex catalytic reactions are amenable to theoretical study. Furthermore, the development of computational techniques, such as the ab initio molecular

Scheme 24

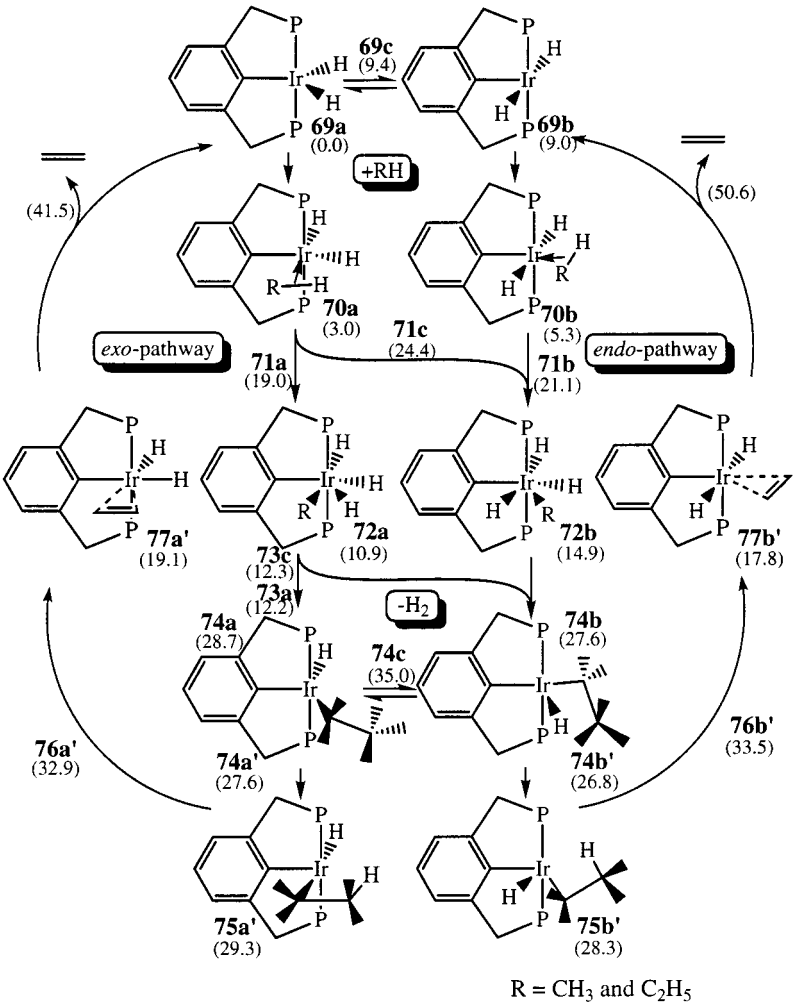

orbital (MO) theory and density functional theory (DFT), has made it possible to carry out kinetic and thermodynamic simulations for catalytic processes and to provide insight into the mechanism of reactions for the rational design and exploration of potential catalysts. Several theoretical studies have been published on the full catalytic cycles for systems such as olefin hydrogenation, olefin hydroformylation, olefin hydroboration, and acetylene silastannation.[3] Recently, together with new experimental findings, theoretical studies of alkane dehydrogenation, CO_2 hydrogenation to formic acid, olefin/CO alternating copolymerization, and olefin polymerization by homogeneous transition-metal catalysts have been reported.

A. Alkane Dehydrogenation

Alkane dehydrogenation catalyzed by transition-metal complexes is a useful process for making various alkene feedstocks from alkanes (reaction 25).[1]

$$\text{Alkanes} \xrightarrow{\text{cat.}} \text{Alkenes} + H_2 \qquad (25)$$

Hall, Niu, and co-workers have reported a series of theoretical studies on alkane dehydrogenation catalyzed by Ir(III) complexes.[125,166] These studies are prompted by the recent experimental findings in this field.[165,185−187] Generally, dehydrogenation of alkanes to produce alkenes, in addition to being highly endothermic (experimentally about 33 kcal/mol), is a symmetry-forbidden reaction and would have an extremely high barrier without a catalyst.[186] Thus, the reaction usually proceeds only under UV irradiation or in the presence of a hydrogen acceptor. Even with a catalyst, the reaction still requires energy and typically occurs only at higher temperatures.[185a] In early work, Crabtree and co-workers described an Ir(III) system, $Ir(H)_2(Me_2CO)(PPh_3)_2^+$, which thermally dehydrogenates cyclopentenes to cyclopentadienyl complexes.[185] Recently, Bergman and co-workers reported another Ir(III) system, $Cp^*Ir(PMe_3)(CH_3)^+$ [$Cp^* = \eta^5$-$C_5(CH_3)_5$], which thermally activates alkanes in the solution phase at unprecedentedly low temperatures to generate olefin complexes.[165] Most recently, Goldman, Jensen, Kaska, and co-workers describe an iridium (III) catalytic system, (PCP)Ir(H)$_2$ [PCP = η^3-$C_6H_3(CH_2PBu^t_2)_2$-1,3], which catalyzes the dehydrogenation of cycloalkanes to the corresponding cycloalkenes and dihydrogen in refluxing cycloalkane (about 200 °C).[187]

On the basis of experimental and theoretical studies on elementary reactions involving iridium(III) systems, Niu and Hall considered two possible path-

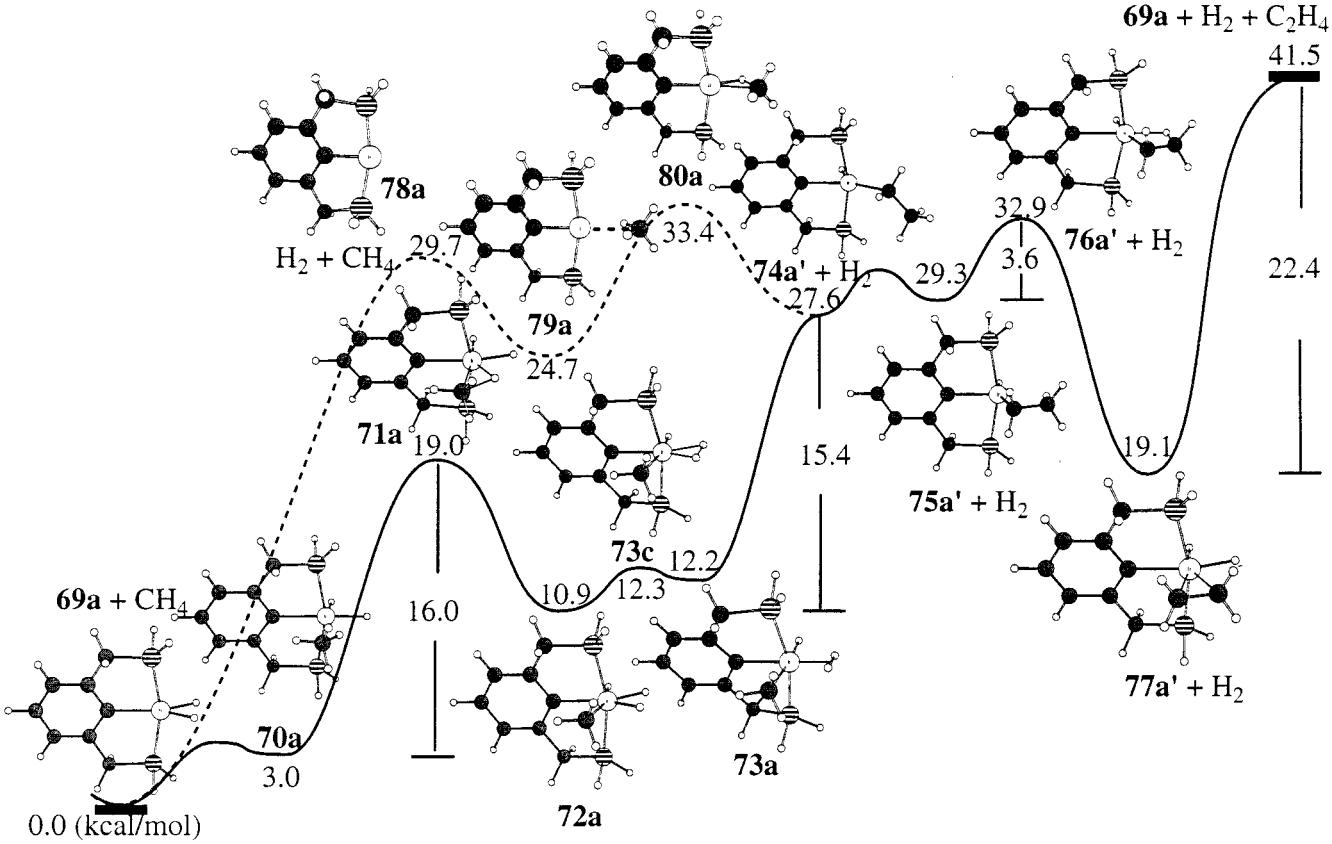

Figure 33. B3LYP potential energy profiles of alkane dehydrogenation along the *exo*-pathway from **69a** and methane/ethane to **69a**, H_2, and C_2H_4. In the OA/RE reaction stage, the energy values are relative to the total energy of reactants, **69a** and CH_4. In the β-H-transfer reaction stage, the energy values are relative to the total energy of reactants, **69a** and C_2H_6.

ways for the alkane dehydrogenation reaction by $(PCP')Ir(H)_2$ [PCP′ = η^3-$C_6H_3(CH_2PH_2)_2$-1,3].[125] As shown in Scheme 24, $(PCP')Ir(H)_2$ exists as two isomers **69a** and **69b**, which differ primarily in the H−Ir−H angle. The *exo*-pathway begins with **69a**, while the *endo*-pathway begins with **69b**. Both pathways proceed from alkane OA and H_2 RE through alkyl β-H transfer and olefin elimination. The calculated relative energies for these two reaction paths at the B3LYP level are shown in Scheme 24. Because of the large energy difference in the olefin elimination steps, the overall reaction favors the *exo*-pathway over the *endo*-pathway. The stationary points and energy profiles along the *exo*-pathway are shown in Figure 33. The alkane dehydrogenation involves the oxidative addition of alkane to form a seven-coordinate iridium(V) alkyl hydride intermediate, followed by the dihydride reductive elimination to a five-coordinate iridium(III) alkyl hydride complex. Both steps are endothermic by 11−15 kcal/mol with moderate activation barriers of 16−19 kcal/mol. Then the reaction proceeds by alkyl β-H transfer to generate an olefin π complex, followed by olefin elimination which returns the system for the next catalytic cycle. The β-H transfer has a low barrier of 4 kcal/mol that forms a relatively stable resting state (π complex), which has a dissociation barrier of 22 kcal/mol. Since in solution the endothermicity for the olefin dissociation would be reduced by solvation of the regenerated catalyst, either alkane OA or H_2 RE could be the rate-determining step. These three similar, low-energy

Scheme 25

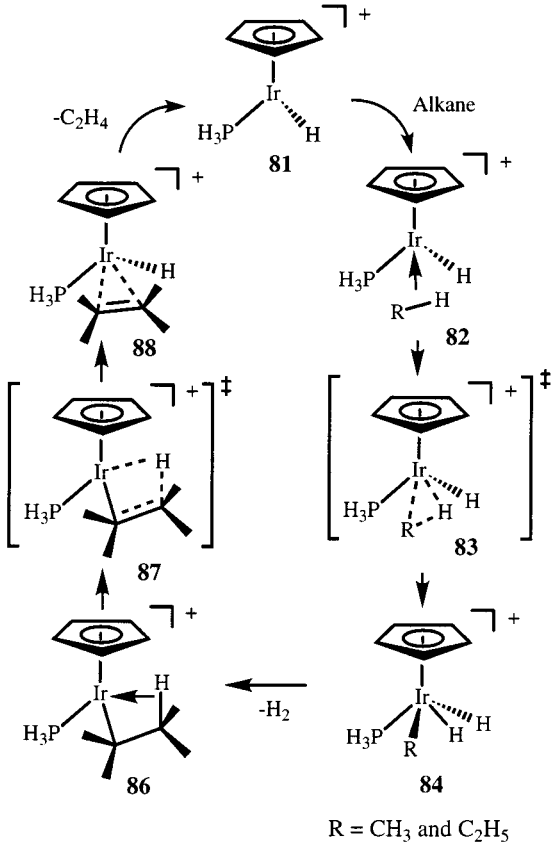

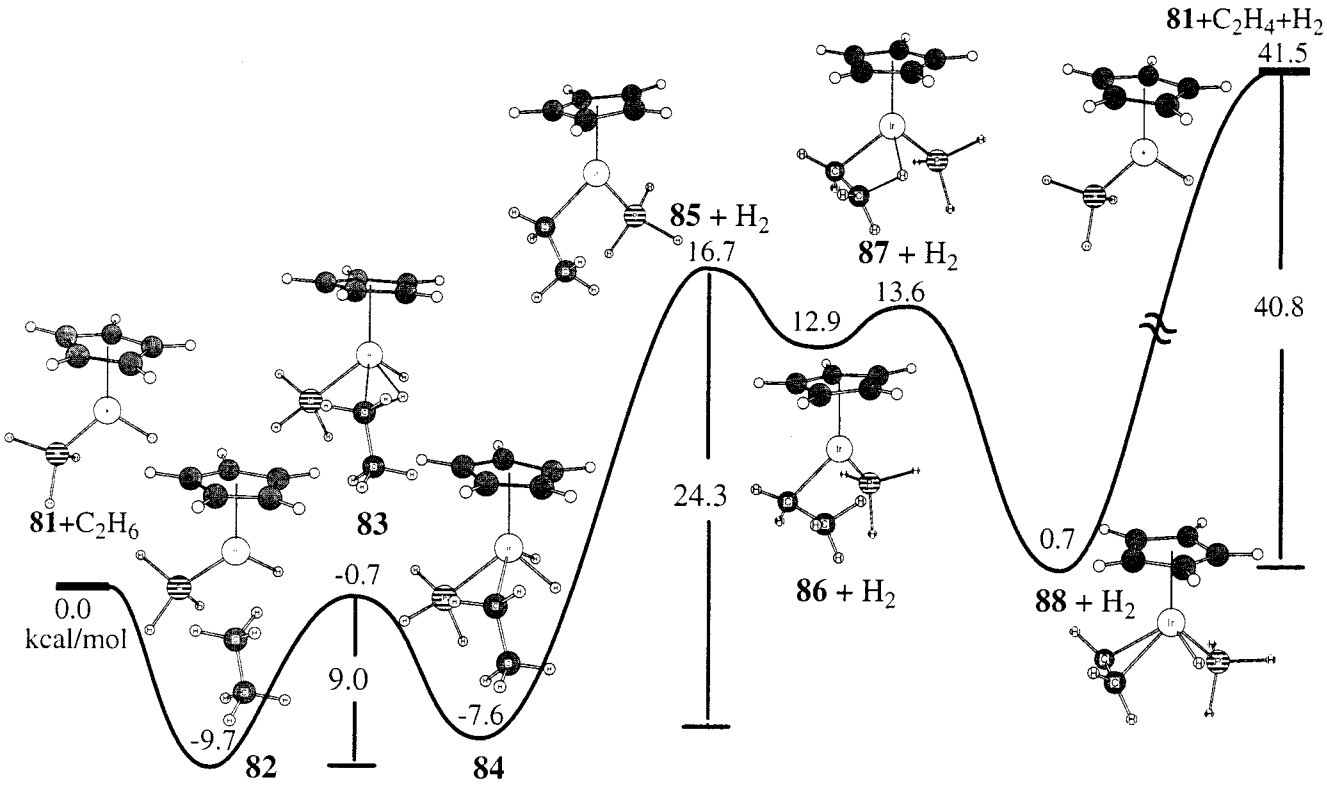

Figure 34. B3LYP energy profiles of ethane dehydrogenation along the OA/RE and β-H transfer pathways from **81** and C_2H_6 through **82′**−**88′** to **81**, H_2, and C_2H_4.

barriers provide a balance in the catalytic cycle of the alkane dehydrogenation by (PCP′)Ir(H)$_2$ so that the reaction's endothermicity is achieved gradually. Although there is another possible reaction pathway from **69a** along Ir(I) species (**78a**, **79a**, and **80a**) to **74a**, the calculations show that these paths have higher barriers.

Niu and Hall also investigated the alkane dehydrogenation process by the CpIr(PH$_3$)(H)$^+$ complex, shown in Scheme 25.[125] This process is somewhat similar to that of (PCP′)Ir(H)$_2$ as the reaction proceeds from alkane OA and H_2 RE through alkyl β-H transfer and olefin dissociation. Overall, as shown in Figure 34, the ethylene dehydrogenation by **81** to the iridium π-complex **88** and H_2 is slightly endothermic. The rate-determining step in the activation of ethane to form olefin complex by CpIr(PH$_3$)(H)$^+$ is the dihydride reductive-elimination step. Although in solution the endothermicity for the dissociation would be reduced by solvation of the regenerated catalyst, olefin elimination seems to be the critical step for this complex's dehydrogenation cycle. The high olefin dissociation energy of 40.8 kcal/mol (**88** to **81** + C_2H_4) is consistent with the fact that only intermediates such as **88** have been observed experimentally and that the Cp*Ir(PMe$_3$)(R)$^+$ system is not catalytic. The higher stability of the Ir(V) complex and the π complex (which has some Ir(V) character) in the CpIr(PH$_3$)(H)$^+$ system is responsible for these differences in the energy of the critical steps. These differences in reactivity can be traced to the singlet−triplet energy splitting of the metal ligand fragments (PCP′)Ir(H) vs CpIr(PH$_3$)$^+$.

B. Carbon Dioxide Hydrogenation

Catalytic CO_2 hydrogenation to formic acid (reaction 26) is an interesting process as it provides a promising approach to the use of CO_2 as a raw material in chemical synthesis.[188]

$$H_2 + CO_2 \xrightarrow{\text{cat.}} \underset{H}{\overset{O}{\diagup\!\!\diagdown}}\!\!\underset{OH}{} \qquad (26)$$

Dedieu and co-workers have investigated the mechanism and kinetics of the rhodium-catalyzed hydrogenation of CO_2 to formic acid by using MP2 and QCISD(T) methods.[178] On the basis of experimental and theoretical results, it is found that the reaction proceeds through the CO_2 insertion to form a coordinatively saturated η^2-O,H complex **92b**, see Scheme 26, followed by H_2 OA/RE or σ-bond metathesis to generate the formic acid complex **95**. Finally, the *trans*-formic acid is released by the elimination of formic acid from **95**. The calculated energy potential profiles (Figure 35) show that the H_2 activation along the OA/RE pathway has an activation barrier of 24.7 kcal/mol and the H_2 activation along the σ-bond metathesis pathway has a lower activation barrier of 14.8 kcal/mol. These results suggest a σ-bond metathesis (pathway B: **92b** → **96** → **97** → **95** → H_2-CO_2H) as an alternative low-energy pathway to a classical oxidative-addition/reductive-elimination sequence (pathway A: **92b** → **93d** → **94** → **95** → H_2-CO_2H) for the reaction of the formate intermediate with dihydrogen. The calculations give detailed in-

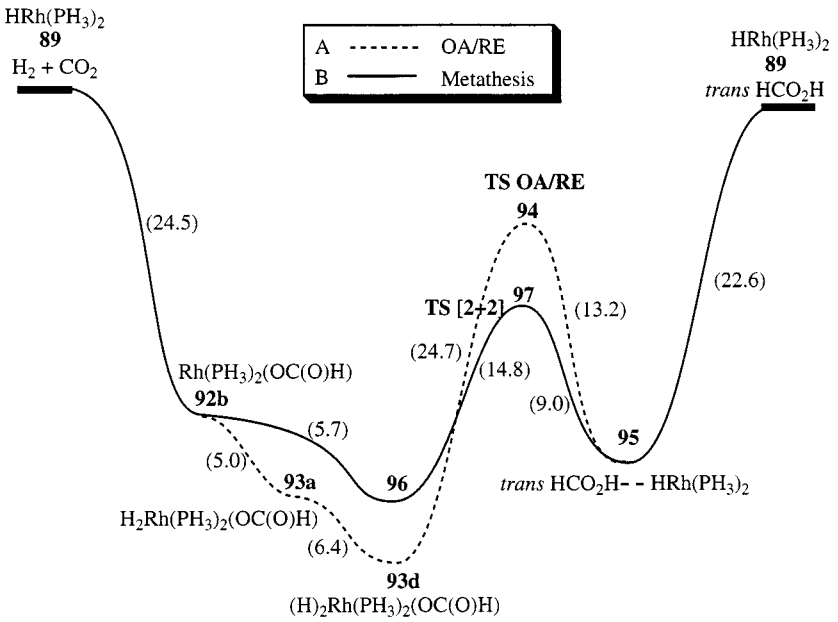

Figure 35. Energy potential profiles of the rhodium-catalyzed hydrogenation of CO_2 to formic acid along the OA/RE pathway and along the σ-bond metathesis pathway.

Scheme 26

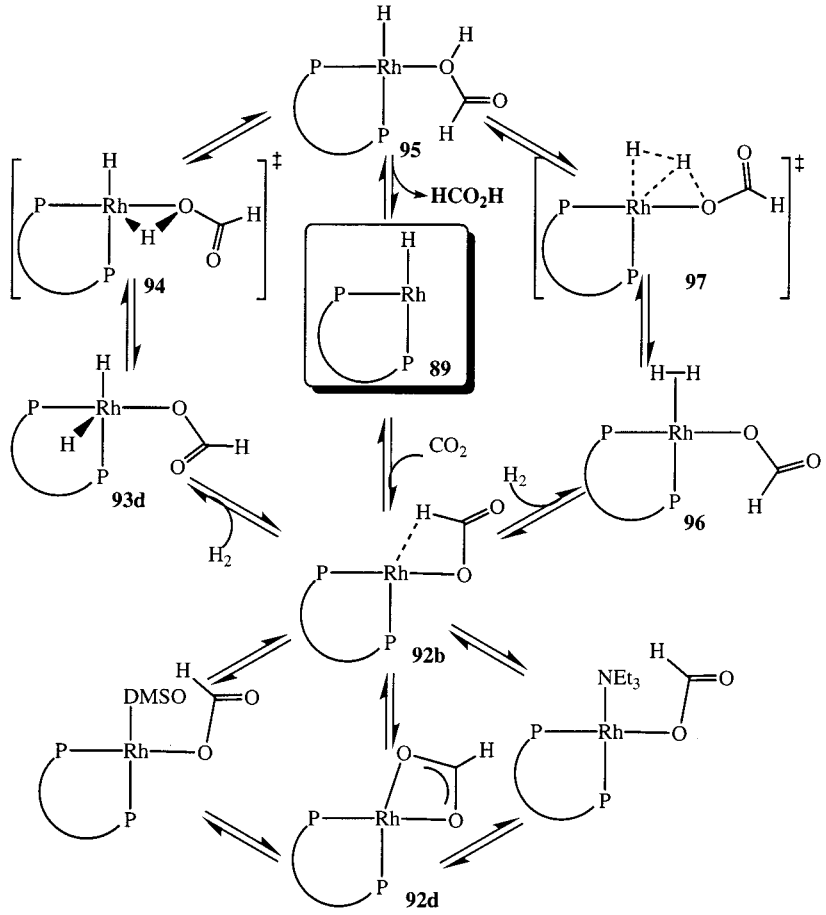

sight into the structure and kinetic behavior of possible intermediates and their transformations during the individual steps.

C. Olefin/CO Copolymerization

Olefin/CO alternating copolymerization is considered to be of technical importance due to the mechanical strength and photodegradation of the copolymers. Recently, Brookhart and co-workers reported kinetic and thermodynamic studies of high-molecular-weight ethylene/CO copolymer from the palladium(II)-catalyzed perfectly alternating copolymerization of ethylene with carbon monoxide (reaction 27).[56]

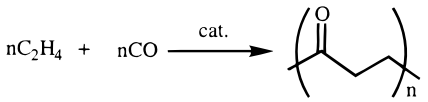

(27)

On the basis of these experimental findings, Hall, Morokuma, Siegbahn, Ziegler, and co-workers investigated the late-transition-metal-catalyzed olefin/CO copolymerization reaction.[59,89,90] The perfectly alternating CO/ethylene migratory insertion reactions depend on the relative binding of CO and ethylene with the palladium complex and the competition between CO and ethylene insertion into the Pd−alkyl or Pd−acyl bonds. Imperfect alternation could lead to the formation of two other polymers or segments of polymer: polyethylene and polyketone; all three possibilities are illustrated in Scheme 27.

Scheme 27

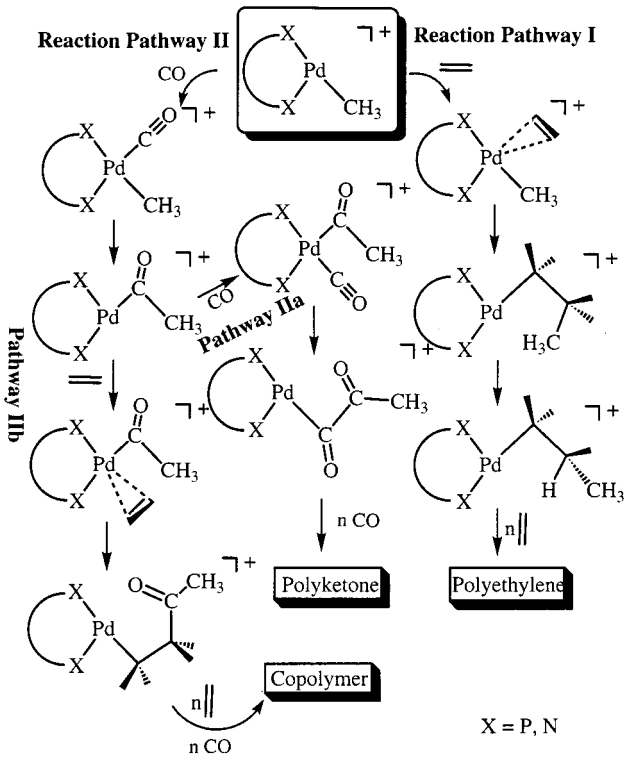

The B3LYP energy profiles for ethylene insertion into the Pd−CH_3 σ bond along pathway I, from reactants (the palladium−methyl complex, **96**, and ethylene) through the π complexes (**97a** and **97b**) and insertion transition state (**99**) to γ- and β-agostic palladium−propyl complexes (**100** and **102**) are shown in Figure 36. The binding energy of ethylene with the palladium−methyl complex (**96**) is −31.8 kcal/mol. The reaction from the π complex, **97a**, to the β-agostic palladium−propyl complex, **102**, is exothermic by 5.5 kcal/mol with an activation barrier of 16.3 kcal/mol.[59] These values are similar to those calculated by Morokuma and Siegbahn.[89] The activation barrier is close to the experimental value of 18.5 kcal/mol.[56] The binding energy of carbon monoxide to the palladium−methyl complex (**96**) to form **103** (pathway II) is −41.4 kcal/mol, about 10 kcal/mol larger than that for ethylene.[59] The migratory insertion to the acetyl complex (**102**) proceeds with a barrier of 15.0 kcal/mol, a value which compares favorably with experiment, $\Delta G^{\ddagger} = 15.4 \pm 0.1$ kcal/mol.[56] The binding energies of ethylene and CO with the palladium acetyl complex (**105**) are −24.1 and −33.9 kcal/mol, respectively. Although the migratory insertion of either ethylene or carbonyl into the Pd−CH_3 σ bond proceeds with a similar activation barrier, there is a large difference in binding affinity (10 kcal/mol) between ethylene and CO with the palladium complex. Thus, the chemical equilibrium favors the CO complex (**106**) (pathway IIa) over the ethylene complex (**109**) (pathway IIb). The reaction from the carbonyl acetyl complex (**106**) through a transition state (**107**) to the diketone complex (**108**) along pathway IIa has a high barrier of 28.9 kcal/mol, while the reaction from the ethylene acetyl complex (**109**) along pathway IIb, through a transition state (**110**) to the chelated acyl complex (**111**), proceeds with a lower activation barrier of 16.8 kcal/mol (exp $\Delta G^{\ddagger} = 16.6 \pm 0.1$ kcal/mol).[4a] In addition, the chelated acyl complex (**111**) is over 28 kcal/mol more stable than the diketone complex (**108**). Thus, ethylene insertion into the Pd−acyl σ bond (pathway IIb) is thermodynamically and kinetically more favorable than CO insertion into the Pd−acyl σ bond (pathway IIa). Furthermore, since the binding affinity of CO with palladium complexes is larger by 10 kcal/mol than that of ethylene, the carbonyl complexes such as **103** and **106** are the resting states.[56] Since **106** is not on the direct route to copolymerization, an essentially barrierless ligand exchange process to form **109** occurs. Therefore, CO insertion into the Pd−alkyl σ bond is thermodynamically more favorable than ethylene insertion into the Pd−alkyl σ bond and ethylene insertion into the Pd−acyl σ bond is kinetically more favorable than CO insertion into the Pd−acyl σ bond.

Ziegler and co-workers investigated the alternative "misinsertion" into a growing polyketone chain using the DFT method.[90] The calculations show that insertion of CO into a Pd−$C_2H_4C(O)R$ bond is favored by a rather stable CO precursor complex (−7.6 kcal/mol) and by a low activation barrier (+11.7 kcal/mol). Ethylene misinsertion into a growing polyketone chain can be ruled out due to the lack of a thermodynamically stable ethylene π complex and the high barrier (+18.6 kcal/mol) associated with the insertion of ethylene into a Pd−$C_2H_4C(O)R$ bond.

Morokuma and co-workers studied the mechanism of polymer chain termination.[89] Among the chain termination processes studied, associative displacement, where the coordinating olefin exchanges with ethylene from solution, is likely to be preferred for diimine−M(II)-based catalysts. The C−H activation and H-exchange chain termination mechanisms are found to be inefficient for diimine−M(II). Hydrogenolysis is also found to be a favorable chain termination process for diimine−M(II). Furthermore, Morokuma and co-workers have found that the Pd-based catalyst has a better selectivity but a lower reactivity in the alternating copolymerization compared to the Ni analogue.

These theoretical results have elucidated the reaction mechanism and important features of the CO/ethylene copolymerization. The calculated data are

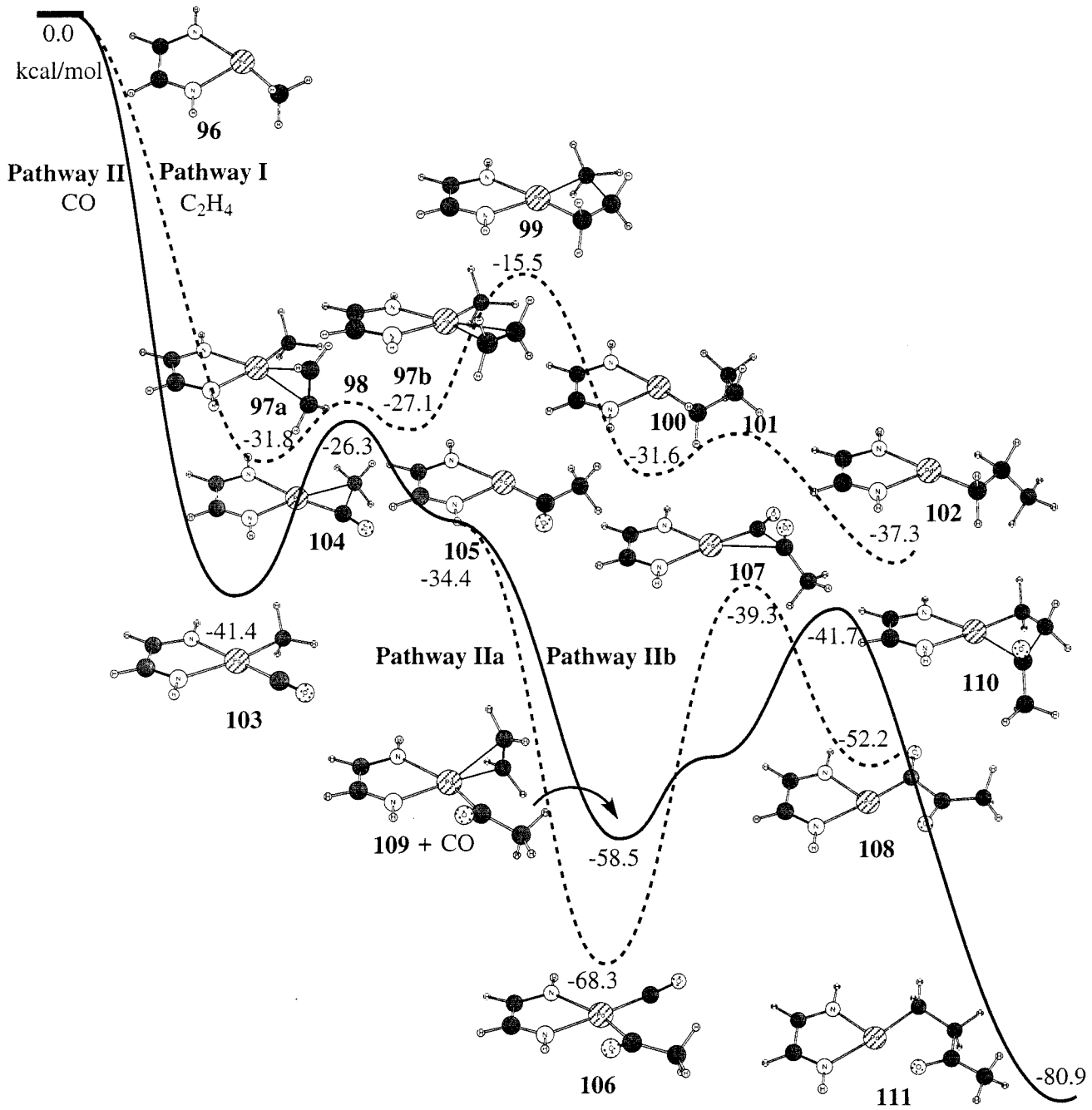

Figure 36. B3LYP energy potential profiles of the diimine palladium(II)-catalyzed polymerization and alternating copolymerization of ethylene with carbon monoxide.

consistent with the reported experimental values and results. The factors responsible for controlling the alternating nature of the copolymerization are confirmed by the DFT energy potential surface.

VII. Conclusion

In this article we reviewed the results of the latest ab initio and DFT studies of transition-metal reactions, both elementary and catalytic ones. With the development of modern computational techniques, particularly recent progress in density functional theory, scientists have a powerful tool to explore kinetic mechanism and thermodynamic properties for catalytic processes and to provide insight for the rational design of new catalysts.

Although DFT calculations may underestimate weak bonding interactions, such as van der Waals interactions,[43] they generally give better and more reliable descriptions of the geometries and relative energies for transition-metal systems than either HF or MP2 methods. During the past several years, hybrid DFT methods, such as B3LYP and B3P86, which have some exact Hartree−Fock exchange included, have become the dominant computational tool for treating the transition-metal reactions because these DFT methods appear to be both more efficient and more accurate. Because electron correlation is treated by the functional rather than through electron excitation as in conventional ab initio methods, DFT methods are less basis-set sensi-

tive. Since many predicted physical and chemistry properties are directly related to the highly accuracy energy computations,[2−5] additional calculations and corrections may need to be applied to achieve the desired accuracy. Generally, corrections may be made for basis-set superposition error (BSSE),[29] zero-point energy (ZPE), thermal effects, solvation, and relativistic (spin−orbit, etc.) effects. As a check of the accuracy of the DFT calculations or if higher accuracy is needed, one may include electron correlation at higher levels of theory; usually, only QCISD, CCSD, or similar techniques with large basis sets are reliably more accurate than DFT.

The studies reviewed here illustrate the general approach one takes in a theoretical investigation. Using the experimental findings, one proposes possible reaction pathways and chooses a reasonable computational method for the studies. When sufficient facts are known about a system, one can design reasonably small numbers of rational models. By determining the structures and energies of reactants, intermediates, transition states, and products, the reaction path can be elucidated. By changing the transition metal, the ligands, and their substituents and by examining the electronic structures of reaction system, one can explore the factors that contribute to the chemical reactivity and selectivity. Through this process one can come to an 'understanding' of the chemistry and create rules on which the rational design of new catalysts can be based.

VIII. References

(1) (a) Elschenbroich, Ch.; Salzer, A. *Organometallics*; VCH Publishers: New York, 1989. (b) Crabtree, R. H. *The Organometallic Chemistry of the Transition Metals*; John Wiley & Sons: New York, 1988. (c) Parshall, G. W. *Homogeneous Catalysis*; Wiley: New York, 1980. (d) Arndtsen, B. A.; Bergman, R. G.; Mobley, T. A.; Peterson, T. H. *Acc. Chem. Res.* **1995**, *28*, 154. (e) Cotton, F. A.; Wilkinson, G. *Advanced Inorganic Chemistry*; John Wiley: New York, 1988. (f) Crabtree, R. H. *Chem. Rev.* **1995**, *95*, 987.

(2) *Reviews in Computational Chemistry*; Lipkowitz, K. B., Boyd, D. B., Eds.; VCH: New York, 1990−1999; Vols. 1−13.

(3) (a) Koga, K.; Morokuma, K. *Chem. Rev.* **1991**, *91*, 823. (b) Musaev, D. G.; Morokuma, K. In *Advances in Chemical Physics*; Rice, S. A., Prigogine, I., Eds.; John Wiley & Sons: New York, 1996; Vol. XCV, p 61. (c) Siegbahn, P. E. M.; Blomberg, M. R. A. In *Theoretical Aspects of Homogeneous Catalysts, Applications of Ab Initio Molecular Orbital Theory*; van Leeuwen, P. W. N. M., van Lenthe, J. H., Morokuma, K., Eds.; Kluwer Academic Publishers: Hingham, MA, 1995. (d) Ziegler, T. *Chem. Rev.* **1991**, *91*, 651. (e) Salahub, D. R.; Castro, M.; Fournier, R.; Calaminici, P.; Godbout, N.; Goursot, A.; Jamorski, C.; Kobayashi, H.; Martinez, A.; Papai, I.; Proynov, E.; Russo, N.; Sirois, S.; Ushio, J.; Vela, A. In *Theoretical and Computational Approaches to Interface Phenomena*; Sellers H., Olab, J., Eds.; Plenum Press: New York, 1995; p 187. (f) Siegbahn, P. E. M. In *Advances in Chemical Physics;* Rice, S. A., Prigogine, I., Eds.; John Wiley & Sons: New York, 1996; Vol. XCIII, p 333. (g) *Transition Metal Hydrides*, Edited by Dedieu, A., VCH Publishers: **1992**. (h) *Theoretical Aspects of Homogeneous Catalysis, Applications of Ab Initio Molecular Orbital Theory*; van Leeuwen, P. W. N. M., van Lenthe, J. H., Morokuma, K., Eds.; The Netherlands, 1994. (i) Yoshida, S.; Sakaki, S.; Kobayashi, H. *Electronic Processes in Catalyst*; VCH: New York, 1992.

(4) Hehre, W. J.; Radom, L.; Schleyer, P. v. R.; Pople, J. A. *Ab initio Molecular Orbital Theory*; John Wiley & Sons: New York, 1986.

(5) Foresman, J. B.; Frish, A. E. *Exploring Chemistry with Electronic Structure Mothods*; Gaussian, Inc.: The Woodlands, TX, 1993.

(6) Parr, R. G.; Yang, W. *Density-functional theory of atoms and molecules*; Oxford University Press: Oxford, 1989.

(7) (a) Møller, C.; Plesset, M. S. *Phys. Rev.* **1936**, *46*, 618. (b) Pople, J. A.; Binkley, J. S.; Seeger, R. *Int. J. Quantum Chem.* **1976**, *10*, 1. (c) Krishnan, R.; Pople, J. A. *J. Chem. Phys.* **1978**, *14*, 91.

(8) (a) Raghavachari, K.; Pople, J. A. *Int. J. Quantum Chem.* **1981**, *20*, 1067. (b) Krishnan, R.; Schlegel, H. B.; Pople, J. A. *J. Chem. Phys.* **1980**, *72*, 4654. (c) Szabo, A.; Ostlund, N. S. *Modern Quantum Chemistry: Introduction to Advanced Electronic Structure Theory*; Macmillan Publishing Co., Inc.: New York, 1982.

(9) Chong, D. P.; Langhoff, S. R. *Int. J. Chem. Phys.* **1986**, *84*, 5606.

(10) Pople, J. A.; Head-Gordon, M.; Raghavachari, K. *J. Chem. Phys.* **1987**, *87*, 5968.

(11) (a) Bartlett, R. J. *Annu. Rev. Phys. Chem.* **1981**, *32*, 359. (b) Scuseria, G. E.; Schaefer, H. F., III *J. Chem. Phys.* **1989**, *90*, 3700.

(12) Raghavachari, K.; Trucks, G. W.; Pople, J. A.; Head-Gordon, M.; *Chem. Phys. Lett.* **1989**, *87*, 5968

(13) (a) Schlegel, H. B. In *Ab Initio Methods in Quantum Chemistry, I*; Lawley, Ed.; John Wiley & Sons Ltd.: New York, 1987. (b) Müller, K. *Angew. Chem., Int. Ed. Engl.* **1980**, *19*, 1.

(14) (a) Gonzalez, C.; Schlegel, H. B. *J. Chem. Phys.* **1989**, *90*, 2154. (b) Gonzalez, C.; Schlegel, H. B. *J. Phys. Chem.* **1990**, *94*, 5523.

(15) Halgren, T. A.; Lipscomb, W. N. *Chem. Phys. Lett.* **1977**, *49*, 225.

(16) (a) Peng, C.; Ayala, P. Y.; Schlegel, H. B.; Frish, M. J. *J. Comput. Chem.* **1996**, *17*, 49. (b) Peng, C.; Schlegel, H. B. *Israel J. Chem.* **1993**, *33*, 449.

(17) (a) Hay, P. J.; Wadt, W. R. *J. Chem. Phys.* **1985**, *82*, 270. (b) Wadt, W. R.; Hay, P. J. *J. Chem. Phys.* **1985**, *82*, 284. (c) Hay, P. J.; Wadt, W. R. *J. Chem. Phys.* **1985**, *82*, 299. (d) Gordon, M. S.; Cundari, T. R. *Coord. Chem. Rew.* **1996**, *147*, 87. (e) Frenking, G.; Antes, I.; Boehme, M.; Dapprich, S.; Ehlers, A. W.; Jonas, V.; Arndt Neuhaus, A.; Otto, M.; Stegmann, R.; Veldkamp, A.; Vyboishchikov, S. F. In *Reviews in Computational Chemistry*; 1996; Vol. 8, p 63.

(18) (a) Pyykkö, P. *Chem. Rev.* **1988**, *88*, 563. (b) Schwarz, W. H. E.; van Wezenbeek, E. M.; Baerends, E. J.; Snijders, J. G. *J. Phys.* **1989**, *B22*, 1515. (c) Wezenbeek, E. M.; Baerends, E. J.; Ziegler, T. *Inorg. Chem.* **1995**, *34*, 238.

(19) (a) Becke, A. D. *Phys. Rev.* **1988**, *A38*, 3098. (b) Becke, A. D. *J. Chem. Phys.* **1993**, *98*, 1372. (c) Becke, A. D. *J. Chem. Phys.* **1993**, *98*, 5648.

(20) Lee, C.; Yang, W.; Parr, R. G. *Phys. Rev. B* **1988**, *37*, 785.

(21) Perdue, J. P. *Phys. Rev. B* **1986**, *33*, 8822.

(22) Perdue, J. P.; Wang, Y. *Phys. Rev. B* **1991**, *45*, 13244.

(23) (a) Weiner, W. P.; White, M. A.; Bergman, R. G. *J. Am. Chem. Soc.* **1981**, *103*, 3612. (b) Seidler, M. D.; Bergman, R. G. *Organometallics* **1983**, *2*, 1897. (c) Weiner, W. P.; Bergman, R. G. *J. Am. Chem. Soc.* **1983**, *105*, 3922.

(24) Niu, S.-Q.; Hall, M. B. *J. Am. Chem. Soc.* **1997**, *119*, 3077.

(25) Niu, S.-Q.; Hall, M. B. *J. Phys. Chem. A* **1997**, *101*, 1360.

(26) (a) Hegarty, D.; Robb, M. A. *Mol. Phys.* **1979**, *38*, 1795. (b) Schlegel, H. B.; Roob, M. A. *Chem. Phys. Lett.* **1982**, *93*, 43.

(27) Lee, T. J.; Scuseria, G. E. In *Quantum Mechanical Electronic Structure Calculations with Chemical Accuracy*; Lanfhoof, S. R., Ed.; Kluwer Academic Publishers: Dordrecht, 1995; pp 47−108.

(28) (a) Mitchell, S. A.; Blitz, M. A.; Siegbahn, P. E. M.; Svensson, M. *J. Chem. Phys.* **1994**, *100*, 423. (b) Fournier, R. *Theor. Chim. Acta* **1995**, *91*, 129.

(29) (a) Davidson, E. R.; Feller, A. *Chem. Rev.* **1986**, *86*, 681. (b) *Ab Initio Methods in Quantum Chemistry, Part I*; Lawley, K. P., Ed.; John Wiley & Sons: New York, 1987. (c) Schlegel, H. B. *J. Chem. Phys.* **1986**, *84*, 4530. (d) Schlegel, H. B. *J. Phys. Chem.* **1988**, *92*, 3075.

(30) (a) Lin, Z.; Hall, M. B. *Coord. Chem. Rev.* **1994**, *135/136*, 845. (b) Siegbahn, P. E. M.; Sevensson, M. *Chem. Phys. Lett.* **1993**, *216*, 147.

(31) (a) Ehlers, A. W.; Frenking, G. *J. Am. Chem. Soc.* **1994**, *116*, 1514. (b) Szilagyi, R. K.; Frenking, G. *Organometallics* **1997**, *16*, 4807. (c) Ehlers, A. W.; Dapprich, S.; Vyboishchikov, S. F.; Frenking, G. *Organometallics* **1996**, *15*, 105. (d) Dapprich, S.; Frenking, G. *Organometallics* **1995**, *14*, 423.

(32) Marsden, C. J.; Wolynec, P. P. *Inorg. Chem.* **1991**, *30*, 1681.

(33) (a) Lin, Z.; Hall, M. B. *Inorg. Chem.* **1992**, *31*, 2791. (b) Li, J.; Schreckenbach, G.; Ziegler, T. *J. Am. Chem. Soc.* **1995**, *117*, 486. (c) Ziegler, T.; Tschinke, V.; Ursenbach, C. J. *J. Am. Chem. Soc.* **1987**, *109*, 4825. (d) Ehlers, A. W.; Ruiz-Morales, Y.; Baerends, E. J.; Ziegler, T. *Inorg. Chem.* **1997**, *36*, 5031.

(34) (a) Angelici, R. *J. Organomet. Chem. Rev. A* **1968**, *3*, 173. (b) Covey, W. D.; Brown, T. L. *Inorg. Chem.* **1973**, *12*, 2820. (c) Centini, G.; Gambino, O. *Atti Acad. Sci. Torino. 1* **1963**, *97*, 1197. (d) Weiner, H. *Angew. Chem., Int. Ed Engl.* **1968**, *7*, 930. (e) Graham, J. R.; Angelici, R. J. *Inorg. Chem.* **1967**, *6*, 2082. (f) Werner, H.; Prinz, R. *Chem. Ber.* **1960**, *99*, 3582. (g) Werner, H.; Prinz, R. *J. Organomet. Chem.* **1966**, *5*, 79.

(35) Bernstein, M.; Simon, J. D.; Peters, J. D. *Chem. Phys. Lett.* **1983**, *100*, 241.

(36) Lewis, K. E.; Golden, D. M.; Smith, G. P. *J. Am. Chem. Chem.* **1984**, *106*, 3905.

(37) (a) Butler, I. S.; Basolo, F.; Pearson, R. G. *Inorg. Chem.* **1967**, *6*, 2074. (b) Green, M.; Westlake, D. J. *J. Chem. Soc. A* **1971**, 367.

(38) Thomas, J. L. C.; Hall, M. B. *Organometallics* **1997**, *16*, 2318.

(39) (a) Schultz, A. J.; Teller, R. G.; Beno, M. A.; Williams, J. M.; Brookhart, M.; Lamanna, W.; Humphrey, M. B. *Science* **1983**, *220*, 197. (b) Brookhart, M.; Noh, S. K.; Timmers, F. J. *Organometallics* **1987**, *6*, 1829.

(40) (a) Wasserman, E. P.; Moore, C. B.; Bergman, R. G. *Science* **1992**, *255*, 315. (b) Bergman, R. G. *Science* **1984**, *223*, 902. (c) Schultz, R. H.; Bengali, A. A.; Tauber, M. J.; Weiller, B. H.; Wasserman, E. P.; Kyle, K. R.; Moore, C. B.; Bergman, R. G. *J. Am. Chem. Soc.* **1994**, *116*, 7369.

(41) (a) Ziegler, T.; Tschinke, V.; Fan, L.-Y.; Becke, A. D. *J. Am. Chem. Soc.* **1989**, *111*, 9177. (b) Song, J.; Hall, M. B. *Organometallics* **1993**, *12*, 3118. (c) Musaev, D.; Morokuma, K. *J. Am. Chem. Soc.* **1995**, *117*, 799. (d) Siegbahn, P. E. M. *J. Am. Chem. Soc.* **1996**, *118*, 1487. (e) Su, M.-D.; Chu, S.-Y. *Organometallics* **1997**, *16*, 1621.

(42) Zaric, S.; Hall, M. B. *J. Phys. Chem. A* **1997**, *101*, 4646.

(43) Cotton, F. A.; Feng, X.-J. *J. Am. Chem. Soc.* **1997**, *119*, 7514.

(44) (a) Baird, M. C. *Chem. Rev.* **1988**, *88*, 1217. (b) Trogler, W. C. *Int. J. Chem. Kinet.* **1987**, *19*, 1025. (c) Howell, J. A. S.; Burkinshaw, P. M. *Chem. Rev.* **1983**, *83*, 557. (d) Lincoln, S. F.; Merbach, A. E. *Adv. Inorg. Chem.* **1995**, *42*, 1.

(45) (a) Basolo, F. *Inorg. Chim. Acta* **1985**, *100*, 3. (b) Basolo, F. *Polyhedron* **1990**, *9*, 1503. (c) Basolo, F. *Pure Appl. Chem.* **1988**, *60*, 1193. (d) Herrington, T. R.; Brown, T. L. J. *J. Am. Chem. Soc.* **1985**, *107*, 5700.

(46) (a) Shi, Q. Z.; Richmond, T. G.; Trogler, W. C.; Basolo, F. *J. Am. Chem. Soc.* **1982**, *104*, 4032. (b) Shi, Q. Z.; Richmond, T. G.; Trogler, W. C.; Basolo, F. *J. Am. Chem. Soc.* **1984**, *106*, 71.

(47) (a) Bader, R. F. W.; MacDougall, P. J.; Lau, C. D. H. *J. Am. Chem. Soc.* **1984**, *106*, 1594. (b) Bader, R. F. W. *Acc. Chem. Res.* **1985**, *18*, 9. (c) Bader, R. F. W. *Atoms in Molecules: A Quantum Theory*; Oxford University Press: New York, 1990.

(48) (a) Basolo, F.; Wojcicki, A. *J. Am. Chem. Soc.* **1961**, *83*, 5290. (b) Day, J. P.; Pearson, R. G.; Basolo, F. *J. Am. Chem. Soc.* **1968**, *90*, 6927. (c) Thorsteinson, E. M.; Basolo, F. *J. Am. Chem. Soc.* **1966**, *88*, 3929. (d) Morris, D. E.; Basolo, F. *J. Am. Chem. Soc.* **1968**, *90*, 2531. (e) Shen, J. K.; Gao, Y. C.; Shi, Q. Z.; Basolo, F. *Inorg. Chem.* **1989**, *28*, 4304.

(49) (a) Wawersik, H.; Basolo, F. *J. Am. Chem. Soc.* **1967**, *89*, 4626. (b) Graham, J. R.; Angelici, R. J. *Inorg. Chem.* **1967**, *6*, 2082.

(50) (a) Sulfab, Y.; Basolo, F.; Rheingold, A. L. *Organometallics* **1989**, *8*, 2139. (b) Brown, D. A.; Sane, R. T. *J. Chem. Soc. A* **1971**, 2088.

(51) Tolman, C. A. *Chem. Soc. Rev.* **1972**, *1*, 337.

(52) Song, J.; Hall, M. B. *J. Am. Chem. Soc.* **1993**, *115*, 327.

(53) (a) Streuli, C. A. *Anal. Chem.* **1960**, *32*, 985. (b) Tolman, C. A. *Chem. Rev.* **1972**, *77*, 313. (c) Rahnan, M. M.; Liu, H. Y.; Prock, A.; Giering, W. P. *Organometallics* **1987**, *6*, 650. (d) Bush, R. C.; Angelici, R. J. *Inorg. Chem.* **1988**, *27*, 681. (e) Poe, A. J. *Pure Appl. Chem.* **1988**, *60*, 1209 and references therein. (f) Sulfab, Y.; Basolo, F.; Rheingold, A. L. *Organometallics* **1989**, *8*, 2139.

(54) (a) Sen, A.; Jiang, Z. *Macromolecules* **1993**, *26*, 9111. (b) Jiang, Z.; Sen, A. *J. Am. Chem. Soc.* **1995**, *117*, 4455. (c) Lai, T.-W.; Sen, A. *Organometallics* **1984**, *3*, 866. (d) Sen, A. *Acc. Chem. Rev.* **1993**, *26*, 333.

(55) (a) Drent, E.; Budzelaar, P. H. M. *Chem. Rev.* **1996**, *96*, 663. (b) Drent, E.; Broekhoven, J. A. M. v.; Doyle, M. J. *J. Organomet. Chem.* **1991**, *417*, 235.

(56) (a) Rix, F. C.; Brookhart, M.; White, P. S. *J. Am. Chem. Soc.* **1996**, *118*, 4746. (b) Johnson, L. K.; Killian, C. M.; Brookhart, M.; White, P. S. *J. Am. Chem. Soc.* **1995**, *117*, 6414. (c) Lapointe, A. M.; Rix, F. C.; Brookhart, M.; White, P. S. *J. Am. Chem. Soc.* **1997**, *119*, 906. (d) Mecking, S.; Johnson, L. K.; Wang, L.; Brookhart, M.; White, P. S. *J. Am. Chem. Soc.* **1998**, *120*, 888. (e) Lapointe, A. M.; Brookhart, M.; White, P. S. *Organometallics* **1998**, *17*, 1530.

(57) (a) Margl, P.; Ziegler, T. *J. Am. Chem. Soc.* **1996**, *118*, 7337. (b) Margl, P.; Ziegler, T. *Organometallics* **1996**, *15*, 5519.

(58) (a) Svensson, M.; Matsubara, T.; Morokuma, K. *Organometallics* **1996**, *15*, 5568. (b) Musaev, D. G.; Svensson, M.; Morokuma, K.; Strömberg, S.; Zetterberg, K.; Siegbahn, P. E. M. *Organometallics* **1997**, *16*, 1933. (c) Siegbahn, P. E. M.; Strömberg, S.; Zetterberg, K. *Organometallics* **1996**, *15*, 1996.

(59) Niu, S.-Q.; Hall, M. B. Unpublished work.

(60) (a) Basolo, F.; Pearson, R. G. *Mechanisms of Inorganic Reactions*; John Wiley: New York, 1968. (b) Langford, C. H.; Gray, H. B. *Ligand Substitution Processes*; W. A. Benjamin: New York, 1965.

(61) (a) Lin, Z.; Hall, M. B. *Inorg. Chem.* **1991**, *30*, 646. (b) Frankcombe, K. E.; Cavell, K. J.; Knott, R. B.; Yates, B. F. *Chem. Commun.* **1996**, 781. (c) Frankcombe, K. E.; Cavell, K. J.; Yates, B. F.; Knott, R. B. *J. Phys. Chem.* **1996**, *100*, 18363. (d) Frankcombe, K. E.; Cavell, K. J.; Yates, B. F.; Knott, R. B. *Organometallics* **1997**, *16*, 3199.

(62) (a) Natta, G. *Nobel Lectures in Chemistry, 1963−1970*; Elsevier: Amsterdam, 1972; p 72. (b) Ziegler, K. *Nobel Lectures in Chemistry, 1963−1970*; Elsevier: Amsterdam, 1972; p 6. (c) Boor, J., Jr. *Ziegler−Natta Catalysts and Polymerizations*; Academic: New York, 1979. (d) Pino, P.; Mulhaupt, R. *Angew. Chem., Int. Ed. Engl.* **1972**, *19*, 857. (e) Eisch, J. J.; Galle, J. E.; Piotrowski, A. M. In *Transition Metal Catalysed Polymerization: Alkenes and Dienes*; Quirk, R. P., Ed.; Harwod: New York, 1983. (f) Eisch, J. J.; Galle, J. E.; Piotrowski, A. M. In *Transition Metal and Organometallics as Catalyst for Olefin Polymerization*; Kaminsky, W., Linn, M., Eds.; Springer-Verlag: Berlin, Heidelberg, 1988. (g) Allen, G. B. *Comprehensive Polymer Science*; Pergamon Press: Oxford, 1989. (h) Albizzati, E.; Giannini, U.; Collina, G.; Noristi, L.; Resconi, L. In *Polypropylene Handbook*; Moore, E. P., Jr., Ed.; Hanser: New York, 1996; p 11.

(63) (a) Scollard, J. D.; McConville, D. H. *J. Am. Chem. Soc.* **1996**, *118*, 10008. (b) Scollard, J. D.; McConville, D. H.; Payne, N. N. C. *Macromolecules* **1996**, *29*, 5241. (c) Shah, S. A. A.; Dorn, H.; Voigt, A.; Roesky, H.; Parisni, E.; Schmidt, H.-G.; Noltemeyer, M. *Organometallics* **1996**, *15*, 3176. (d) Fokken, S.; Spaniol, T. P.; Kang, H.-C.; Massa, W.; Okuda, J. *Organometallics* **1996**, *15*, 5069. (e) van der Linden, A.; Schaverien, C. J.; Meijboom, N.; Ganter, C.; Orpen, A. G. *J. Am. Chem. Soc.* **1995**, *117*, 3008. (f) Warren, T. H.; Schrock, R. R.; Davis, W. M. *Organometallics* **1996**, *15*, 562. (g) Brand, H.; Capriotti, J. A.; Arnold, J. *Organometallics* **1994**, *13*, 4469. (h) Tjaden, E. B.; Swenson, D. C.; Jordan, R. F.; Petersen, J. L. *Organometallics* **1995**, *14*, 371. (i) Horton, A. D.; de With, J.; van der Linden, A. J.; van de Weg, H. *Organometallics* **1996**, *15*, 2672. (j) Fuhrmann, H.; Brenner, S.; Arndt, P.; Kempe, R. *Inorg. Chem.* **1996**, *35*, 6742. (k) Cozzi, P. G.; Gallo, E.; Floriani, C.; Chiesi-Villa, A.; Rizzoli, C. *Organometallics* **1995**, *14*, 4994. (l) Cloke, F. G. N.; Geldbach, T. J.; Hitchcock, P. B.; Love, J. B. *J. Organomet. Chem.* **1996**, *506*, 343. (m) Uhrhammer, R.; Black, D. G.; Gandner, T. G.; Olsen, J. D.; Jordan, R. F. *J. Am. Chem. Soc.* **1993**, *115*, 8493. (n) Long, D. P.; Bianconi, P. A. *J. Am. Chem. Soc.* **1996**, *118*, 12453. (o) Aoyagi, K.; Gantzel, P. K.; Kalai, K.; Tilley, T. D. *Organometallics* **1996**, *15*, 923. (p) Jia, L.; Yang, X.; Stern, C.; Marks, T. J. *Organometallics* **1994**, *13*, 3755. (q) Murphy, V. J.; Turner, H. *Organometallics* **1997**, *16*, 2495. (r) Antonelli, D. M.; Leins, A.; Stryker, J. M. *Organometallics* **1997**, *16*, 2500. (s) Strauss, S. H. *Chem. Rev.* **1993**, *93*, 927. (t) Crowther, D. J.; Borkowsky, S. L.; Swenson, D.; Meyer, T. Y.; Jordan, R. F. *Organometallics* **1993**, *12*, 2897. (u) Kaminsky, W.; Kulper, K.; Brintzinger, H. H.; Wild, F. R. W. P. *Angew. Chem., Int. Ed. Engl.* **1992**, *31*, 1347.

(64) (a) Cossee, P. *J. Catal.* **1964**, *3*, 80. (b) Arlman, E. J.; Cossee, P. *J. Catal.* **1964**, *3*, 99.

(65) Lauher, J. W.; Hoffmann, R. *J. Am. Chem. Soc.* **1976**, *98*, 1729.

(66) (a) Koga, N.; Obara, S.; Morokuma, K. *J. Am. Chem. Soc.* **1984**, *106*, 4625. (b) Koga, N.; Obara, S.; Kitaura, K.; Morokuma, K. *J. Am. Chem. Soc.* **1985**, *107*, 7109. (c) Koga, N.; Morokuma, K. *J. Am. Chem. Soc.* **1988**, *110*, 108. (d) Kawamura-Kuribayashi, H.; Koga, N.; Morokuma, K. *J. Am. Chem. Soc.* **1992**, *114*, 2359. (e) Kawamura-Kuribayashi, H.; Koga, N.; Morokuma, K. *J. Am. Chem. Soc.* **1992**, *114*, 8687. (f) Endo, J.; Koga, N.; Morokuma, K. *Organometallics* **1993**, *12*, 2777. (g) Yoshida, T.; Koga, N.; Morokuma, K. *Organometallics* **1995**, *14*, 746. (h) Froese, R. D. J.; Musaev, D. G.; Matsubara, T.; Morokuma, K. *J. Am. Chem. Soc.* **1997**, *119*, 7190. (i) Das, P. K.; Dockter, D. W.; Fahey, D. R.; Lauffer, D. E.; Hawkins, G. D.; Li, J.; Zhu, T.; Cramer, C. J.; Truhlar, D. G.; Dapprich, S.; Froese, R. D. J.; Holthausen, M. C.; Liu, Z.; Mogi, K.; Vyboishchikov, S.; Musaev, D. G.; Morokuma, K. In *Transition State Modeling for Catalysis*; Truhlar, D. G., Morokuma, K., Eds.; ACS Symposium Series 721; Oxford University Press: 1999; p 208.

(67) Jolly, C. A.; Marynick, D. S. *J. Am. Chem. Soc.* **1989**, *111*, 7896.

(68) (a) Castonguay, L. A.; Rappé, A. K. *J. Am. Chem. Soc.* **1992**, *114*, 5832. (b) Hart, J. R.; Rappé, A. K. *J. Am. Chem. Soc.* **1993**, *115*, 6159.

(69) (a) Weiss, H.; Haase, F.; Ahlrichs, R. *Chem. Phys. Lett.* **1992**, *194*, 492. (b) Weiss, H.; Haase, F.; Ahlrichs, R. *J. Am. Chem. Soc.* **1992**, *116*, 4919.

(70) (a) Gleiter, R.; Hyla-Kryspin, I.; Niu, S.; Erker, G. *Organometallics* **1993**, *12*, 3828. (b) Hyla-Kryspin, I.; Niu, S.; Gleiter, R. *Organometallics* **1995**, *14*, 964. (c) Hyla-Kryspin, I.; Silverio, S. J.; Niu, S.; Gleiter, R. *J. Mol. Catal. A: Chem.* **1997**, *115*, 183.

(71) (a) Mohr, R.; Berke, H.; Erker, G. *Helv. Chim. Acta* **1993**, *76*, 1389. (b) Janiak, C. *J. Organomet. Chem.* **1993**, *452*, 63.

(72) Petitjean, L.; Pattou, D.; Ruiz-López, M. F. *J. Phys. Chem.* **1999**, *103*, 27.

(73) (a) Siegbahn, P. E. M. *J. Am. Chem. Soc.* **1993**, *115*, 5803. (b) Siegbahn, P. E. M. *Chem. Phys. Lett.* **1993**, *205*, 290. (c) Jensen, V. R.; Siegbahn, P. E. M. *Chem. Phys. Lett.* **1993**, *212*, 353.

(74) Bierwagen, E. B.; Bercaw, J. E.; Goddard, W. A., III *J. Am. Chem. Soc.* **1994**, *116*, 1481.

(75) (a) Woo, T. K.; Fan, L.; Ziegler, T. *Organometallics* **1994**, *13*, 432. (b) Woo, T. K.; Fan, L.; Ziegler, T. *Organometallics* **1994**, *13*, 2252. (c) Fan, L.; Harrison, D.; Woo, T. K.; Ziegler, T. *Organometallics* **1995**, *14*, 2018. (d) Lohrenz, J. C. W.; Woo, T. K.; Ziegler, T. *J. Am. Chem. Soc.* **1995**, *117*, 12793. (e) Woo, T. K.; Margl, P. M.; Lohrenz, J. C. W.; Blöchl, P. E.; Ziegler, T. *J. Am. Chem. Soc.* **1996**, *118*, 13021. (f) Woo, T. K.; Margl, P. M.; Ziegler, T.; Blöchl, P. E. *Organometallics* **1997**, *16*, 3454. (g) Margl, P. M.; Deng, L.; Ziegler, T. *Organometallics* **1998**, *17*, 933. (h) Margl, P. M.; Deng, L.; Ziegler, T. *J. Am. Chem. Soc.* **1998**, *120*, 5517.

(76) Sini, G.; Macgregor, S. A.; Eisenstein, O.; Teuben, H. H. *Organometallics* **1994**, *13*, 1049.
(77) Meier, R. J.; Doremaele, G. H. J. V.; Iarlori, S.; Buda, F. *J. Am. Chem. Soc.* **1994**, *116*, 7274.
(78) Støvneng, J. A.; Rytter, E. *J. Organomet. Chem.* **1996**, *519*, 277.
(79) Prosenc, M.-H.; Brintzinger, H.-H. *Organometallics* **1997**, *16*, 3889.
(80) (a) Cavallo, L.; Guerra, G.; Corradini, P. *J. Am. Chem. Soc.* **1998**, *120*, 2428. (b) Boero, M.; Parrimello, M.; Terakura, K. *J. Am. Chem. Soc.* **1998**, *120*, 2746.
(81) (a) Dawoodi, Z.; Green, M. L. H.; Mtetwa, V. S. B.; Prout, K. *J. Chem. Soc., Chem. Commun.* **1982**, 802. (b) Dawoodi, Z.; Green, M. L. H.; Mtetwa, V. S. B.; Prout, K. *J. Chem. Soc., Chem. Commun.* **1982**, 1410. (c) Brookhart, M.; Green, M. L. H.; Mtetwa, V. S. B.; Prout, K. *J. Organomet. Chem.* **1983**, *250*, 1410.
(82) Mashima, K.; Fujikawa, S.; Tanaka, Y.; Urata, H.; Oshiki, T.; Tanaka, E.; Nakamura, A. *Organometallics* **1995**, *14*, 2633.
(83) (a) Scollard, J. D.; McConville, D. H. *J. Am. Chem. Soc.* **1996**, *118*, 10008. (b) Scollard, J. D.; McConville, D. H.; Payne, N, C.; Vittal, J. J. *Macromolecules* **1996**, *29*, 5241. (c) Shah, S. A. A.; Dorn, H.; Voigt, A.; Roesky, H.; Parisini, E.; Schmidt, H.-G.; Noltemeyer, M. *Organometallics* **1996**, *15*, 3176. (d) Crackness, R. B.; Orpen, A. G.; Spencer, J. L. *J. Chem. Soc., Chem. Commun.* **1984**, 326. (e) Brookhart, M.; Schmidt, G. F.; Lincoln, D.; Rivers, D. S. In *Transition Metal Catalyzed Polymerizations*; Quirk, R., Ed.; Cambridge University Press: Cambridge, 1988. (f) Schmidt, G. F.; Brookhart, M. *J. Am. Chem. Soc.* **1985**, *107*, 1443. (g) Freemantle, M. *Chem. Eng. News* **1998**, *76* (15), 12.
(84) (a) Johnson, L. K.; Killian, C. M.; Brookhart, M. J. *J. Am. Chem. Soc.* **1995**, *117*, 6414. (b) Johnson, L. K.; Killian, C. M.; Brookhart, M. J. *J. Am. Chem. Soc.* **1996**, *118*, 267. (c) Killian, C. M.; Tempel, D. J.; Johnson, L. K.; Brookhart, M. J. *J. Am. Chem. Soc.* **1996**, *118*, 11664.
(85) (a) Thorn, D. L.; Hoffmann, R. *J. Am. Chem. Soc.* **1978**, *100*, 2079. (b) Silvestre, J.; Calhorda, M. J.; Hoffman, R.; Stoutland, P. O.; Bergman, R. G. *Organometallics* **1986**, *5*, 1841. (c) Albright, T. A.; Burdett, J. K.; Whangbo, M. H. *Orbital Interactions in Chemistry*; Wiley: New York, 1985.
(86) (a) Koga, N.; Morokuma, K. In *Quantum Chemistry: The Challenge of Transition Metals and Coordination Chemistry*; Veillard, A., Ed.; NATO ASI Series 176; Reidel: Dordrecht, 1986; p 351. (b) Koga, N.; Daniel, C.; Han, J.; Fu, X. Y.; Morokuma, K. *J. Am. Chem. Soc.* **1987**, *109*, 3455. (c) Daniel, C.; Koga, N.; Han, J.; Fu, X. Y.; Morokuma, K. *J. Am. Chem. Soc.* **1988**, *110*, 3773. (d) Koga, N.; Jin, S.-Q.; Morokuma, K. *J. Am. Chem. Soc.* **1988**, *110*, 3417.
(87) (a) Sakaki, S.; Ogawa, M.; Musashi, Y.; Arai, T. *J. Am. Chem. Soc.* **1994**, *116*, 7258. (b) Sakaki, S.; Ogawa, M.; Musashi, Y. *J. Organomet. Chem.* **1997**, *535*, 25. (c) Sugimoto, M.; Yamasaki, I.; Mizoe, N.; Anzai, M.; Sakaki, S. *Theor. Chem. Acc.* **1999**, *102*, 377.
(88) Creve, S.; Oevering, H.; Coussens, B. B. *Organometallics* **1999**, *18*, 1967.
(89) (a) Sevensson, M.; Matsubara, T.; Morokuma, K. *Organometallics* **1996**, *15*, 5569. (b) Musaev, D. G.; Froese, R. D. J.; Sevensson, M.; Morokuma, K. *J. Am. Chem. Soc.* **1997**, *119*, 367. (c) Musaev, D. G.; Sevensson, M.; Morokuma, K.; Strömberg, S.; Zetterberg, K.; Siegbahn, P. E. M. *Organometallics* **1997**, *16*, 1933. (d) Musaev, D. G.; Froese, R. D. J.; Morokuma, K. *New J. Chem.* **1997**, *21*, 1269. (e) Froese, R. D. J.; Musaev, D. G.; Morokuma, K. *J. Am. Chem. Soc.* **1998**, *120*, 1581. (f) Musaev, D. G.; Froese, R. D. J.; Morokuma, K. *Organometallics* **1998**, *17*, 1850.
(90) (a) Deng, L.; Margl, P.; Ziegler, T. *J. Am. Chem. Soc.* **1997**, *119*, 1094. (b) Deng, L.; Woo, T. K.; Cavallo, L.; Margl, P.; Ziegler, T. *J. Am. Chem. Soc.* **1997**, *119*, 6177. (c) Woo, T. K.; Margl, P.; Deng, L.; Cavallo, L.; Ziegler, T. in *Transition State Modeling for Catalysis*; Truhlar, D. G., Morokuma, K., Eds.; ACS Symposium Series 721; Oxford University Press: New York, 1999; p 173. (d) Margl, P.; Ziegler, T. *Organometallics* **1996**, *15*, 15519. (e) Margl, P.; Ziegler, T. *J. Am. Chem. Soc.* **1996**, *118*, 7337.
(91) (a) Siegbahn, P. E. M.; Strömberg, S.; Zetterberg, K. *Organometallics* **1996**, *15*, 5542. (b) Strömberg, S.; Zetterberg, K.; Siegbahn, P. E. M. *J. Chem. Soc., Dalton Trans.* **1997**, 4147.
(92) Albert, K.; Gisdakis, P.; Rösch, N. *Organometallics* **1998**, *17*, 1608.
(93) Ohanessian, G.; Goddard, W. A., III *Acc. Chem. Res.* **1990**, *23*, 386.
(94) Walch, S. P.; Bauschlicher, C. W., Jr. In *Comparison of Ab Initio Quantum Chemistry with Experiment*; Bartlett, R., Ed.; Reidel: Boston, MA, 1985; p 17.
(95) Niu, S.-Q.; Zaric, S.; Bayse, C. A.; Strout, D. L.; Hall, M. B. *Organometallics* **1998**, *17*, 5139.
(96) Han, Y.; Deng, L.; Ziegler, T. *J. Am. Chem. Soc.* **1997**, *119*, 5939.
(97) (a) McDade, C.; Bercaw, J. E. *J. Organomet. Chem.* **1985**, *279*, 281. (b) Thompson, M. E.; Baxter, S. M.; Bulls, A. R.; Burger, B. J.; Nolan, M. C.; Santarsiero, B. D.; Schaefer, W. P.; Bercaw, J. E. *J. Am. Chem. Soc.* **1987**, *109*, 203. (c) Burger, B. J.; Thompson, M. E.; Cotter, W. D.; Bercaw, J. E. *J. Am. Chem. Soc.* **1990**, *112*, 1566. (d) Christ, C. S., Jr.; Eyler, J. R.; Richardson, D. E. *J. Am. Chem. Soc.* **1990**, *112*, 596. (e) Horton, A. D.; Orpen, A. G. *Organometallics* **1992**, *11*, 8.
(98) (a) Eish, J. J.; Piotrowski, A. M.; Brownstein, S. K.; Gable, E. J.; Lee, F. L. *J. Am. Chem. Soc.* **1985**, *107*, 7219. (b) Horton, A. D.; Orpen, A. G. *Organometallics* **1991**, *10*, 3910. (c) Erker, G. *Nachr. Chem. Technol. Lab.* **1992**, *40*, 1099. (d) Rottger, D.; Erker, G. *Angew. Chem., Int. Ed. Engl.* **1997**, *36*, 812.
(99) (a) Trost, B. M.; Sorum, M. T.; Chan, C.; Harms, A. E.; Rühter, G. *J. Am. Chem. Soc.* **1997**, *119*, 698. (b) Slugovc, C.; Mereiter, K.; Zobetz, E.; Schmid, R.; Kirchner, K. *Organometallics* **1996**, *15*, 5275.
(100) Rappé, A. K. *Organometallics* **1990**, *9*, 466.
(101) Nakamura, E.; Miyachi, Y.; Koga, N.; Morokuma, K. *J. Am. Chem. Soc.* **1992**, *114*, 4. 6686.
(102) Niu, S.-Q.; Hall, M. B. Unpublished work.
(103) de Vaal, P.; Dedieu, A. *J. Organomet. Chem.* **1994**, *478*, 121.
(104) Zakharov, I. I.; Zakharov, V. A.; Zhidomirov, G. M. *Macromolecular Theory Simulations* **1996**, *5*, 837.
(105) (a) Evans, D.; Osborn, J. A.; Wilkinson, *J. Chem. Soc. A* **1968**, 3133. (b) Evans, D.; Yagupsky, G.; Wilkinson, *J. Chem. Soc. A* **1968**, 2660.
(106) (a) Calderazzo, F.; Cotton, F. A. *Inorg. Chem.* **1962**, *1*, 30. (b) Kuhlmann, E. K.; Alexander, J. J. *J. Coord. Chem. Rev.* **1980**, *33*, 195. (c) Kurfee, L. D.; Rothwell, I. P. *Chem. Rev.* **1988**, *88*, 1059.
(107) (a) Berke, H.; Hoffmann, R. *J. Am. Chem. Soc.* **1978**, *100*, 7224. (b) Hofmann, P.; Stauffert, P.; Tatsumi, K.; Nakamura, A.; Hoffmann, R. *Organometallics* **1985**, *4*, 404. (c) Hofmann, P.; Stauffert, P.; Tatsumi, K.; Nakamura, A.; Hoffmann, R. *J. Am. Chem. Soc.* **1985**, *107*, 4440.
(108) Curtis, M. D.; Shiu, K.-B.; Butler, W. M. *J. Am. Chem. Soc.* **1986**, *108*, 1550.
(109) Ziegler, T.; Versluis, L.; Tschinke, V. *J. Am. Chem. Soc.* **1986**, *108*, 612.
(110) Axe, F. U.; Marynick, D. S. *Organometallics* **1987**, *6*, 572.
(111) Axe, F. U.; Marynick, D. S. *J. Am. Chem. Soc.* **1988**, *110*, 3728.
(112) (a) Sakaki, S.; Kitaura, K.; Morokuma, K.; Ohkabo, K. *J. Am. Chem. Soc.* **1983**, *105*, 2280. (b) Koga, N.; Morokuma, K. *J. Am. Chem. Soc.* **1985**, *107*, 7230. (c) Koga, N.; Morokuma, K. *J. Am. Chem. Soc.* **1986**, *108*, 6136.
(113) Rappé, A. K. *J. Am. Chem. Soc.* **1987**, *109*, 5605.
(114) Blomberg, M. R. A.; Karlsson, C. A. M.; Siegbahn, P. E. M. *J. Phys. Chem.* **1993**, *97*, 9341.
(115) (a) Matsubara, T.; Koga, N.; Ding, Y. P.; Musaev, D. G.; Morokuma, K. *Organometallics* **1997**, *16*, 1065. (b) Markies, B. A.; Wijkens, P.; Dedieu, A.; Boersma, J.; Spek, A. L.; van Koten, G. *Organometallics* **1995**, *14*, 5628. (c) Groen, J. H.; de Zwart, A.; Vlaar, M. J. M.; Ernsting, J. M.; van Leeuwen, P. W. N. M.; Vrieze, K.; Kooijman, H.; Smeets, W. J. J.; Spek, A. L.; Budzelaar, P. H. M.; Xiang, Q.; Thummel, R. P. *Eur. J. Inorg. Chem.* **1998**, 1129.
(116) Cao, Z. X.; Niu, S. Q.; Hall, M. B. *J. Phys. Chem.*, submitted.
(117) Richter-Addo, G. B.; Legzdins, P. *Metal Nitrosyls*; Oxford University Press: New York, 1992.
(118) Culotta, E.; Koshland, D. E., Jr. *Science* **1992**, *258*, 1862.
(119) Feldman, P. L.; Griffith, O. W.; Stuehr, D. J. *Chem. Eng. News* **1993**, *71*(5), 26.
(120) Sulfab, Y.; Basolo, F.; Rheingold, A. L. *Organometallics* **1989**, *8*, 2139.
(121) Legzdins, P.; Wassink, B.; Einstein, F. W. B.; Willis, A. C. *J. Am. Chem. Soc.* **1986**, *108*, 317.
(122) Goldhaber, A.; Vollhart, K. P. C.; Walborsky, E. C.; Wolfgruber, M. *J. Am. Chem. Soc.* **1986**, *108*, 516.
(123) (a) Weiner, W. P.; White, M. A.; Bergman, R. G. *J. Am. Chem. Soc.* **1981**, *103*, 3612. (b) Seidler, M. D.; Bergman, R. G. *Organometallics* **1983**, *2*, 1897. (c) Weiner, W. P.; Bergman, R. G. *J. Am. Chem. Soc.* **1983**, *105*, 3922.
(124) Margl, P.; Deng, L.; Ziegler, T. *J. Am. Chem. Soc.* **1999**, *121*, 154.
(125) Niu, S.-Q.; Hall, M. B. *J. Am. Chem. Soc.* **1999**, *121*, 3992.
(126) Lin, Z.; Hall, M. B.; Guest, M. F.; Sherwood, P. *J. Organomet. Chem.* **1994**, *478*, 197.
(127) (a) Brookhart, M.; Lincoln, D. M.; Volpe, A. F., Jr.; Schmidt, G. F. *Organometallics* **1989**, *8*, 1212. (b) Brookhart, M.; Lincoln, D. M.; Bennett, M. A. *J. Am. Chem. Soc.* **1990**, *112*, 2691.
(128) (a) Fan, L.; Krzywicki, A.; Somogyvari, A.; Ziegler, T. *Inorg. Chem.* **1996**, *35*, 4003. (b) Fan, L.; Krzywicki, A.; Somogyvari, A.; Ziegler, T. *Stud. Surf. Sci. Catal.* **1996**, *100*, 507.
(129) Muller, U.; Keim, K.; Kruger, C.; Betz, P. *Angew. Chem., Int. Ed. Engl.* **1989**, *28*, 1011.
(130) (a) Yoshida, T.; Otsuka, S. *J. Am. Chem. Soc.* **1977**, *99*, 2134. (b) Fornies, J.; Green, M.; Spencer, J. L.; Stone, F. G. *J. Chem. Soc., Dalton Trans.* **1977**, 1006. (c) Yoshida, T.; Yamagata, T.; Tulip, T. H.; Ibers, J. A.; Otsuka, S. *J. Am. Chem. Soc.* **1978**, *100*, 2063. (d) Paonessa, R. S.; Trogler, W. C. *J. Am. Chem. Soc.* **1982**, *104*, 1138. (e) Packett, D. L.; Jensen, C. M.; Cowan, R. L.; Strouse, C. E.; Trogler, W. C. *Inorg. Chem.* **1985**, *24*, 3578. (f)

Packett, D. L.; Trogler, W. C. *J. Am. Chem. Soc.* **1986**, *108*, 5036. (g) Packett, D. L.; Trogler, W. C. *Inorg. Chem.* **1988**, *27*, 1768.
(131) (a) Abis, L.; Sen, A.; Halperin, J. *J. Am. Chem. Soc.* **1978**, *100*, 2915. (b) Gillie, A.; Stille, J. K. *J. Am. Chem. Soc.* **1980**, *102*, 4933.
(132) (a) Low, J. J.; Goddard, W. A., III *J. Am. Chem. Soc.* **1984**, *106*, 6928. (b) Low, J. J.; Goddard, W. A., III *J. Am. Chem. Soc.* **1984**, *106*, 8321. (c) Low, J. J.; Goddard, W. A., III *Organometallics* **1986**, *5*, 609. (d) Low, J. J.; Goddard, W. A., III *J. Am. Chem. Soc.* **1986**, *108*, 6115.
(133) (a) Blomberg, M. R. A.; Siegbahn, P. E. M. *J. Chem. Phys.* **1983**, *78*, 986. (b) Blomberg, M. R. A.; Siegbahn, P. E. M. *J. Chem. Phys.* **1983**, *78*, 5682. (c) Blomberg, M. R. A.; Brandemark, U.; Siegbahn, P. E. M. *J. Am. Chem. Soc.* **1983**, *105*, 5557. (d) Siegbahn, P. E. M.; Blomberg, M. R. A. *Organometallics* **1994**, *13*, 354. (e) Siegbahn, P. E. M. *Organometallics* **1994**, *13*, 2833. (f) Siegbahn, P. E. M.; Svensson, M. *J. Am. Chem. Soc.* **1994**, *116*, 10124. (g) Wittborn, A. M. C.; Costas, M.; Blomberg, M. R. A.; Siegbahn, P. E. M. *J. Chem. Phys.* **1997**, *107*, 4318.
(134) (a) Obara, S.; Kitaura, K.; Morokuma, K. *J. Am. Chem. Soc.* **1984**, *106*, 7482. (b) Musaev, D. G.; Morokuma, K. *J. Am. Chem. Soc.* **1995**, *117*, 799. (c) Matsubara, T.; Maseras, F.; Koga, N.; Morokuma, K. *J. Phys. Chem.* **1996**, *100*, 2573. (d) Svensson, M.; Humbel, S.; Froese, R. D. J.; Matsubara, T.; Sieber, S.; Morokuma, K. *J. Phys. Chem.* **1996**, *100*, 19357.
(135) (a) Noell, J. O.; Hay, P. J. *J. Am. Chem. Soc.* **1982**, *104*, 4578. (b) Hay, P. J. In *Transition Metal Hydrides*; Dedieu, A., Ed.; VCH Publishers: 1992; p 127. (c) Hay, P. J. *New J. Chem.* **1991**, *15*, 735.
(136) (a) Sakaki, S.; Leki, M. *J. Am. Chem. Soc.* **1991**, *113*, 5063. (b) Sakaki, S.; Leki, M. *J. Am. Chem. Soc.* **1993**, *115*, 2373. (c) Sakaki, S.; Ogawa, M.; Musashi, Y.; Arai, T. *Inorg. Chem.* **1994**, *33*, 1660. (d) Sakaki, S.; Ogawa, M.; Kinoshita, M. *J. Phys. Chem.* **1995**, *99*, 9933. (e) Sakaki, S.; Biswas, B.; Sugimoto, M. *J. Chem. Soc., Dalton Trans.* **1997**, 803. (f) Sakaki, S.; Biswas, B.; Sugimoto, M. *Organometallics* **1998**, *17*, 1278. (g) Sakaki, S.; Mizoe, N.; Musashi, Y.; Biswas, B.; Sugimoto, M. *J. Phys. Chem. A* **1998**, *102*, 8027.
(137) Su, M.-D.; Chu, S.-Y. *Inorg. Chem.* **1998**, *37*, 3400.
(138) (a) Chock, P. B.; Halpern, J. *J. Am. Chem. Soc.* **1966**, *88*, 3511. (b) Halpern, J. *Acc. Chem. Res.* **1970**, *3*, 386. (c) Vaska, L. *Acc. Chem. Res.* **1968**, *1*, 335. (d) Ugo, R.; Pasini, A.; Fusi, A.; Cenini, S. *J. Am. Chem. Soc.* **1972**, *94*, 7364. (e) Collman, J. P. *Acc. Chem. Res.* **1968**, *1*, 136. (f) Burk, M. J.; McGrath, M. P.; Wheeler, R.; Grabtree, R. H. *J. Am. Chem. Soc.* **1988**, *110*, 5034. (g) Evans, D.; Osborn, J. A.; Wilkinson, G. *J. Chem. Soc. A* **1968**, 3133. (h) Evans, D.; Yagupsky, G.; Wilkinson, G. *J. Chem. Soc. A* **1968**, 2660. (i) Evans, D.; Wilkinson, G. *J. Chem. Soc. A* **1970**, 2753.
(139) (a) Janowicz, A. H.; Bergman, R. G. *J. Am. Chem. Soc.* **1982**, *104*, 352. (b) Hoyano, J. K.; Graham, W. A. G. *J. Am. Chem. Soc.* **1982**, *104*, 3723. (c) Crabtree, R. H.; Mellea, M. F.; Mihelsie, J. M.; Quick, J. M. *J. Am. Chem. Soc.* **1982**, *104*, 107. (d) Jones, W. D.; Feher, F. J. *J. Am. Chem. Soc.* **1982**, *104*, 4240.
(140) (a) Koga, N.; Morokuma, K. *J. Phys. Chem.* **1990**, *94*, 5454. (b) Koga, N.; Morokuma, K. *J. Am. Chem. Soc.* **1993**, *115*, 6883. (c) Wakatsuki, Y.; Koga, N.; Werner, H.; Morokuma, K. *J. Am. Chem. Soc.* **1997**, *119*, 360.
(141) Margl, P.; Ziegler, T.; Blöchl, P. E. *J. Am. Chem. Soc.* **1995**, *117*, 12625.
(142) (a) Krogh-Jesperson, K.; Goldman, A. S. In *Transition State Modeling for Catalysis*; Truhlar, D. G., Morokuma, K., Eds.; ACS Symposium Series 721; Oxford University Press: New York, 1999; p 151. (b) Rosini, G. P.; Liu, F.; Krogh-Jesperson, K.; Goldman, A. S.; Li, C.; Nolan, S. P. *J. Am. Chem. Soc.* **1998**, *120*, 9256.
(143) (a) Cundari, T. R. *J. Am. Chem. Soc.* **1994**, *106*, 340. (b) Benson, M. T.; Cundari, T. R. *Inorg. Chim. Acta* **1997**, *259*, 91.
(144) Hill, G. S.; Puddephatt, R. J. *Organometallics* **1998**, *17*, 1478.
(145) Avdeev, V. L.; Zhidomirov, G. M. *Kinet. Catal.* **1996**, *37*, 722.
(146) (a) Fisher, B. J.; Eisenberg, R. *Inorg. Chem.* **1984**, *23*, 3216. (b) Johnson, C. E.; Fisher, B. J.; Eisenberg, R. *J. Am. Chem. Soc.* **1983**, *105*, 7772. (c) Johnson, C. E.; Eisenberg, R. *J. Am. Chem. Soc.* **1985**, *107*, 3148. (d) Johnson, C. E.; Eisenberg, R. *J. Am. Chem. Soc.* **1985**, *107*, 6531.
(147) (a) Sargent, A. L.; Hall, M. B.; Guest, M. F. *J. Am. Chem. Soc.* **1992**, *114*, 517. (b) Sargent, A. L.; Hall, M. B. *Inorg. Chem.* **1992**, *31*, 317. (c) Sargent, A. L.; Hall, M. B. In *Topics in Physical Organometallic Chemistry*; Gielen, M. Ed.; Freund Pub.: London, 1992; Chapter 1, Vol. 4, p 1.
(148) (a) Abu-Hasanayn, F.; Krogh-Jespersen, K.; Goldman, A. S. *Inorg. Chem.* **1993**, *32*, 495. (b) Abu-Hasanayn, F.; Goldman, A. S.; Krogh-Jespersen, K. *Inorg. Chem.* **1994**, *33*, 5122. (b) Abu-Hasanayn, F.; Goldman, A. S.; Krogh-Jespersen, K. *J. Phys. Chem.* **1993**, *97*, 5890.
(149) Hammord, G. S. *J. Am. Chem. Soc.* **1955**, *77*, 334.
(150) Musaev, D. J.; Morokuma, K. *J. Organomet. Chem.* **1995**, *504*, 93.
(151) (a) Spillet, C. T.; Ford, P. C. *J. Am. Chem. Soc.* **1989**, *111*, 1932. (b) Duckett, S. B.; Eisenberg, R. *J. Am. Chem. Soc.* **1993**, *115*, 5292.
(152) Wang, W.; Weitz, E. *J. Phys. Chem.* **1997**, *101*, 2358.
(153) Wang, W.; Narducci, A.; House, P.; Weitz, E. *J. Am. Chem. Soc.* **1996**, *118*, 8654.
(154) (a) Wasserman, E. P.; Moore, C. B.; Bergman, R. G. *Science* **1992**, *255*, 315. (b) Schultz, R. H.; Bengali, A. A.; Tauber, M. J.; Weiller, B. H.; Wasserman, E. P.; Kyle, K. R.; Moore, C. B.; Bergman, R. G. *J. Am. Chem. Soc.* **1994**, *116*, 7369. (c) Stoutland, P. O.; Bergman, R. G.; Nolan, S. P.; Hoff, C. D. *Polyhedron* **1988**, *7*, 1429. (d) Bengali, A. A.; Bergman, R. G.; Moore, C. B. *J. Am. Chem. Soc.* **1995**, *117*, 3879.
(155) (a) Hofmann, P.; Padmanabhan, M. *Organometallics* **1983**, *2*, 1273. (b) Hoffmann, R. *Angew. Chem., Int. Ed. Engl.* **1982**, *21*, 711.
(156) Jiménez-Cataño, R.; Hall, M. B. *Organometallics* **1996**, *15*, 1889.
(157) Bosque, R.; Clot, E.; Fantacci, S.; Maseras, F.; Eisenstein, O.; Perutz, R. N.; Renkema, K. B.; Caulton, K. G. *J. Am. Chem. Soc.* **1998**, *120*, 12638.
(158) (a) Su, M.-D.; Chu, S.-Y. *Organometallics* **1997**, *16*, 1621. (b) Su, M.-D.; Chu, S.-Y. *Chem. Eur. J.* **1999**, *5*, 198.
(159) (a) Bell, T. W.; Brough, S.-A.; Partridge, M. G.; Perutz, R. N.; Rooney, A. D. *Organometallics* **1993**, *12*, 2933. (b) Bell, T. W.; Haddleton, D. M.; McCamley, A.; Partridge, M. G.; Willner, H. *J. Am. Chem. Soc.* **1990**, *112*, 9212. (c) Ghosh, C. K.; Hoyano, J. K.; Krentz, R.; Graham, W. A. G. *J. Am. Chem. Soc.* **1989**, *111*, 5480.
(160) (a) Jiménez-Cataño, R.; Niu, S.-Q.; Hall, M. B. *Organometallics* **1997**, *16*, 1962. (b) Zaric, S.; Hall, M. B. *J. Phys. Chem. A* **1998**, *102*, 1963.
(161) (a) Lian, T.; Bromberg, S. E.; Yang, H.; Proulx, G.; Bergman, R. G.; Harris, C. B. *J. Am. Chem. Soc.* **1996**, *118*, 3769. (c) Bromberg, S. E.; Yang, H.; Asplund, M. C.; Lian, T.; McNamara, B. K.; Kotz, K. T.; Yeston, J. S.; Wilkens, M.; Frei, H.; Bergman, R. G.; Harris, C. B. *Science* **1997**, *278*, 260.
(162) (a) Kubas, G. J. *Acc. Chem. Res.* **1988**, *21*, 120. (b) Kubas, G. J.; Unkefer, C. J.; Swanson, B. I.; Fukishima, E. *J. Am. Chem. Soc.* **1986**, *108*, 7000.
(163) Jean, Y.; Eisenstein, O.; Volatron, F.; Maouche, B.; Sefta, F. *J. Am. Chem. Soc.* **1986**, *108*, 6587.
(164) Hay, P. *J. Am. Chem. Soc.* **1987**, *109*, 305.
(165) (a) Arndtsen, B. A.; Bergman, R. G. *Science* **1995**, *270*, 1970. (b) Burger, P.; Bergman, R. G. *J. Am. Chem. Soc.* **1993**, *115*, 10462. (c) Lohrenz, J. C. W.; Hacobsen, H. *Angew. Chem., Int. Ed. Engl.* **1996**, *35*, 1305.
(166) (a) Strout, D.; Zarić, S.; Niu, S.-Q.; Hall, M. B. *J. Am. Chem. Soc.* **1996**, *118*, 6068. (b) Niu, S.-Q.; Strout, D.; Zarić, S.; Bayes, C. A.; Hall, M. B. In *Transition State Modeling for Catalysis*; Truhlar, D. G., Morokuma, K., Eds.; ACS Symposium Series 721; Oxford University Press: New York, 1999; p 138. (c) Niu, S.-Q.; Hall, M. B. *J. Am. Chem. Soc.* **1998**, *120*, 6169. (d) Niu, S.-Q.; Hall, M. B. Unpublished work.
(167) (a) Hinderling, C.; Plattner, D. A.; Chen, P. *Angew. Chem., Int. Ed. Engl.* **1997**, *36*, 243. (b) Hinderling, C.; Feichtings, D.; Plattner, D. A.; Chen, P. *J. Am. Chem. Soc.* **1997**, *119*, 10793.
(168) Luecke, H. F.; Bergman, R. G. *J. Am. Chem. Soc.* **1997**, *119*, 11538.
(169) Su, M.-D.; Chu, S.-Y. *J. Am. Chem. Soc.* **1997**, *119*, 5373.
(170) (a) Katz, T. J. *Adv. Organomet. Chem.* **1977**, *16*, 283. (b) Calderon, N.; Lawrence, J. P.; Ofstead, E. A. *Adv. Organomet. Chem.* **1979**, *17*, 449.
(171) Herisson, J. L.; Chauvin, Y. *Makromol. Chem.* **1970**, *141*, 161.
(172) Steigerwald, M. L.; Goddard, W. A., III *J. Am. Chem. Soc.* **1984**, *106*, 308.
(173) (a) Ziegler, T.; Folga, E. *J. Am. Chem. Soc.* **1993**, *115*, 636. (b) Ziegler, T.; Folga, E. *J. Organomet. Chem.* **1994**, *478*, 57. (c) Folga, E.; Ziegler, T. *Can. J. Chem.* **1992**, *70*, 333.
(174) Thompson, M. E.; Buxter, S. M.; Bulls, A. R.; Burger, B. J.; Nolan, M. C.; Santarsiero, B. D.; Schaefer, W. P.; Bercaw, J. E. *J. Am. Chem. Soc.* **1987**, *109*, 203.
(175) Harrod, J. F.; Ziegler, T.; Tschinke, V. *Organometallics* **1990**, *9*, 897.
(176) Siegbahn, P. E. M.; Crabtree, R. H. *J. Am. Chem. Soc.* **1996**, *118*, 4442.
(177) (a) Shilov, A. E. *Activation of Saturated Hydrocarbons by Transition Metal Complexes*; D. Riedel: Dordrecht, The Netherlands, 1984. (b) Shilov, A. E. In *Activation and Functionalization of Alkanes*; Hill, C. L., Ed.; Wiley: New York, 1984.
(178) (a) Hutschka, F.; Dedieu, A.; Leitner, W. *Angew. Chem., Int. Ed. Engl.* **1995**, *34*, 1742. (b) Hutschka, F.; Dedieu, A.; Eichberger, M.; Fornika, R.; Leitner, W. *J. Am. Chem. Soc.* **1997**, *119*, 4432. (c) Milet, A.; Dedieu, A.; Kapteijin, G.; van Koten, G. *Inorg. Chem.* **1997**, *36*, 3223. (d) Dedieu, A.; Hutschka, F.; Milet, A. In *Transition State Modeling for Catalysis*; Truhlar, D. G., Morokuma, K., Eds.; ACS Symposium Series 721; Oxford University Press: New York, 1999; p 100. (e) Hutschka, F.; Dedieu, A. *J. Chem. Soc., Dalton Trans.* **1997**, 1899. (f) Milet, A.; Dedieu, A.; Canty, A. J. *Organometallics* **1997**, *16*, 5331.

(179) (a) Sakaki, S.; Nishikawa, M.; Ohyoshi, A. *J. Am. Chem. Soc.* **1980**, *102*, 4062. (b) Eisenstein, O.; Hoffmann, R. *J. Am. Chem. Soc.* **1980**, *102*, 6148. (c) Nakamura, S.; Dedieu, A. *Theor. Chim. Acta* **1982**, *61*, 587. (d) Dedieu, A.; Nakamura, S. *Nouv. J. Chim.* **1984**, *8*, 317. (e) Fujimoto, H.; Yamasaki, T. *J. Am. Chem. Soc.* **1986**, *108*, 578. (f) Sakaki, S.; Maruta, K.; Ohkubo, K. *Inorg. Chem.* **1987**, *26*, 2499. (g) Sakaki, S.; Maruta, K.; Ohkubo, K. *J. Chem. Soc., Dalton Trans.* **1987**, 361.

(180) Siegbahn, P. E. M. *J. Phys. Chem.* **1996**, *100*, 14672.

(181) Crabtree, R. H.; Siegbahn, P. E. M.; Eisenstein, O.; Rheingold, A. L.; Koetzle, T. F. *Acc. Chem. Res.* **1996**, *29*, 348.

(182) Peris, E.; Lee, J. C.; Rambo, J. R.; Eisenstein, O.; Crabtree, R. H. *J. Am. Chem. Soc.* **1995**, *117*, 3485.

(183) (a) Pavlov, M.; Siegbahn, P. E. M.; Blomberg, M. R. A.; Crabtree, R. H. *J. Am. Chem. Soc.* **1998**, *120*, 548. (b) Pavlov, M.; Siegbahn, P. E. M.; Blomberg, M. R. A. *Int. J. Quantum Chem.* **1999**, *73*, 197.

(184) Niu, S.-Q.; Thomson, L. M.; Hall, M. B. *J. Am. Chem. Soc.* **1999**, *121*, 4000.

(185) (a) Burk, M. J.; Crabtree, R. H.; McGrath, D. V. *J. Chem. Soc., Chem. Commun.* **1985**, 1829. (a) Crabtree, R. H.; Mihelcic, J. M.; Quirk, J. M. *J. Am. Chem. Soc.* **1979**, *101*, 7738. (b) Baudry, M. J.; Ephritikine, M.; Felkin, H.; Holmes-Smith, R. *J. Chem. Soc., Chem. Commun.* **1983**, 788. (c) Baudry, M. J.; Crabtree, R. H.; Parnell, C. P.; Uriarte, R. J. *Organometallics* **1984**, *3*, 816.

(186) (a) Atkins, P. W. *Physical Chemistry*; Oxford University Press: New York, 1990. (b) NIST Standard Reference Database Number 69, 1996, http://webbook.nist.gov/chemistry/.

(187) (a) Xu, W.-W.; Rosini, G. P.; Gupta, M.; Jensen, C. M.; Kaska, W. C.; Krogh-Jespersen, K.; Goldman, A. S. *J. Chem. Soc., Chem. Commun.* **1997**, 2273. (b) Jensen, C. M.; Gupta, M.; Hee, A.; Hagen, C.; Hoffmann, S.; Kaska, W. C.; Pak, E.; Zidan, R. *215th Am. Chem. Soc. National Meeting Dallas, TX, March 29*, 1998, *Div. Inorg. Chem.*, Paper 11. (c) Lee, D. W.; Kaska, W. C.; Jensen, C. M. *Organometallics* **1998**, *17*, 1. (d) Gupta, M.; Hagen, C.; Kaska, W. C.; Cramer, R. E.; Jensen, C. M. *J. Chem. Soc., Chem. Commun.* **1996**, 2083. (e) Gupta, M.; Hagen, C.; Kaska, W. C.; Cramer, R. E.; Jensen, C. M. *J. Am. Chem. Soc.* **1997**, *119*, 840. (f) Gupta, M.; Kaska, W. C.; Jensen, C. M. *J. Chem. Soc., Chem. Commun.* **1997**, 461.

(188) (a) Jessop, P. G.; Ikariya, T.; Noyori, R. *Chem. Rev.* **1995**, *95*, 259. (b) Leitner, W. *Angew. Chem., Int. Ed. Engl.* **1995**, *34*, 2207. (c) Graf, E.; Leitner, W. *Chem. Ber.* **1996**, *129*, 91.

CR980404Y